HEATSTORE

Uncertainty Management in Underground Thermal Energy Storage Development and Operation

Prepared by: Antoine Armandine Les Landes, BRGM
Jérémy Rohmer, BRGM
Annick Loschetter, BRGM
Charles Maragna, BRGM
Lorenzo Perozzi, University of Geneva
Luca Guglielmetti, University of Geneva
Thomas G. Vangkilde-Pedersen, GEUS

With collaboration of: Peter Meier (Geo-Energie)
Dieter Ollinger (Geo-Energie)

Checked by: Jean-Charles Manceau, BRGM

Approved by: Marc Perreaux, Storengy (WP5 leader)
Holger Cremer, TNO (HEATSTORE coordinator)

Please cite this report as: Armandine Les Landes A., Rohmer J., Loschetter A., Maragna C., Perozzi L., Guglielmetti, L., Vangkilde-Pedersen,T.G., 2021: Uncertainty Management in Underground Thermal Energy Storage Development and Operation, GEOTHERMICA – ERA NET Cofund Geothermal, 73 p.

This report represents HEATSTORE project deliverable number D5.5

HEATSTORE (170153-4401) is one of nine projects under the GEOTHERMICA – ERA NET Cofund aimed at accelerating the uptake of geothermal energy by 1) advancing and integrating different types of underground thermal energy storage (UTES) in the energy system, 2) providing a means to maximise geothermal heat production and optimise the business case of geothermal heat production doublets, 3) addressing technical, economic, environmental, regulatory and policy aspects that are necessary to support efficient and cost-effective deployment of UTES technologies in Europe.

This project has been subsidized through the ERANET cofund GEOTHERMICA (Project n. 731117), from the European Commission, RVO (the Netherlands), DETEC (Switzerland), FZJ-PtJ (Germany), ADEME (France), EUDP (Denmark), Rannis (Iceland), VEA (Belgium), FRCT (Portugal), and MINECO (Spain).

About HEATSTORE

High Temperature Underground Thermal Energy Storage

The heating and cooling sector is vitally important for the transition to a low-carbon and sustainable energy system. Heating and cooling is responsible for half of all consumed final energy in Europe. The vast majority – 85% - of the demand is fulfilled by fossil fuels, most notably natural gas. Low carbon heat sources (e.g. geothermal, biomass, solar and waste-heat) need to be deployed and heat storage plays a pivotal role in this development. Storage provides the flexibility to manage the variations in supply and demand of heat at different scales, but especially the seasonal dips and peaks in heat demand. Underground Thermal Energy Storage (UTES) technologies need to be further developed and need to become an integral component in the future energy system infrastructure to meet variations in both the availability and demand of energy.

The main objectives of the HEATSTORE project are to lower the cost, reduce risks, improve the performance of high temperature (~25°C to ~90°C) underground thermal energy storage (HT-UTES) technologies and to optimize heat network demand side management (DSM). This is primarily achieved by 6 new demonstration pilots and 8 case studies of existing systems with distinct configurations of heat sources, heat storage and heat utilization. This will advance the commercial viability of HT-UTES technologies and, through an optimized balance between supply, transport, storage and demand, enable that geothermal energy production can reach its maximum deployment potential in the European energy transition.

Furthermore, HEATSTORE also learns from existing UTES facilities and geothermal pilot sites from which the design, operating and monitoring information will be made available to the project by consortium partners.

HEATSTORE is one of nine projects under the GEOTHERMICA – ERA NET Cofund and has the objective of accelerating the uptake of geothermal energy by 1) advancing and integrating different types of underground thermal energy storage (UTES) in the energy system, 2) providing a means to maximize geothermal heat production and optimize the business case of geothermal heat production doublets, 3) addressing technical, economic, environmental, regulatory and policy aspects that are necessary to support efficient and cost-effective deployment of UTES technologies in Europe. The three-year project will stimulate a fast-track market uptake in Europe, promoting development from demonstration phase to commercial deployment within 2 to 5 years, and provide an outlook for utilization potential towards 2030 and 2050.

The 23 contributing partners from 9 countries in HEATSTORE have complementary expertise and roles. The consortium is composed of a mix of scientific research institutes and private companies. The industrial participation is considered a very strong and relevant advantage, which is instrumental for success. The combination of leading European research institutes together with small, medium and large industrial enterprises, will ensure that the tested technologies can be brought to market and valorised by the relevant stakeholders.

Document Change Record

This section shows the historical versions, with a short description of the updates.

Version	Short description of change
2021.07.26	First version
2021.08.17	Revised version (integration of revisions proposed by Jean-Charles Manceau)
2021.09.24	Definitive version to be published on Heatstore website

Table of Content

1 Introduction

The design of complex systems such as Underground Thermal Energy Storage (UTES) requires not only the modelling of the whole installation and optimisation of the overall design but also to consider the large variety of different uncertainty sources that affect each stage of the modelling chain. A dedicated task on uncertainty management was proposed in the HEATSTORE project, described in the work plan as follows:

> **Task 5.5: Uncertainty management (BRGM, STY, GEUS, UPC, UniGe)**
> It is important to recognize two basic kinds of uncertainties: natural and epistemic uncertainty. Whereas the former is described as arising from inherent variability or randomness in the studied systems (for instance the average monthly temperature), the latter stems from sparse, incomplete and imprecise information such as expert's beliefs about some unknown parameter. The first subtask will thus be to assess the sources of uncertainty on the different parameters, and to propose a framework for uncertainty representation (either a pure probabilistic one or a hybrid probabilistic-possibilistic one). Once identified and represented, uncertainties have to be propagated in models. Depending on the models computational cost, it may be necessary to use methods for uncertainty propagation. Finally, after proper representation and propagation of uncertainties, an effort will be made to make the results understandable and useable depending on the context and on the users' level of knowledge. The number of investigated technologies and demo sites will be adapted to match with the available resources.
>
> - STORENGY / BRGM: assessment of sources of uncertainty on the different parameters, and proposition of a framework for uncertainty representation. Propagation of uncertainties in models. Depending on the models computational cost, it may be necessary to use state-of-the-art methods for uncertainty propagation that are parsimonious. Making the results understandable and useable depending on the context and on the users' level of knowledge will be the final step.
> - GEUS: will contribute to development of strategies for uncertainty management, especially regarding geological/reservoir uncertainty.
> - UniGe and UPC will assess the remaining uncertainty of the subsurface models
>
> Deliverable: D5.5 Report on uncertainty management in UTES development and operation

The present report addresses the following key questions:

1) How to account for different origins of uncertainties, i.e. aleatory (aka randomness) which is inherent to the physical environment or engineered system under study and represents its intrinsic variability, and epistemic uncertainty which is not intrinsic to the system under study and stems from the incomplete/imprecise nature of available information? This question is very important in the context of energy storage, because data are often scarce, incomplete or imprecise, and thus the systematic and only use of the probabilistic framework may be debatable.

   → Section 2: we provide an overview of different methods that are available to deal with uncertainties, to discuss how they may be helpful for decision-making in a high-uncertainty context, and to highlight their advantages and limitations. For sake of explanation of the whole chain (identification of uncertainty and information gathering, representation of uncertain parameters, propagation of uncertainties, sensitivity analysis, decision making), we chose a fictive case study that consists of making a decision based on the expected efficiency of an aquifer seasonal storage. A simple analytical model available in the literature was used.

   → Section 3: the exercise was initiated on a real case study, the Bern demo site. We focused on preliminary steps of the uncertainty treatment: identification of context and model requirements, refinement of the decision-making process, parameter identification, uncertainty elicitation, uncertainty representation, preliminary modelling, elaboration of a work programme to complete the analysis with such a complex model. This section is very complementary to section 2 since it illustrates the numerous issues and difficulties, which occur when we confront with a real and complex case study, and how they can be addressed.

2) How to conduct the analysis of the parametric uncertainties affecting the system when using complex time-consuming numerical models (with typical computation time cost of the order of several hours)?

   ➞ Section 4: this section provides a framework for uncertainty analysis using long-running numerical simulations by relying on metamodeling techniques. An inter-seasonal heat storage system within the Dogger aquifer is used as a real application case.

3) How to predict and quantify uncertainties concerning reservoir properties?

   ➞ Section 5: this section explains the main challenges related to geological modelling and introduces the two different kinds of assessments that may be deployed: qualitative assessment vs. quantitative assessment.

   ➞ Section 6: this section explains how to capture the stochastic uncertainty related to inference of reservoir properties away from primary data (e.g. wells) and with correlated secondary data (e.g. seismic), using geostatistics and machine learning techniques.

2 An overview of methods to make a decision in uncertain situations: illustration on a fictive case study

2.1 Objective

The objective of the present section is to provide an overview on the different methods that are available to deal with uncertainties, to discuss how they may be helpful for decision-making, and to highlight their advantages and limitations. We tried to make explanations as clear and accessible as possible through a fictive case study based on an analytical model. The content presented in this section was prepared for an internal workshop (March 9th, 2021), with the idea of sharing knowledge and finding a real case study that could be further investigated.
Focusing on a simple illustrative case study, we will be able to demonstrate the different steps of uncertainty treatment (Figure 1):

- Identification of uncertainty and information gathering;
- Mathematical representation of uncertain parameters;
- Propagation of uncertainties;
- Sensitivity analysis: this step enables identifying the most influential parameters;
- Decision making;
- It may then be necessary to reduce epistemic uncertainty by new data acquisition and by re-starting the information-gathering step.

In the case study presented here, we will first present identification and information gathering, which is common to all frameworks. The exercise of representation, propagation, and use for decision-making will be presented first with a very basic tool called OAT (One-At-a-Time), then in the probabilistic framework and finally in extra-probabilistic framework i.e. a framework that combines different mathematical tools (like probabilities, intervals, fuzzy sets, etc.) for treating the different types of uncertainties.

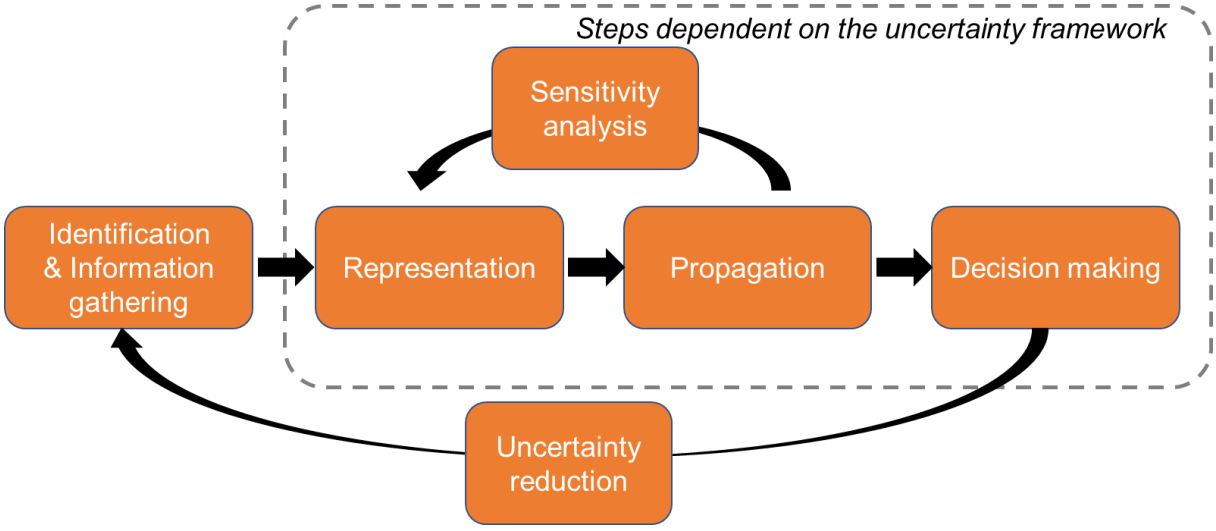

Figure 1: Dealing with uncertainty is a several-step process.

2.2 Illustrative case study

2.2.1 Decision making context

Dealing with uncertainty may be interesting *per se* in some situations. However, in most cases the interest of uncertainty treatment relies on its link with decision-making. It is therefore important to spend time to elaborate the decision-making context.
For the present fictive case study, we propose the following decision making context: a new project is in preparation to store high temperature water (~90°) in an aquifer for seasonal storage. We assume a reservoir

thickness around 21 m, an initial temperature around 20 °C, horizontal and vertical permeabilities respectively around 15 D and 1,5 D. We also assume that the same volume will be stored and produced, around 55 000 m^3/y and that there is no regional groundwater flow.
The decision-maker has to establish the go/no-go decision based on economic considerations and on preliminary assessment. We assume that according to the business plan, the storage efficiency needs to be over 50 % in order to reach economical profitability, after the transient regime.
The storage efficiency is defined as the ratio of energy that can be recovered compared to the energy injected. Assuming equal volumes of injection and production and neglecting variations of water volumetric heat capacity, the energy efficiency is assessed through:

$$Eff = \frac{T\_produced - T\_aquifer}{T\_injection - T\_aquifer}$$

With:

Eff: the recovery efficicency (%)
T_produded: the temperature of the water produced during the production phase (°C)
T_injection: the temperature of the water injected during the storage phase (°C)
T_aquifer: the temperature of the water in the aquifer (°C)

In context with high level of uncertainties, it is rare to circumvent sufficiently the level of uncertainties and to make a decision using a simple threshold, like 50 % in the present case. The threshold should be associated to a probability of non-exceedance. For the present case study, we propose the following: the threshold for decision-making is that the probability of getting an efficiency below 50 % should not overtake 5 %.

2.2.2 Model

We propose to use the analytical model proposed in Schout et al. (2014). The processes that control the energy efficiency include thermal conduction, dispersion, regional groundwater flow and density-driven flow. Taking into account all these processes requires complex numerical modelling, with significant computation time. Based on a number of numerical simulations using HstWin-2D (Figure 2), the authors established a correlation between the dimensionless Rayleigh number (a measure of the relative strength of free convection) and the calculated recovery efficiencies for seasonal storage. The analytical solution takes the following form to estimate the recovery efficiency of a 21 m-thick aquifer:

$$Eff = A\, e^{(B\, Ra^*)}$$

With:

$$A = A_1 - \frac{1{,}7}{H^{1,2}}$$

$$B = 2{,}2 \times 10^{-3} - \frac{B_1}{H^{1,35}}$$

$$Ra^* = 1634\, \frac{\rho\, H^{2.5} \sqrt{k_v k_h}\, \Delta T}{\mu \sqrt{V_i}}$$

Where :

Eff is the recovery efficiency (as afore-defined, %)
H is the aquifer thickness (m)
A_1 is a model parameter, equal to 0.82 in Sought et al. (2014)
B_1 is a model parameter, equal to 2.2x10^{-3} in Sought et al. (2014)
ΔT is the temperature difference between the injected and ambient groundwater (K)
μ is the dynamic viscosity of water (kg.m^{-1}.s^{-1})
ρ is the density of water (kg.m^{-3})
k_v is the vertical equivalent permeability (m²)
k_h is the horizontal equivalent permeability (m²)
Vi is the injected/produced volume (m³)
Ra* is the modified Rayleigh number (see Schout et al. 2014)

The density and the viscosity have to be assessed at the “average system temperature”, i.e. the mean of ambient groundwater temperature and injected water temperature.
It is assumed that the cold well has not a significant influence on the main well. In addition, the reservoir is assumed homogeneous, and confined by impermeable clay layers.

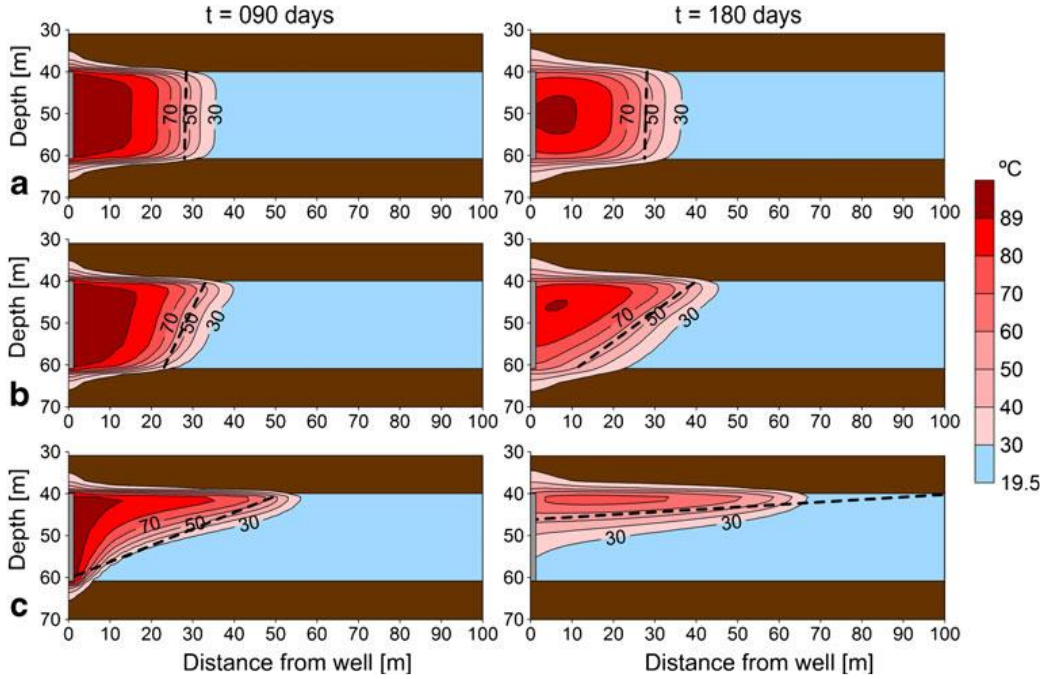

Figure 2: Contour plots of the calculated groundwater temperatures at the end of the injection period (t=90 days; left panel) and at the end of the storage period (t=180 days; right panel) for horizontal and vertical permeabilities respectively equal to: 25 D and 0.1 D (a); 15 D and 1.5 D (b); 50 D and 25 D (c) (source: Sought et al., 2014).

2.3 Identification of uncertain parameters and information gathering

The analytical model presented in section 2.2.2 requires information on seven parameters related to the reservoir and engineering. Two additional parameters were added to take into account uncertainties concerning the analytical model, which approximates results obtained through numerical model.

Once parameters are identified, it is necessary to gather information on these parameters. When dealing with underground objects, we are systematically confronted with a high level of uncertainties on parameters in the first phases of a project. It is useful to distinguish two facets of uncertainty:

- Random uncertainty, also called aleatory uncertainty or variability: these uncertainties correspond to “real” variability intrinsic to the physical system under study (e.g., temporal evolution of rainfall magnitude); as a consequence, it cannot be reduced.
- Knowledge-based uncertainty, also referred to as epistemic uncertainty. These uncertainties stem from limited knowledge, measurement capability and modelling capability on the part of the analyst. They can be reduced, and in the extreme case of perfect knowledge they could be equal to zero.

This distinction is important in the perspective of decision-making. For a decisional context such as the one proposed in this section, the decision maker has in fact three choices:

- Grant the project a go;
- Cancel the project;
- Inquire further investigation prior to making the decision.

With that in mind, the decision maker needs to be able to quantify the uncertainty that could be reduced through further investigations and the uncertainty which is by nature un-reducible.

The distinction is theoretically easy between variability and epistemic uncertainty. In practice, it may be tricky to classify uncertainties in both categories. We illustrate it here, considering the parameters and model of the present case study:

- For aquifer thickness: at the injection point, the true thickness is not variable; the uncertainty is thus purely epistemic. But if we consider the storage footprint, the thickness is not identical in any point, and variability may be meaningful. In the present model, we consider that the aquifer thickness is an equivalent aquifer thickness, and a fixed value is expected for the model. It can thus be considered that the nature of uncertainty for the equivalent aquifer thickness is epistemic. If we had a numerical model with more sophisticated capabilities, the aquifer thickness could be considered as simultaneously tainted by variability and epistemic uncertainty.
- The same reasoning is applicable for aquifer horizontal and vertical permeabilities.
- Concerning the temperature difference: i. the aquifer temperature (prior to storage) may vary spatially within the footprint of the storage and may also fluctuate temporally in the cold well; ii. the injection temperature at a given instant is a fixed value, but it may vary with time. The temperature difference is thus by nature variable, but once again if we consider that the input parameter should be an equivalent parameter (summarizing both spatial and time variability) for the simple model considered here, it may be considered that uncertainties can be summarized as epistemic-only.
- Concerning the volume injected/produced, once again it may fluctuate with time, but the equivalent average volume is only tainted with epistemic uncertainty.
- Viscosity and density are fixed for a given water composition, temperature, pressure. The uncertainty should thus be considered as mainly epistemic. With a more complex numerical model, the pressure, temperature and water composition may vary in the different cells of the mesh, and in this case it would be necessary to compute density and viscosity cell by cell. The uncertainty would remind mostly epistemic.
- Concerning the model regression parameters, they can be classified as model uncertainties and stem from the lack of knowledge we have on the model. They are thus purely epistemic. In the present case, we are confronted with a special case, since the analytical model is itself an approximation of a numerical model (a sort of metamodel). The uncertain parameters introduced here will convey the level of uncertainties that arises from the transition between numerical and analytical model. It should be kept in mind that model uncertainty related to the numerical model is not taken into account here.

For the sake of the illustrative case study, we retained values proposed in Shout et al. (2014) for the base case values: the aquifer thickness is 21 m, horizontal and vertical permeabilities are respectively 15 and 1.5 D, the temperature difference is 70 °C, the volume injected/produced is 55 000 m^3 (see Table 1, column “base case value”).
Concerning viscosity, Benno Drijvner informed that the following relation was used (personal communication, co-author of Schout et al. 2014):

$$\mu(T) = 10^{-3}(1 + 0.015512(T - 20))^{-1.572}$$

This yields:

$$\mu(T = 55°C) = 5.06 \times 10^{-4}\ kg.m^{-1}.s^{-1}$$

It should be noted that the viscosity also depends on the water composition. Considering the illustrative dimension of the case study, the assessment of viscosity was not further investigated.
Concerning density, we also used the relation provided by B. Drijvner, which yields 985 kg/m^3.

$$\rho(T) = 996.9(1 - 3.17 \times 10^{-4}(T - 25) - 2.56 \times 10^{-6}(T - 25)^2)$$

2.4 Information gathering

Once the case study and the parameters are well identified, it becomes necessary to gather information that will subsequently be used, whatever the framework considered for uncertainty treatment. When operated through workshops with expert, this phase often takes the form of expert elicitation. It may be a tricky step, especially when it relies on a workshop with a pool of experts who may emit contradictory opinions.
In order to make the illustrative case study interesting from uncertainty point of view, we made choices that may be debatable. Besides, the values retained are in part arbitrary. The information provided in Table 1 (column “information gathering”) should be considered as illustrative only.

Table 1: Uncertain parameters and representation in the different frameworks; PDF means Probability Distribution Function. The grey columns will be discussed in sections 2.5, 2.6 and 2.7.

Symbol	Unit	Description	Base case value	Information gathering (information indicated here can be considered as expressed by fictive experts).	Range of values for OAT	Representation in probabilistic framework	Representation in extra-probabilistic framework
H	m	Aquifer thickness	21	There is a close drilling where it is 21 m, but any value between 18 and 25 m could be possible .	[18 ;25]	Uniform PDF between 18 and 25	Triangular possibility distribution (18;21;25)
ΔT	°C	Temperature difference	90-20 =70	The aquifer temperature is very close to 20°C (±0.5°). The storage temperature target is 90° but we don't exclude values between 80 and 95°	[60 ;75]	Uniform PDF between 60 and 75	Triangular possibility distribution (60;70;75)
k_h	D	Horizontal permeability	15	We have numerous values in this aquifer. Normal law (15,2) fits very well with our data	[10 ;20]	Normal PDF (15,2)	Normal PDF (15,2)
k_v	D	Vertical permeability	1.5	We have fewer measurements. We have different sets of values (values between 0.7 and 4), see Figure 3. We don't expect values above 4 or below 0.5.	[0.5 ;4]	Uniform PDF between 0.5 and 4	Imprecise probability : an envelope of PDF may be used (black curves in Figure 3).
V_i	m^3/y	Volume injected/produced	55 000	It may vary depending on heat source and heat demand at the surface. 55 000 is the target but we cannot exclude values between 45 000 and 65 000 m^3/y.	[45 000 ;65 000]	Uniform PDF between 45000 and 65000	Triangular possibility distribution (45 000; 55 000;65 000)
μ	kg/m.s	Viscosity	5.06 $x10^{-4}$	It would be necessary to further investigate the literature to verify how it varies with temperature, pressure and mineral content. In a first approach between $4.5x10^{-4}$ and $6x10^{-4}$ kg/m.s is a relevant range.	[$4.5x10^{-4}$; $6x10^{-4}$]	Uniform PDF between $4.5x10^{-4}$ and $6x10^{-4}$	Interval possibility distribution ($4.5x10^{-4}$; $6x10^{-4}$)
ρ	kg/m^3	Density	985	The density is comprised between 975 and 990 kg/m^3 based on the data we have.	[975 ;990]	Uniform PDF between 975 and 990	Interval possibility distribution (975;990)
A_1	/	Model regression parameter	0.82	Between 0.81 and 0.85 we capture quite all values – between 0.8 and 0.88 we capture absolutely all values. See Figure 4.	[0.8 ;0.88]	Uniform PDF between 0.8 and 0.88	Trapezoidal possibility distribution (0.80;0.81;0.85;0.88)
B_1	/	Model regression parameter	1.2	Between 1.2 and 1.5 we capture quite all values – between 1.1 and 2.2 for absolutely all values. See Figure 4.	[1.1 ;2.2]	Uniform PDF between 1.1 and 2.2	Trapezoidal possibility distribution (1.1;1.2;1.5;2.2)

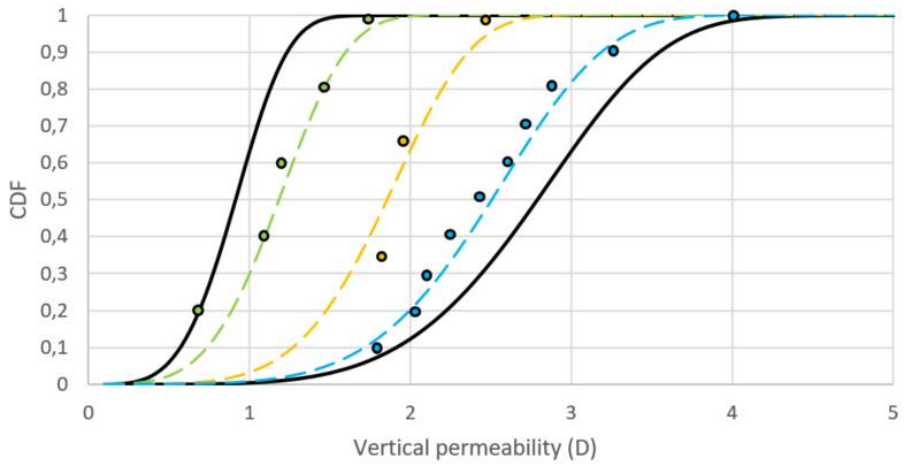

Figure 3: Cumulative Distribution Function denoted CDF for the vertical permeability. We assume that we have 3 sets of values at different locations (respectively 5, 3 and 10 measures): each set of data may be approximated by a probability distribution function (green, yellow, blue lines). The lowest value is 0.7 and the highest value is 4 D. The black curves correspond to the probability box used in the extra-probabilistic framework (see section 2.7).

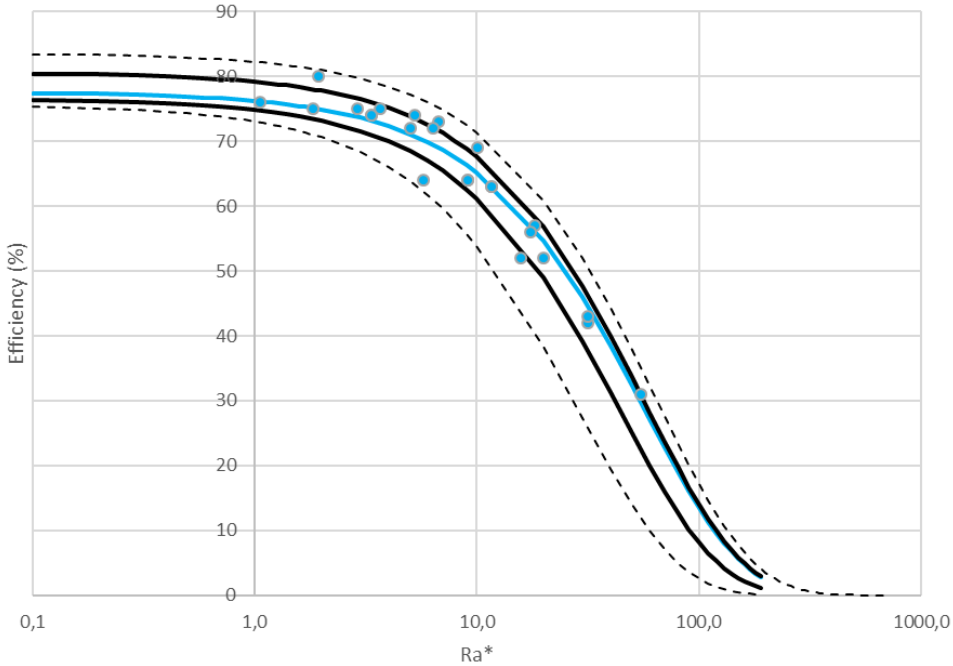

Figure 4: Approximation of numerical results by an analytical equation to compute the storage efficiency (%) depending on the modified Rayleigh number (plot elaborated from results presented in Schout et al. 2014). The blue points correspond to the results of numerical modelling. The blue line corresponds to approximation by an analytical equation, with best estimates for A_1 and B_1, respectively 0.82 and 1.2. The dark full lines correspond to a first envelope that enables to capture most points, with A_1 and B_1 respectively equal to 0.81/0.85 and 1.2/1.5 for left/right curves. The dark dotted lines correspond to an envelope that enables to capture all points, with A_1 and B_1 respectively equal to 0.8/0.88 and 1.1/2.2 for left/right curves.

2.5 Getting a first idea with OAT (One-At-a-Time) approach

2.5.1 Presentation

A very simple method, which is often used in order to give an idea of the influence of input uncertainties on results is the OAT approach ("tornado diagram"). Its implementation is accessible to non-specialists. Starting from the base case, it consists in varying one parameter only to its extreme minimal value, and then to its extreme maximal value, in order to estimate the range of variation on the output. Let's take an example: with the present model and base case values identified in Table 1, the computed efficiency is 66 %. In the decision-making context, we chose a decision threshold of 50 % for efficiency in order to make a positive decision. The idea of OAT is to give insight into orders of magnitude of influence of one parameter on results: for example, the aquifer thickness varies between 18 and 25 m, which leads to efficiency variation between 65 and 67 %. This method conveys a first intuition to identify the most influential parameters and to estimate the level of influence.

2.5.2 Representation and propagation

For the representation of uncertainties, we need to identify the plausible ranges of variations for the different uncertain parameters. This exercise was carried out for the present case study based on information gathered in previous step (see Table 1, column "range of values for OAT").
The propagation is very simple for such a monotonous model: two computations are performed for each uncertain parameter, one for the lowest plausible value, and one for the highest plausible value. In total, this represents: 1 simulation for the base case and 2x9=18 supplementary computations, i.e. 19 computations. This method is thus very economical in terms of computation time. It should be noted that for a model with non-monotonous behavior, or with non-established monotony, it would be necessary to use more sophisticated mathematical tools to identify the output minimal and maximal values.
Results are presented in Figure 5: from this analysis, the most influential parameter is the model regression parameter B_1: when it increases to 2.2, the efficiency drops to 57 %. The density appears as low-influential in the range considered.

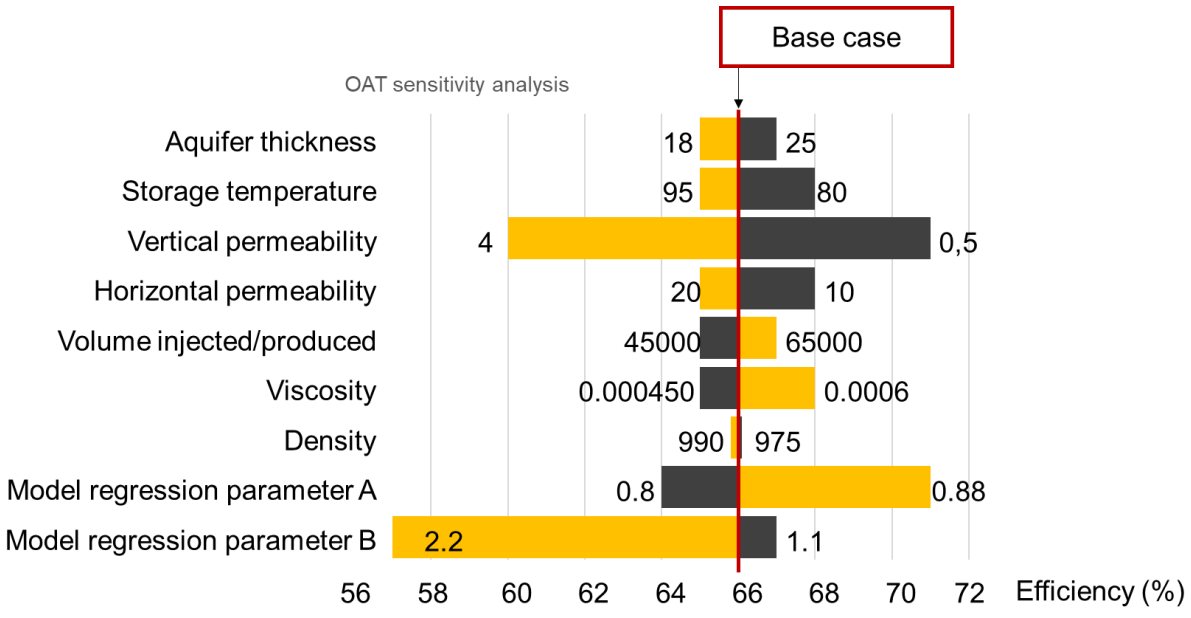

Figure 5: Illustration of OAT sensitivity analysis results for the fictive case study.

2.5.3 Towards decision

The counterpart of simplicity is that the range of exploration of inputs is very limited; thus the results should be considered very cautiously for decision-making. In the present case, it should not be concluded that the efficiency never drops below 50 %. If several parameters are simultaneously degraded, the efficiency is likely to decrease. When the decision-making deals with a risk, the OAT is not appropriate at all, because it is non-conservative: the range of variation of the output is artificially tightened by the method.
Even if this approach is not appropriate for decision-making, it enables to elaborate simply and at low computation cost a first sensitivity analysis to get a first idea of most influential parameters.

2.6 Probabilistic framework

2.6.1 Presentation

In order to avoid the limitations presented in the previous section, it is necessary to explore the whole range of parameters, which can be done in the probabilistic framework. It consists in representing the different uncertainties by probabilistic distribution functions (PDF); then sets of values are drawn aleatory for the different parameters, and a model simulation is carried out for each set. When the number of simulations increases, the (Cumulative Distribution Function) CDF of the output settles. This classical approach is often called Monte Carlo sampling.

2.6.2 Representation

In the absence of further information, we represent uncertain parameters by uniform PDF between the minimal and maximal values identified. The choices made for the present case study are identified in Table 1, column “Representation in probabilistic framework” and illustrated in Figure 6. All parameters are represented by uniform CDFs, except the horizontal permeability for which it was assumed that a normal PDF was appropriate. For some parameters, a range of value was elicited, and a more probable value within this range was suggested. Another option could be to represent these parameters by a triangular PDF. This choice was not made here in order to have a conservative representation of extreme values.

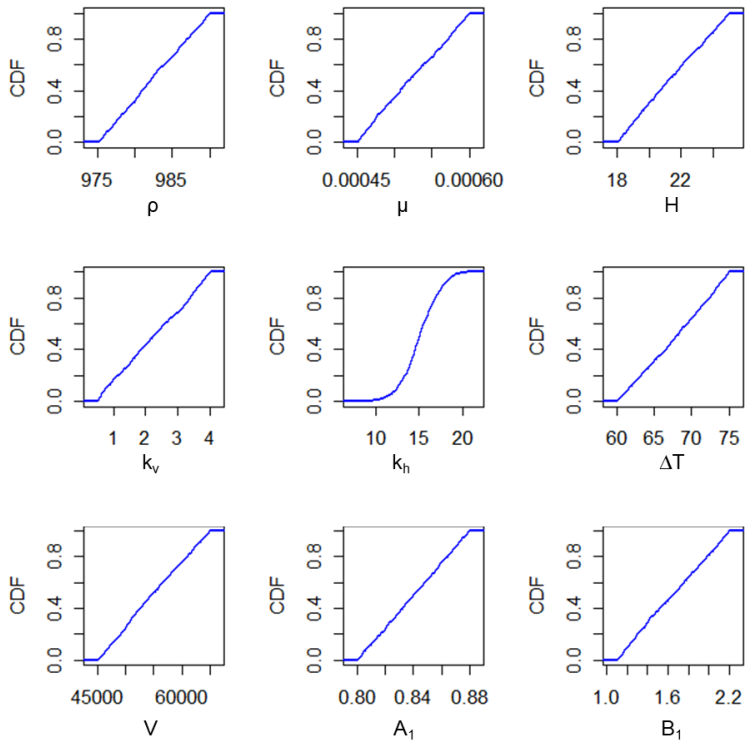

Figure 6: Representation of uncertain parameters in the probabilistic framework.

2.6.3 Propagation

As afore-mentioned, the propagation consisted in drawing randomly 1000 sets of inputs' values (independently for all parameters), and in computing the 1000 corresponding values of efficiency . The CDF presented in Figure 7 summarizes the results. Within the range of parameters investigated, the efficiency varies between 45 and 75 %.

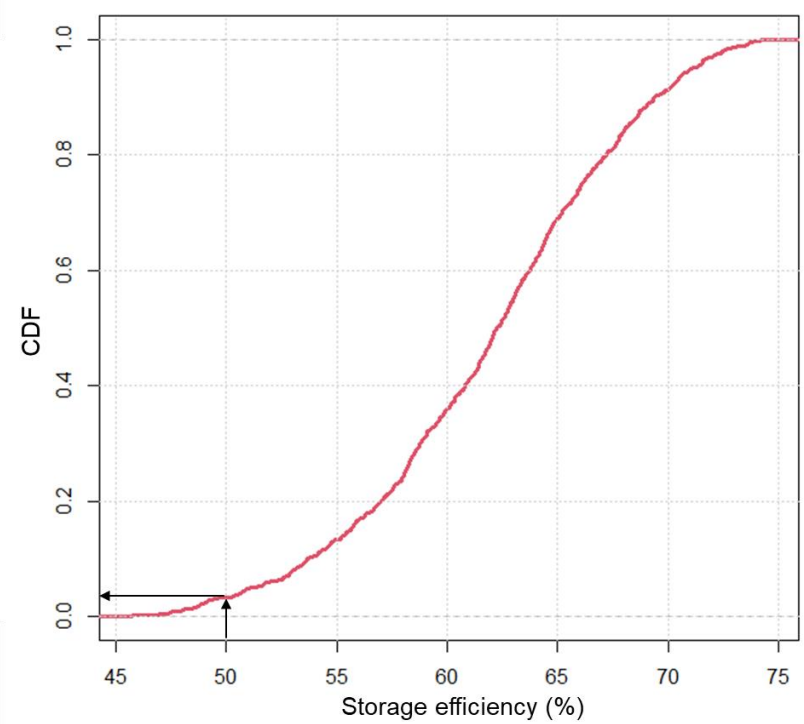

Figure 7: CDF obtained for the storage efficiency in the probabilistic framework. The probability of having a storage efficiency below 50 % is 4 % (as indicated by black arrows).

2.6.4 Towards decision

According to results presented in Figure 7, the probability to have insufficient efficiency (below 50 %) is 4 %. The decision threshold was identified as 5 %, so it could be concluded that the level of uncertainties is acceptable to launch the project.
Since conservative assumptions were made, and since the result is favourable, further investigations in the form of sensitivity analysis on parameters are not indispensable. Where appropriate, it could be possible to carry out sensitivity analysis in the probabilistic framework with variance-based global sensitivity analysis (Saltelli et al., 2008). For the interested reader, this tool is presented and illustrated in section 4.

2.6.5 Advantages and limitations

This framework remains quite simple in its application, but the number of simulations to settle the CDF for the output is relatively important (1000 simulations here). This method enables exploring the whole range of parameters, but the use of probabilities for mathematically representing the uncertainties imposes to add information about the likelihood within the variation range of each input variable; for instance, making the assumption of a uniform PDF implies that each value within the given interval has the same probability weight. This information may not be justified in our case due to lack of knowledge, and thus it introduces new information, which may at the end convey the impression that the situation is better known than in reality.

2.7 Extra-probabilistic framework

2.7.1 Presentation

In order to overpass some limitations of the probabilistic framework, an extra-probabilistic (also called “hybrid” or “possibilistic”) framework was established. It relies on new mathematical tools for parameters that cannot be represented by probabilistic distribution without introduction of additional information. An overview of alternative mathematical representation tools is available in Dubois and Guyonnet (2011): probability boxes, possibility distributions, Dempster-Shafer structures, etc. In the present report, the mathematical concepts are not exposed in details. The presentation is oriented for potential users.

For parameters that can be characterized by an interval of values (eventually with a more plausible value or with a more plausible interval within), a possibility distribution is used instead of a probability distribution. It is a flexible mathematical representation tool that enables accounting for all data and pieces of information, but without introducing unwarranted assumptions (e.g. Baudrit et al; 2007, Beer et al. 2013). The simplest situation corresponds to an imprecise parameter, i.e. a parameter whose value is ill-known. The simplest tool to represent this imprecision is the interval, which is defined by a lower and an upper bound. Yet, the expert may provide in some cases more information by expressing preferences. An illustration is given in Figure 8: the expert is sure that the distribution is comprised between 0 and 5, and considers 2 as a more plausible value. Using both pieces of information, the imprecision can be represented by a triangular possibility distribution. The interval [0 ; 5] is the support of the distribution, i.e. the interval with the highest level of confidence (the expert is sure that the value is not outside). Inside this interval, he is able to indicate other imbricated intervals that are more precise, but for which he is less confident (as illustrated in Figure 8).

Imprecise probability distribution may also be used within this extra-probabilistic framework. A parameter was voluntarily characterized in this sense for the sake of illustration here: for the vertical permeability, we assumed that it was clear for experts that it followed a CDF, but that best estimates of the law were poorly known. As illustrated in Figure 3, the most appropriate approach for this parameter is to encompass the possible CDF in an envelope of lower and upper possible CDF.

Based on these extra-probabilistic representation tool, it is possible to propagate uncertainties in models without introducing new assumptions. Instead of drawing random values for the parameters, we draw imprecise range of values that correspond to different confidence level. As an output, we obtain a set of output intervals that can be sorted for producing an envelope of CDF (we remind that the probabilistic framework leads to a set of output values resulting in a single CDF); this envelope translates the true level of uncertainty that was elicited from experts.

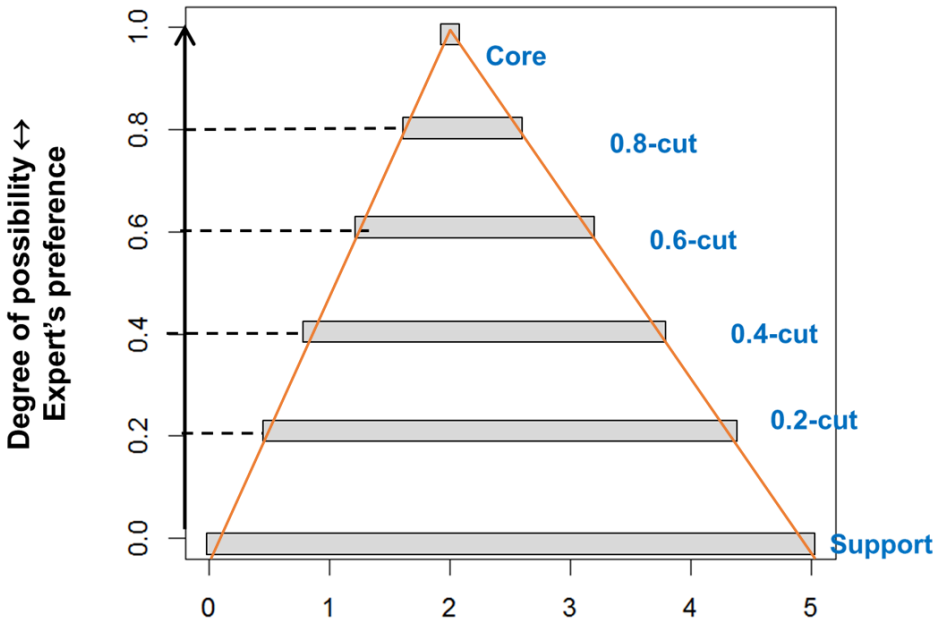

Figure 8: Illustration of the mathematical representation tool used for possibilistic representation of uncertainties.

The work presented here is performed using an R package, HYRISK, dedicated to jointly handling different mathematical representation tools, namely probabilities, possibility distributions and probability functions with imprecise parameters, for the different stages of uncertainty treatment (i.e. uncertainty representation, propagation, sensitivity analysis and decision-making) (Rohmer et al. 2018).

2.7.2 Representation

The representation of the different parameters in the extra-probabilistic framework is summarized in Table 1, column “representation in the extra-probabilistic framework”. Figure 9 illustrates the mathematical tool used for the representation of each parameter. For the horizontal permeability, a known PDF could be assumed, and it is thus represented in the probabilistic framework (in this sense, this kind of approach can be considered as hybrid, since the different mathematical tools may co-exist). The vertical permeability is represented by imprecise probabilities. Other parameters are represented by possibility distribution functions, either intervals, triangular distributions or trapezoidal distributions.

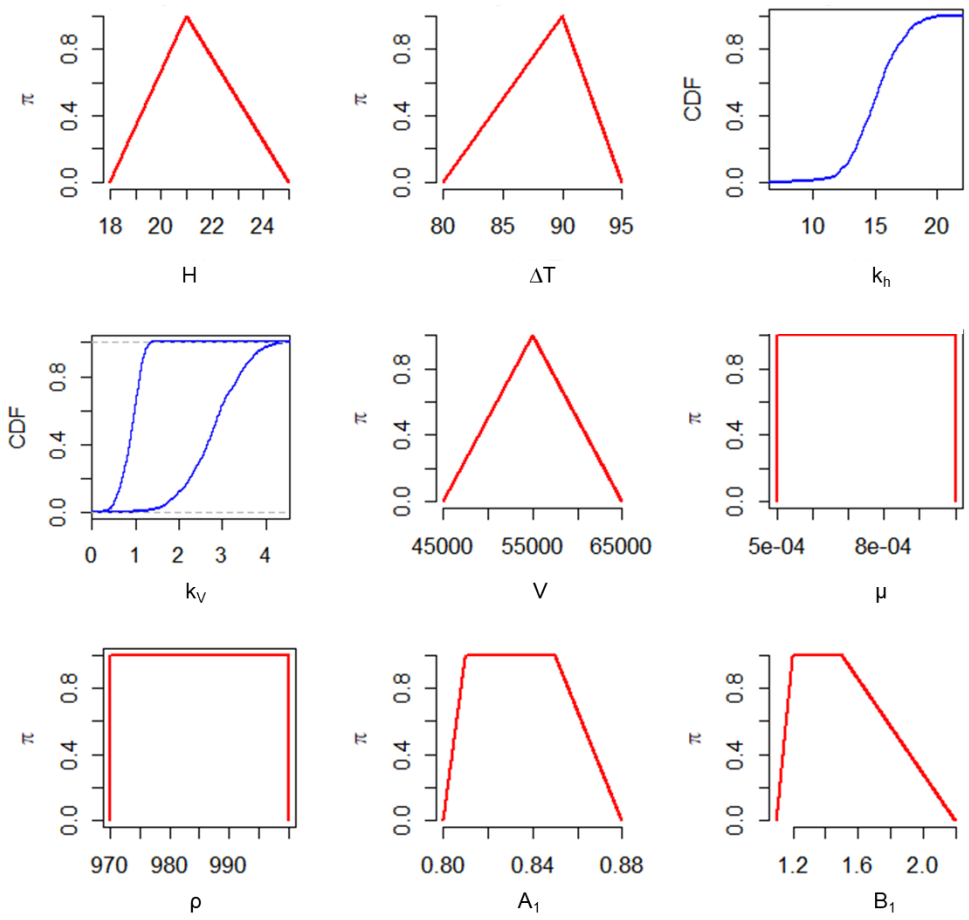

Figure 9: Representation of uncertain parameters in the extra-probabilistic framework.

2.7.3 Propagation

The propagation was performed with the Hyrisk package (code R), which implements the Monte-Carlo-based algorithm of Baudrit et al. (2007) for jointly handling possibility and probability distributions and the algorithm of Baudrit et al. (2008) for jointly handling possibility, probability distributions and p-boxes. We used 1000 random draws. For each draw, we obtain for each parameter either a precise value or an interval. It is then necessary to identify the minimal and maximal corresponding efficiency. If all parameters have monotonous behavior, the number of necessary simulations is 2000, but if one or several parameters present non-monotonous or non-established behavior, it is necessary to use an optimization method (here quasi-Newton method with multi-start), and the number of simulations may get quickly higher.

The envelope of CDF presented in Figure 10 summarizes the results: the probability of having a storage efficiency below 50 % is comprised between 0 % and 63 %. The following section will present how one may make use of these results within a decision making process.

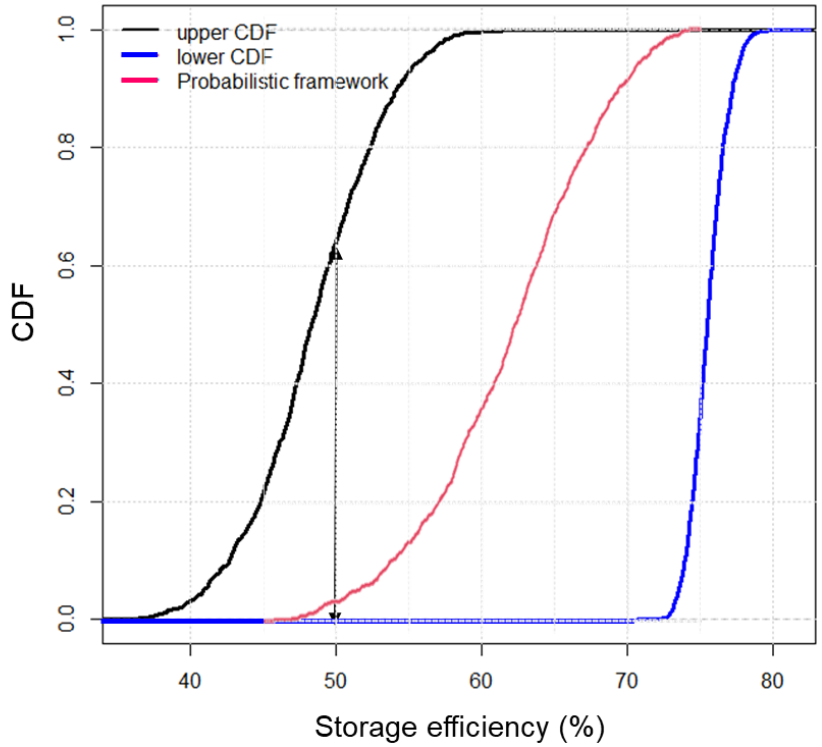

Figure 10: Envelope of CDF obtained for the storage efficiency in the extra-probabilistic framework. The probability of having a storage efficiency below 50 % is comprised between 0 % and 63 % (as indicated by black arrow). The red curve is just a reminder of the result obtained in the probabilistic framework for sake of comparison.

2.7.4 Towards decision

An important question is now: how to use such a result for decision-making? In order to make a positive decision, we expected that the probability to have a storage efficiency below 50 % would be inferior to 5 %. Considering the high level of uncertainty without additional assumptions, it appears that the only thing that can be asserted at this stage is that this probability is comprised between 0 and 63 %. This is very low-informative, and the decision maker may be confused by this sophisticated framework and by the very fuzzy results. These results need to be largely explained, so that the decision maker becomes aware that these latter results reflect better the real level of uncertainty than the results produced with the probabilistic framework, since the number of additional assumptions is very limited.

In order to help the decision maker confronted with such a difficult decision, the following tasks may be pursued:

- Identification of most influential parameters in the extra-probabilistic framework (see section 2.8).
- Once influential parameters are identified, it is worth coming back to the information gathering step, or even to the expert elicitation exercise in order to check the assumptions that were made, and to verify if any other data could be available in order to enrich the analysis.
- If the uncertainty cannot be reduced using existing information an option could be to acquire new data. The cost of such data acquisition should be balanced with regard to the stakes of the decision. This exercise may benefit from Value of Information (VOI) approach.

In case the decision maker needs to take the decision without additional information, the upper and lower curves presented above can be summarized in a single one, with integration of an additional parameter which is linked to the decision maker risk aversion (i.e. attitude of the decision-maker to risk). That amounts to considering a single CDF as for the probabilistic framework, but in this case, there is an intermediary step, where a CDF envelope is produced, that enables raising awareness on the context of high uncertainty.

2.8 Sensitivity analysis

In the present case, the level of uncertainty is very high, which can be seen by the CDF envelope width and area. In order to reduce the level of uncertainty, a first step is to identify the most influential parameters. In order to perform sensitivity analysis in the extra-probabilistic framework, we used the method of Ferson and Tucker (2006). It consists in pinching the value of a parameter at a given value (for instance the base case value), and we restart the exercise. In order to illustrate how it works, we selected the parameter B_1: instead of representing it by a trapezoidal possibility distribution, for the sensitivity analysis it is assumed that its value is known; all other parameters remain represented as previously. Instead of obtaining the black and blue CDF for the envelope of the storage efficiency (see Figure 11), we obtain the grey and orange curves. The area between curves is 35 % lower than previously. This quantifies to what extent the output is sensitive to the parameter B_1. If we had obtained the same curves, it could be concluded that the parameter investigated has very low influence. On the contrary, if the curves are deeply tightened when pinching the parameter, it means that it is very influential. If we have a look at the 50 % threshold here, we can see that if we were able to characterize sufficiently B_1 to consider a value of 1.2 for sure, we would be able to say that the probability to have a storage efficiency below 50 % is insignificant.
The analysis is not presented for all parameters here, but the results show that model parameters A_1 and B_1 have an important influence on results. In a first approach, these parameters were characterized in a very conservative way. In order to help the decision-maker, we could advice to re-consider these model parameters and to better characterize the level of uncertainty. Maybe a more important set of numerical simulations could be performed in order to elaborate a refined metamodel. Even with the present set of simulation, the model regression parameters could be characterized more rigorously, for instance taking into account the interdependence between both parameters A_1 and B_1.

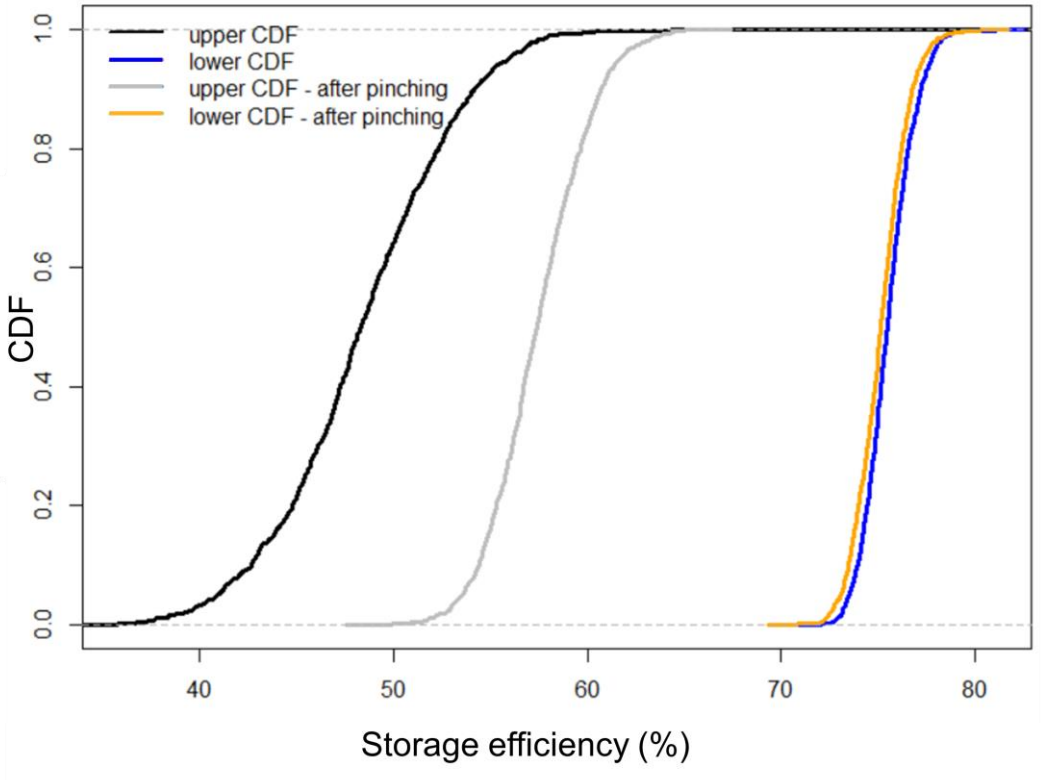

Figure 11: Sensitivity analysis in the extra-probabilistic framework for the parameter B_1.

2.9 Advantages and limitations

This framework is more sophisticated and requires an important number of simulations, especially if the monotony of the model cannot be established. Moreover, the decision-maker may feel confused by the form of the result and by the conveyed information and should be guided to interpret and use results. Despite these limitations, it is a very interesting framework since it provides flexibility for representing the different types of uncertainties depending on the data/knowledge that are at disposal while minimizing the impact of the mathematical representation's assumptions (contrary to the fully probabilistic framework).

2.10 Conclusion

We summarize the main features in Table 2.
We indicate in this table to what extent each framework can be considered as reliable in terms of uncertainty quantification. We remind that, independently of the uncertainty framework considered, the reliability of the results depend on the choice of the model and on the data used. For instance, for the present case study, in case there is an influential groundwater flow or an influence of the cut-off temperature, since the model does not take it into account, the results can obviously not reflect the related influence and uncertainties, whatever the choice of the uncertainty framework. The same is valid if inappropriate data is used. The quality of the uncertainty framework deployed is not a guarantee of reliability, and in some situations, it may be a priority to improve the model and the acquisition of data before spending time on uncertainty framework. However, once we have a relevant model and appropriate data and expertise to discuss parameters, it becomes worth investing in a convenient framework to tackle uncertainties, on adequacy with the means and the model complexity. It should be kept in mind that using a sophisticated extra-probabilistic framework with a complex numerical model remains today a challenge, but a panel of solutions may be further investigated for such cases. This point will be further discussed on the Bern case study (section 0).

Table 2: Dealing with uncertainty, summary of tools afore-presented.

	Computational cost	Characteristics
OAT	Very simple	Simple sensitivity analysis tool Not appropriate for decision-making, only very limited and non-conservative sets of values are investigated
Probabilistic framework	Moderate to high	The entire range of values is investigated. Additional assumptions are made at the representation step. The results can be used for decision-making, but should be considered cautiously, since they underestimate the uncertainty. It is possible to perform sensitivity analysis.
Extra-probabilistic framework	High	The entire range of values is investigated. The number of additional assumptions is very limited. The results can be used for decision-making and gives a good idea of the “true” level of uncertainty with the possibility to distinguish the different origins of uncertainties (randomness, epistemic). The decision-maker may feel confused by the form of the result and should be guided to interpret and use results. It is possible to perform sensitivity analysis.

3 Dealing with uncertainty for the Bern case study: towards a comprehensive analysis

3.1 Introduction

The work in section 0 was presented at a HEATSTORE internal workshop in order to initiate collaboration on a real case study with project partners. Geo-Energie proposed the Bern demo site as a possible case study.
The pilot project in Bern aims to store waste heat from the nearby power generation site Bern-Forsthaus. The power generation site is operated by the local utility company Energie Wasser Bern (EWB) and contains a combined-cycle plant, waste-to-energy plant and wood-fired power station for electricity and heat production. The heat user is an existing district network, which presents an increasing heat demand and a planned expansion in the city of Bern. The project consists in storing waste heat during the low-demand season, and in delivering it during heating seasons, thus replacing the standard gas heat production.
For the pilot heat storage system, an exploration well, around 500 m deep will be drilled to reach the Lower Freshwater Molasse (USM for Untere SüsswasserMolasse). The goal of this project is to assess the feasibility of the ATES system and if the results are positive, to drill more wells to realize a fully functional heat storage system, which, in its final implementation is aimed to store lost heat at a storage temperature of 120°C maximum.

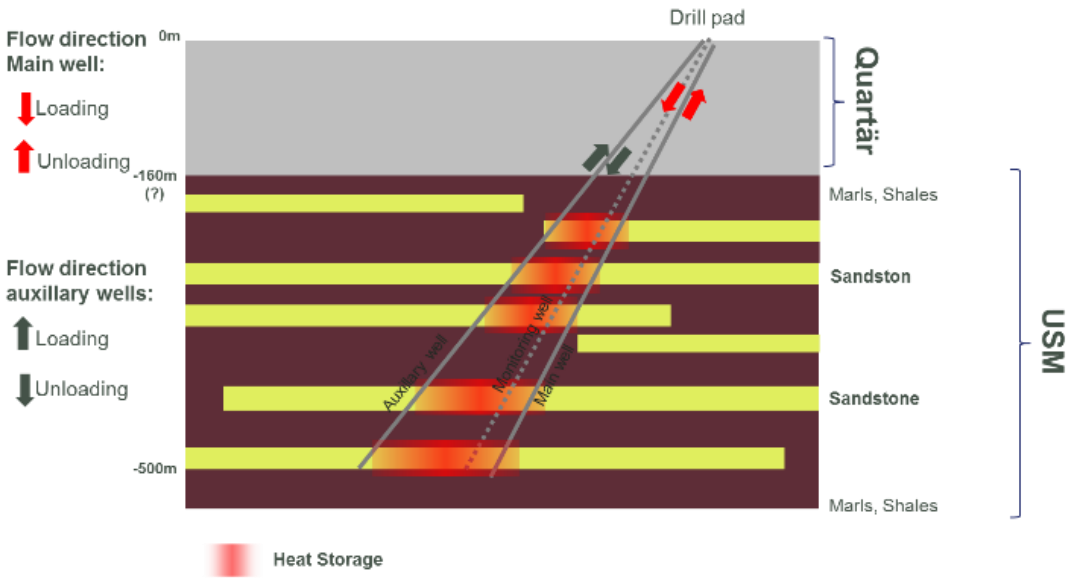

Figure 12: Illustration of the Bern case study.

The overall project is divided into different phases. The pre-drilling and the first well drilling are part of HEATSTORE project. When we initiated discussion with Geo-Energie, it was already decided to drill the first well, but the drilling had not begun. Geo-Energie did preliminary modelling in order to support the first decision concerning the go/no go for the first drilling. At this stage, the exploitation scenario was not fixed and data was very scarce. In this very uncertain context, Geo-Energie established a 2D radial numerical model, and simulated 3 scenarios (corresponding to 3 different storage temperatures), with expert estimations for the different parameters, based on the available data. The modelling results seem to foreshadow appropriate storage performance, and the drilling was validated. Uncertainties were not considered at this stage to make the decision.
After discussion, we decided to go back in time to elaborate a case study. We assumed that the choice of drilling the first well had not been made, and that we had to support this decision through a comprehensive analysis of uncertainties.

3.2 Preliminary work

3.2.1 Presentation of preliminary modelling

For the preliminary modelling, a 2D radial configuration was used, with a main central well. The base case values are indicated in Table 3. In order to represent auxiliary wells (where cold water is pumped during load phase and where water is reinjected after use during unload), a drainage boundary condition was used on the boundary.

Table 3: Preliminary modelling for the Bern case study.

Parameter	Description	Value
Rock properties		
ρ_r	Density of rock [kg/m³]	2535
C_r	Specific heat capacity of rock [J/kg/K]	750
λ_r	Thermal conductivity of rock [W/m/K]	2,67
Fluid properties		
ρ_f	Density of fluid [kg/m³]	985
C_f	Specific heat capacity of fluid [J/kg/K]	4180
λ_f	Thermal conductivity of rock [W/m/K]	0,6
Impermeable layers		
Φ_i	Porosity [%]	0,5
k_i	Pemeability [m^2]	$2{,}60\times10^{-17}$
Permeable layers		
Φ_p	Porosity [%]	10
k_p	Pemeability [m^2]	$3{,}45\times10^{-13}$
Fluid circulation		
Q	Total circulation rate [L/s]	25
$T_{inj,main}$	Injection temperature at main well (load phase) [°C]	90
$T_{inj,border}$	Injection temperature at "drainage" boundary (unload phase) [°C]	50
T_{thr}	Threshold temperature for unload cycle [°C]	55
Reservoir design		
R	Radius of radial symetric cylinder model [m]	300
r	Radius of the well [m]	0,25
$R_{drainage}$	Radius of the "drainage" boundary	60
H	Height of the cylinder model [m]	500
N_{mesh}	Number of mesh points	9200
Initial conditions		
T_0	Initial rock temperature [°C]	13
Time scheme load :unload cycle		
t_{load}	Load cycle [days]	217
t_{unload}	Unload cycle [days]	148
N_{cycles}	Number of cycles	20

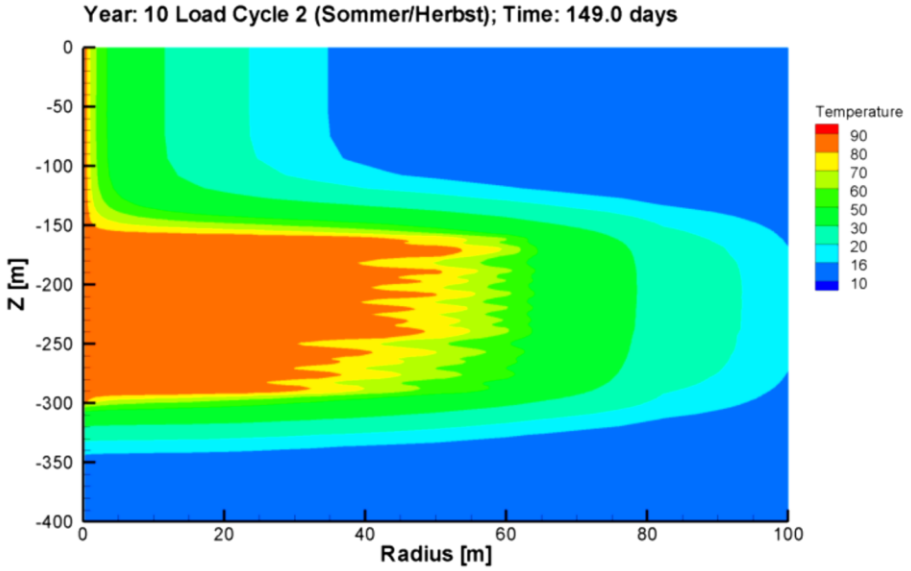

Figure 13: Results of preliminary modelling obtained by Geo-Energie. Temperature field after 10 cycles, at the end of the load cycle.

The modelling code SUTRA was used (Figure 13). The evolution of temperature and of flow rates was quantified in order to assess the recovery factor. It increases to 80 % after several cycles.

3.2.2 Context and model requirements

In first discussions, we indicated that for the sake of the uncertainty exercise, it would be recommended to have a model as simple as possible in order to be able to carry out the same kind of exercise as for the fictive case study. However, rapidly, we came to the conclusion that a simple model would be inappropriate to capture the complexity of the case study. From uncertainty viewpoint, it appeared interesting to confront with the reality of the case study, to highlight difficulties and imagine solutions instead of twisting facts to have a quite simple case study. The counterpart is that we could not follow through within the HEATSTORE project time and budget constraints.

In order to carry out a comprehensive uncertainty analysis for the Bern case study, we would need a significant number of simulations. It has not been possible to launch such a high number of simulations in parallel with SUTRA, and therefore, it has been decided to build the same model with COMPASS (code developed at BRGM), which offers the possibility to increase the number of simulations. COMPASS is a parallel numerical code to simulate gas liquid compositional thermal flow in high energy geothermal reservoirs or energy storages. Considering the model, a 2D radial model may be used, but in order to reproduce the storage process as faithfully as possible, a 3D model is more appropriate (Figure 14) as it allows accounting for a groundwater flow and finite strip-shaped layers.

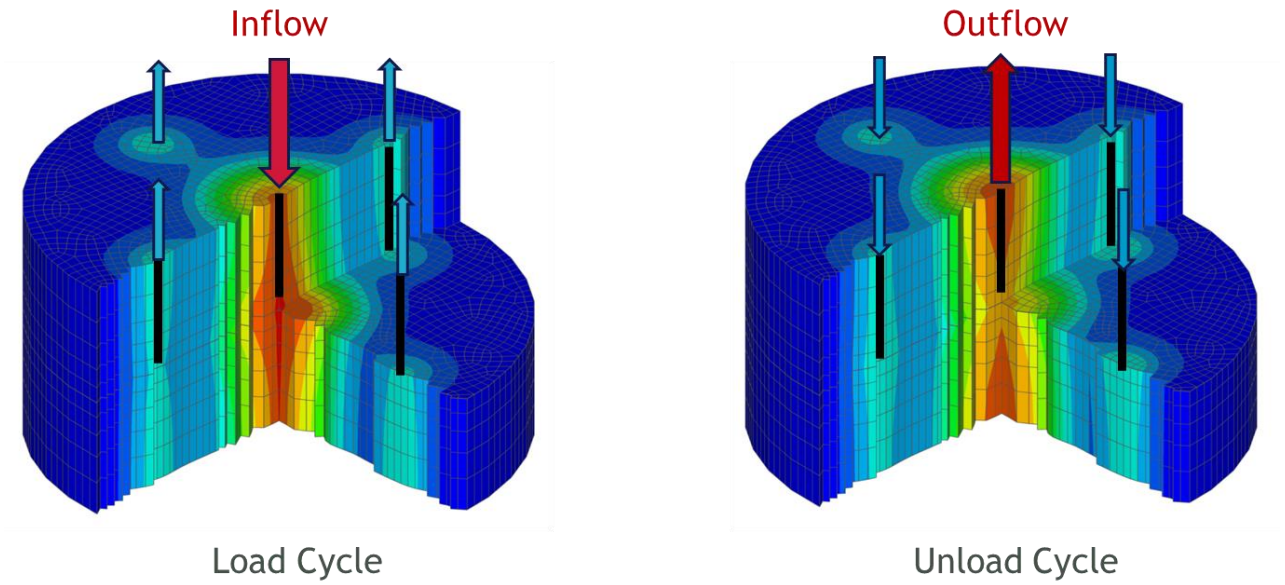

Figure 14: Choice of configuration for modelling the Bern case study (Author: Geo-Energie).

3.2.3 Frame of the decision making process

As mentioned, we decided to go back in time and to assume that the first decision concerning the go/no go for the first drilling had not been made. Data is very scarce concerning underground at the project location. However, we assumed that the ideal exploitation scenario had already been optimized by engineers, considering upstream and downstream constraints:

- The targeted configuration is one main well and 4 auxiliary wells (injection in the main well during load phase and production during the unload phase);
- During the storage phase (load phase), the injection pressure will be 3 MPa in the main well. The extraction rate in auxiliary wells will be adjusted to have a similar mass flow rate, by checking that the pressure drop remains inferior to 1.2 MPa;
- During the production phase (unload phase), the injection pressure will be 3 MPa in auxiliary wells. The extraction rate in the main well will be adjusted to have a similar mass flow rate, by checking that the pressure drop remains inferior to 1.2 MPa;
- The phases durations are considered as fixed: 217 days for load, 148 days for unload.
- The injection temperature during the load phase is 90 °C. The re-injection temperature is 50 °C. The threshold temperature during production is 55 °C (if the temperature drops to 55 °C, then the production is interrupted until next cycle).
- The distance between main well and auxiliary wells is assumed to be 45 m.

In practice, these different values are not definitively fixed. However, from our discussion, it appeared that optimization of engineering parameters is an exercise which is different from dealing with uncertainties. It could be interesting to investigate the robustness of storage performance for different chosen exploitation scenarios, taking into account the underground uncertainties, but considering the complexity of the case study, we preferred decorrelating both subjects.
Assuming this exploitation scenario, we discussed the decision criteria. The objective of the project is to reach economic performance, without neglecting environmental and societal issues. Underground numerical simulations provide information that is limited to technical points and marginally to environmental aspects. Not all decisional criteria can thus be addressed through numerical modelling. We identified the following criteria and associated indicators:

- Criterion 1: recover high part of energy stored, measured by Indicator 1 “Recovery efficiency: number of kWh recovered/number of kWh injected [%]”;
- Criterion 2: store high volume of energy, measured by “number of kWh recovered during one cycle [kWh]”

The following criteria were also discussed, but we decided to leave them out for the following reasons:

- Enable a rapid contribution of the storage, which could be measured by the duration of the transitory regime. It was left out because the most important point is the performance on long term, according to Geo-Energie;
- Limit the environmental footprint of the storage, for instance in a perspective of conflictual interest for underground uses. It could be measured for instance by the maximal distance where the temperature or pressure is modified more than 10 % compared to its initial value. It was left out because there are currently no other existing or planned uses for the targeted reservoir at this location;
- Limit the risk of induced seismicity: this criterion is indirectly considered in the exploitation scenario modelling choices. There are 2 options for implementation of injection in models: either the injection is controlled by an injection flow rate (and the resulting injection pressure can be measured) or the injection is controlled by an injection pressure (and the resulting flow rate is measured). The latter choice was made, which guarantees a moderate pressure at the injection well. This condition is not a sufficient condition to assess the risk of induced seismicity, but in a first approach it may be an interesting parameter to enlighten the situation.

Concerning the retained criteria, it is necessary to choose how they will be measured in simulations: average value over N cycles, value over 1 cycle after transitory regime, etc. As afore-mentioned, the intention is to focus on permanent regime for decision making in the present case. We decided to perform a number of preliminary simulations in order to better characterize the duration of transitory regime for the base case but also for more extreme cases, and to choose the number of iterations that guarantees the achievement of stable values for both indicators (denoted cycle number X in the following). From this analysis, it will appear that focusing on the cycle number X would give a good estimate by optimizing the computation time. Preliminary modelling is presented in next section for assessment of X.

In the decision making analysis, we have 2 options:

- Either both criteria are analysed independently, thus leading to observation of two output curves;
- Or both criteria are agglomerated in a single decision variable. The aggregation method could be the following: first perform a set of simulations, to obtain range of values for both outputs; then establish scoring scales with decision makers (not necessarily linear) to translate each indicator value in a score. Both scores could then be averaged.

In the present case, considering the limited number of indicators, it may be easier in a first approach to analyse outputs independently, and to compare the values with tangible and direct thresholds values. However, it induces a limitation in the analysis: it will not be possible to discriminate if simulations presenting bad score on one output are correlated (or inversely correlated) with the simulations presenting bad scores on the other output. For this reason, we recommend the use of the second approach. Once the first set of simulations will be performed, it will be necessary to elaborate the scoring scales with experts and decision makers, and to discuss the scoring thresholds for decision-making.

As a conclusion, the summary of this step is the following:
The decision-making associated with numerical modelling will consider the two following:

- Indicator 1: “Recovery efficiency: number of kWh recovered/number of kWh injected [%]” at cycle N°X
- Indicator 2: “Number of kWh recovered during one cycle [kWh]” at cycle N°X

Scoring scales will be established to translate values in scores. Both scores will be averaged for decision making. Decision thresholds will be refined through a workshop that will gather decision makers and experts.

3.3 Elaboration of a preliminary numerical model and parameter identification

As afore-mentioned, we decided to elaborate a three dimensional model with COMPASS. Prior to uncertainty treatment, it is necessary to grasp the possibility and complexity of modelling. Preliminary simulations are launched with the following objectives:

1. Check the feasibility of the three-dimensional model and the refinement possibility in terms of mesh to have a reasonable computing time.
2. Implement the specificity of the model: in the present case, it is necessary to implement injection pressure and balance with flow rates in production wells, and to check the pressure drop in production wells.
3. Choose the number of iterations that guarantees stable values for both indicators.
4. Make some modelling choices, such as the lateral and vertical dimensions of the model.
5. Assess the computation time in order to estimate the number of possible simulations that will conditions the uncertainty treatment approach.
6. Identify all input parameters.
7. Perform preliminary modelling in order to reduce the high number of parameters and quantify the influence of modelling choices.

A first model was established with base case values presented in Table 3 (Figure 15). For this model, we chose 2500 m for the lateral extent of the model and 500 m for vertical height. A first mesh with one cell per layer was considered. If we analyse the pressure and temperature fields, the dimensions appear to be appropriate, the lateral boundary conditions are far enough from the wells (as shown in Figure 15). The appropriateness of these dimensions needs to be confirmed on more extreme cases once the ranges of values for the different parameters will be established.

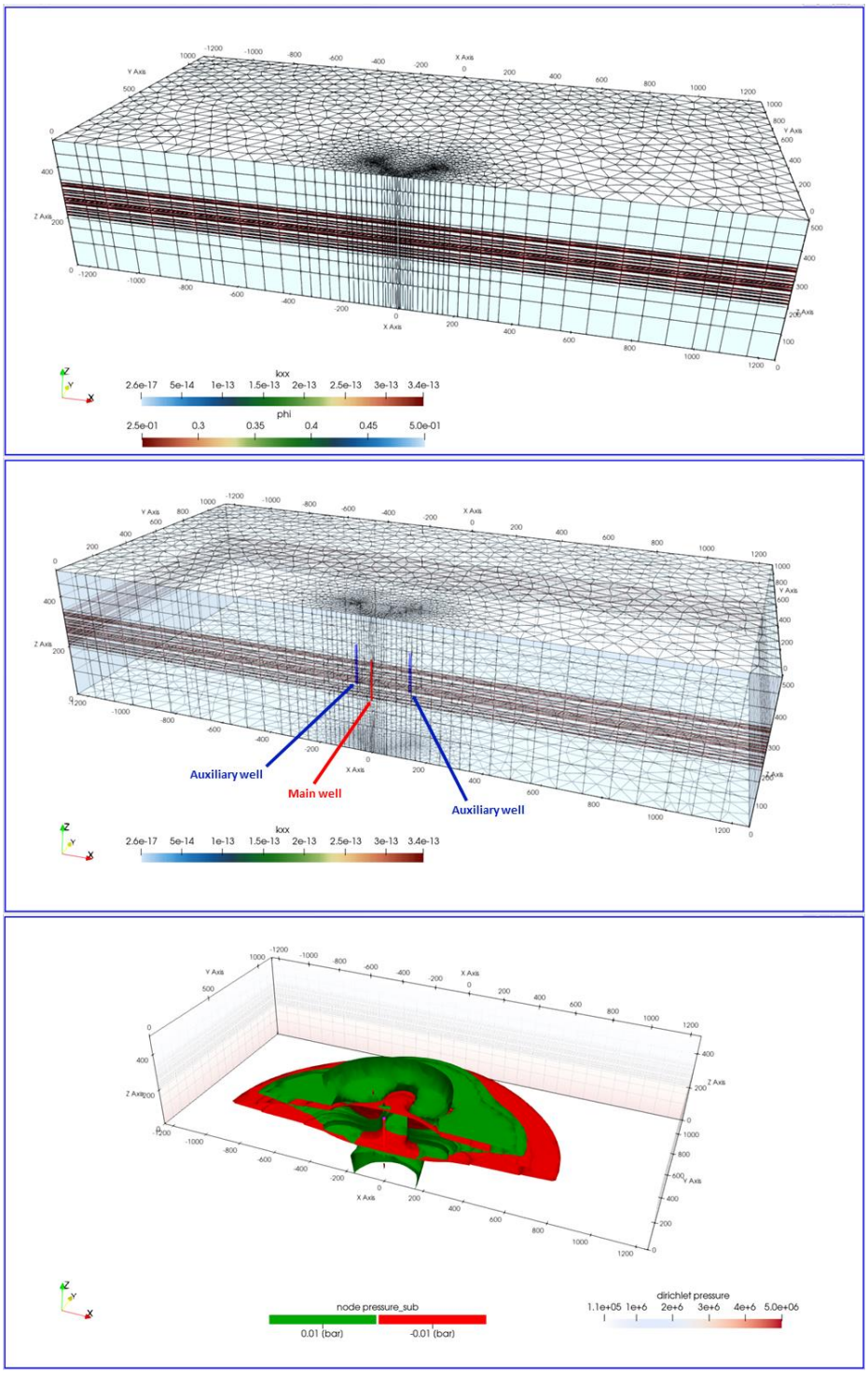

Figure 15: Illustration of the preliminary modelling. Top: Illustration of the mesh for the base case. Middle: Location of main well and auxiliary wells. Bottom: Illustration of pressure fields.

We deployed the same approach in order to estimate the duration of the transient regime, in a first time for the base case model. The evolution of temperatures (at the main well and one of the auxiliary well) cycle by cycle is presented in Figure 16. We see that the temperatures start to stabilize at the end of the simulation (after around 9 cycles). Once again, it will be necessary to check this behavior on other sets of inputs values in order to choose a conservative value. For this simulation (over a hundred cells), for 11 cycles, the computation time was around 6 hours (using 6 cores). Analysing indicators at cycle 10 may be a good compromise between stability and limited computation cost.

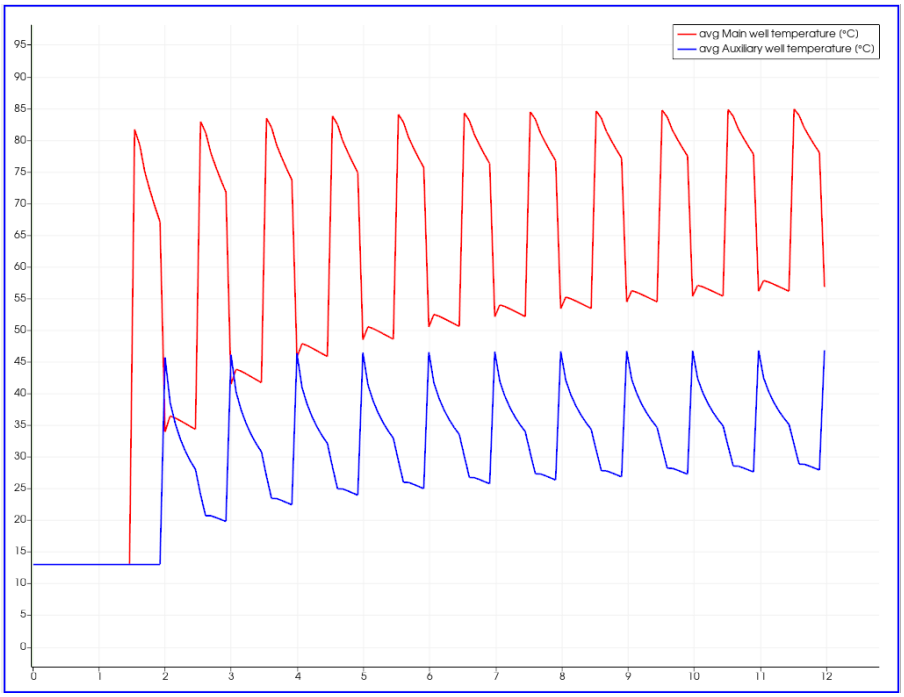

Figure 16: Illustration of transitory regime for one simulation with COMPASS (base case). The temperatures at the wells are shown (main well in red and auxiliary well in blue).

Concerning the mesh discretization in the lateral directions, we made some tests with coarser and finer meshes in order to see if it had influence on the results. The fineness of the mesh close to the wells requires specific attention and must be adapted to the simulation parameters. However, the mesh used for the base case (the mesh size increases with distance to the well, see Figure 15) appears adapted and sufficiently fine to provide consistent results.

Concerning the vertical discretization, in a first approach we considered only one cell per layer. But regarding the vertical distribution of permeable and impermeable layers and their geometries (variable heights) as well as the temperature difference between the initial fluid in place and the injected fluid, some effects on the results are expected.

In order to investigate the impact of the vertical discretization on the results and then represent processes as faithfully as possible, it would be necessary to use a refined vertical discretization. A first test was carried out, with discretization in 2 layers for each permeable layer. In that case, the computation time increased by a factor of 1.4 in comparison with the reference case (using twice as many cores). The comparison of results for a single cell per layer and for a refined mesh are presented in Figure 17. We can observe that the volume of heat storage within the reservoir is similar between the two simulations. However, the time series of temperature for the main well are clearly different during the loading phase. The coarse mesh seems to provide an overestimated value of temperature. Note that the difference (temperatures between the two simulations) is higher for the first cycles, therefore it appears that the difference decreases with the number of cycle (even if the differential is still of 7°C at the 11 cycles). Then, it appears that using a non-refined mesh in the vertical discretization may provide an overestimate of the temperature at the well. This constraint (vertical discretization) requires a specific attention and the optimal configuration (vertical discretization – geological layers – consistent results - computing time) must be sought prior to embarking on the detailed analysis.

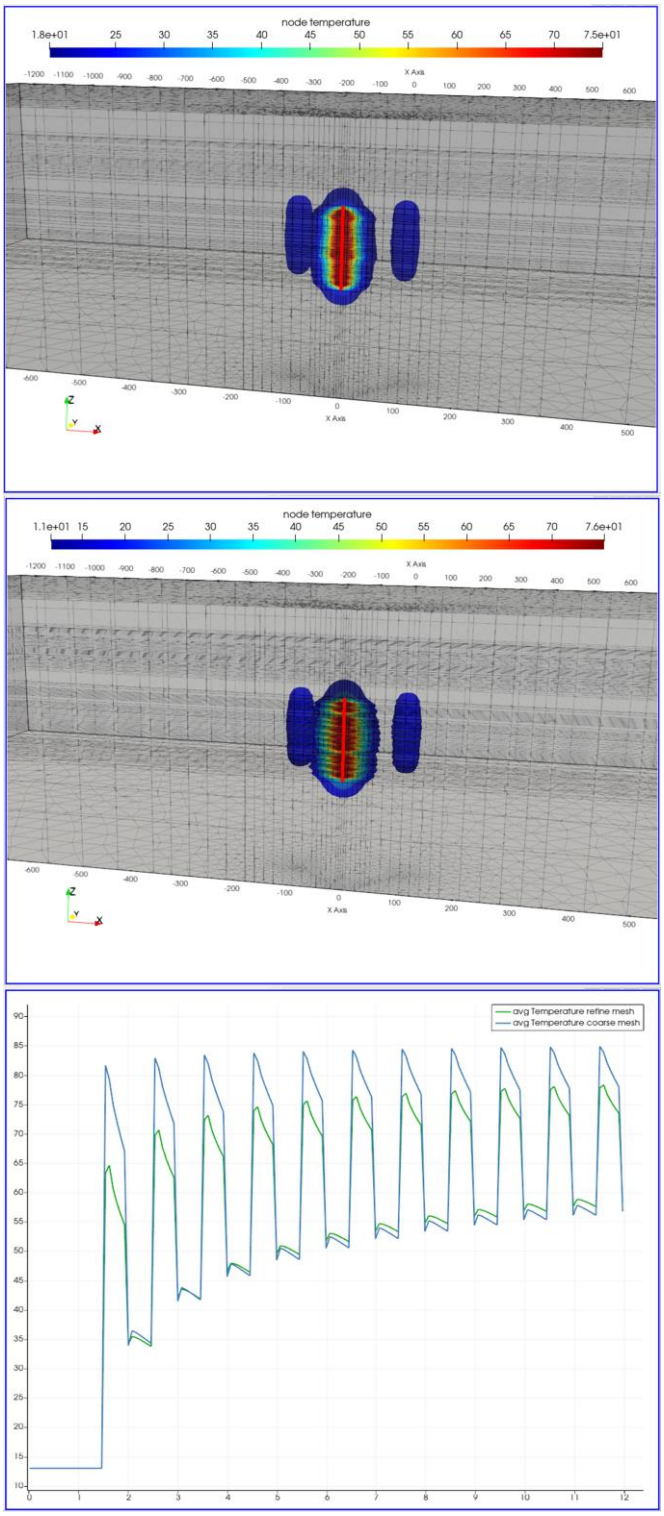

Figure 17: Contours of temperature around the wells at the last cycle (Top : coarse mesh ; Middle : Refined mesh). Bottom : Temperature time series at the main well (blue : coarse mesh ; green : refined mesh).

Last but not least, the preliminary modelling exercise permitted to discuss the choice of input parameters (see next section).

3.4 Information gathering

Discussion concerning the choice of parameters' values and information gathering are detailed in subsections below, per category. Table 4 summarizes the results.

Table 4: Input parameters, collect of information and possible representations.

Parameter	Description	Base case value	Information collected	Range of variations	Probabilistic representation	Possibilistic representtaion
Design						
r	Radius of the well [m]	0,25	Engineering choice	No uncertainty	Fixed value	Fixed value
α	Orientation of wells with respect to the X direction [°]	0	Engineering choice and assumption concerning geology	[-10° ; +10°]	Uniform PDF [-10 ; +10]	Triangular possibilistic distribution [-10 ; 0 ; +10]
d	Distance between main well and auxiliary wells [m]	45	Optimization scenario, uncertainties just from drilling operations	[40 ; 50]	Uniform PDF [40 ; 50]	Triangular possibilistic distribution [40 ; 45 ; 50]
D_1	Drilling depth [m]	500	Optimization scenario, uncertainties just from drilling operations	[490 ; 510]	Uniform PDF [490 ; 510]	Triangular possibilistic distribution [490 ; 500 ; 510]
Storage geometry						
D_2	Reservoir top depth [m]	160	Contour lines Geoportal	[145 ; 175]	Uniform PDF [145 ; 175]	Triangular possibilistic distribution [145 ; 160 ; 175]
$t_{reservoir}$	Total reservoir thickness [m]	D_1-D_2	Computed from other inputs	No uncertainty considered	/	/
Reservoir constitution/geometry						
$N_{permeable}$	Number of permeable layers intersected	16	Deduced from Burgdorf data	[11 ; 21]	Uniform PDF [11 ; 21]	Triangular possibilistic distribution [11 ; 16 ; 21]

Parameter	Description	Base case value	Information collected	Range of variations	Probabilistic representation	Possibilistic representtaion
$R_{p/total}$	Ratio [sum of thickness permeable layers]/[reservoir thickness]	0.3	Deduced from Burgdorf data	[0.2 ;0.4]	Uniform PDF [0.2 ; 0.4]	Triangular possibilistic distribution [0.2 ; 0.3 ; 0.4]
$\sigma_{thick\_permeable}$	Standard deviation of permeable layers thickness	1.8	Deduced from Burgdorf data	[1 ; 3]	Uniform PDF [1 ; 3]	Triangular possibilistic distribution [1 ; 1.8 ; 3]
$\sigma_{thick\_impermeable}$	Standard deviation of impermeable layers thickness	1.4	Deduced from Burgdorf data	[1 ; 3]	Uniform PDF [1 ; 3]	Triangular possibilistic distribution [1 ; 1.4 ; 3]
$w_{permeable}$	Average width of permeable layers [m]	60	To be further discussed	[25 ; 100]	Uniform PDF [25 ; 100]	Triangular possibilistic distribution [25 ; 60 ; 100]
Rock properties						
ρ_r	Density of rock [kg/m³]	2535	Databases	[2400 ; 2650]	Uniform PDF [2400 ; 2650]	Triangular possibilistic distribution [2400 ; 2535 ; 2650]
C_{r_i}	Specific heat capacity of rock for impermable layers [x10^6 J/kg/K]	2.188	Databases	[1.868 ; 2.653]	Uniform PDF [1.868 ; 2.653]	Triangular possibilistic distribution [1.868 ; 2.188 ; 2.653]
C_{r_p}	Specific heat capacity of rock for permeable layers [x10^6 J/kg/K]	2.253	Databases	[1.736 ; 2.610]	Uniform PDF [1.736 ; 2.610]	Triangular possibilistic distribution [1.736 ; 2.253 ; 2.610]
λ_{r_p}	Thermal conductivity of rock for impermable layers [W/m/K]	2.4	Databases	[2.1 ; 2.8]	Uniform PDF [2.1 ; 2.8]	Triangular possibilistic distribution [2.1 ; 2.4 ; 2.8]
λ_{r_i}	Thermal conductivity of rock for permeable layers [W/m/K]	2.4	Databases	[2 ; 2.8]	Uniform PDF [2 ; 2.8]	Triangular possibilistic distribution [2; 2.4 ; 2.8]
Fluid properties						
C_f	Specific heat capacity of fluid [J/kg/K]	4180	Litterature	[4050 ; 4250]	Uniform PDF [4050 ; 4250]	Triangular possibilistic distribution [4050 ; 4180 ; 4250]

Parameter	Description	Base case value	Information collected	Range of variations	Probabilistic representation	Possibilistic representtaion
λ_f	Thermal conductivity of fluid [W/m/K]	0,6	Litterature	[0.60 ; 0.66]	Uniform PDF [0.60 ; 0.66]	Triangular possibilistic distribution [0.60 ; 0.60 ; 0.66]
Impermeable layers						
Φ_i	Porosity [%]	0,5	Conceptualization, completely impermeable	No uncertainty considered	/	/
k_i	Permeability [m²]	$2{,}60\times10^{-17}$	Conceptualization, completely impermeable	No uncertainty considered	/	/
Permeable layers						
Φ_p	Porosity [%]	20	Deduced from Burgdorf data	[10 ; 20]	Uniform PDF [10 ; 20]	Trapezoidal possibilistic distribution [10 ; 15 ; 20 ; 20]
σ_Φ	Standard deviation of permeable layers porosity (variability inter-layers) [%]	0	Expert opinion (to be confirmed)	[0 ; 5]	Uniform PDF [0 ; 5]	Interval [0 ; 5]
k_p	Permeability [m²]	$3{,}45\times10^{-13}$	Deduced from Burgdorf data	[1×10^{-13} ; 10×10^{-13}]	Uniform PDF [1×10^{-13} ; 10×10^{-13}]	Triangular possibilistic distribution [1×10^{-13} ; $3{,}45\times10^{-13}$; 10×10^{-13}]
σ_k	Standard deviation of permeable layers permeability, X direction (variability inter-layers) [m²]	0	Expert opinion (to be confirmed)	[0 ; 2×10^{-13}]	Uniform PDF [0 ; 2×10^{-13}]	Interval [0 ; 2×10^{-13}]
k_y/k_x	Ratio permeability Y vs. X	1	Expert opinion and observations	[0.1 ; 1]	Uniform PDF [0.1 ; 1]	Interval [0.1 ; 1]
k_z/k_x	Ratio permeability Z vs. X	0.25	Expert opinion and observations	[0.1 ; 0.5]	Uniform PDF [0.1 ; 0.5]	Interval [0.1 ; 0.5]
Initial conditions						
T_0	Initial rock temperature [°C]	13	Measurements	[11 ; 15]	Uniform PDF [11 ; 15]	Triangular possibilistic distribution [11 ; 13 ; 15]
q	Natural hydraulic gradient (%)	0	Expert opinion	[0 ; 5]	Uniform PDF [0 ; 5]	Triangular possibilistic distribution

Parameter	Description	Base case value	Information collected	Range of variations	Probabilistic representation	Possibilistic representtaion
						[0 ; 0 ; 5]
Exploitation scenario						
$P_{injection}$	Injection pressure (identical load/unload) [MPa]	3	Engineering choice	/	/	/
P_{drop_max}	Maximal drop pressure in production well [MPa]	1.2	Engineering choice	/	/	/
$T_{inj,main}$	Injection temperature at main well (load phase) [°C]	90	Engineering choice	/	/	/
$T_{inj,border}$	Injection temperature in auxiliary wells (production) [°C]	50	Engineering choice	/	/	/
T_{thr}	Threshold temperature for unload cycle [°C]	55	Engineering choice	/	/	/
t_{load}	Duration of load cycle [days]	217	Engineering choice	/	/	/
t_{break}	Break days	0	Engineering choice	/	/	/
t_{unload}	Duration of unload cycle [days]	148	Engineering choice	/	/	/
Modelling choices						
H	Height of the cylinder model [m]	500	Preliminary modelling choice	/	/	/
R	Radius of radial symetric cylinder model [m]	2500	Preliminary modelling choice	/	/	/
N	Number of cells	10	Preliminary modelling choice	/	/	/
N_{cycles}	Number of cycles	Over a hundred cells	Preliminary modelling choice	/	/	/

3.4.1 Main sources of information

We present in this section the main sources of information, which were used, in addition to expert opinion. Most documents are in German (not translated).

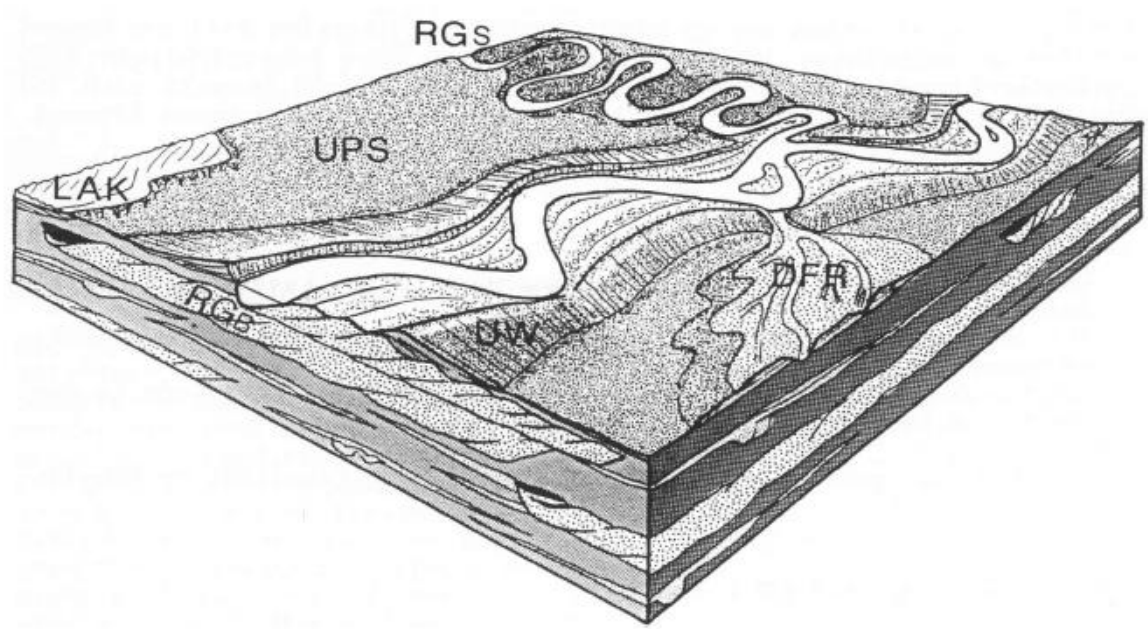

Figure 18: Representation of the formation of geological facies in the reservoir (source: NAGRA, 2005).

As illustrated in Figure 18, the targeted formation originates from sedimentary fluviatil deposits, thus permeable layers have longitudinal shapes. The location of permeable layers evolved with the former riverbed location. This is illustrated in Figure 12. Even at limited drilling distances, the number and characteristics of permeable layers may evolve. Thus the level of uncertainty is relatively high.

Concerning the other sources of available information, we have at our disposal data on a well located at 47.057260233, 7.622510062 (distance 20 km from the present project). On this well, we have the following information (Figure 19):

- Geological profile;
- Structural elements of the USM;
- Porosities;
- Transmissivities.

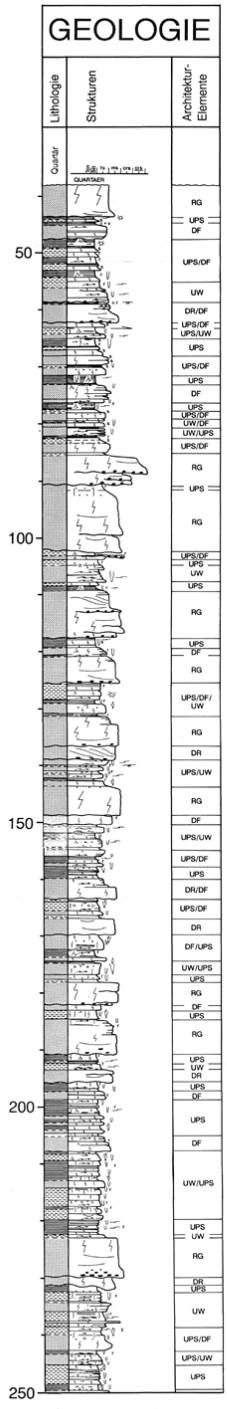

Position Zufluss (m ab OKT)	Zufluss-Mächtigkeit H (m)		Transmissivität T BORE (1E-6 m²/s)	Hydraul. Durchlässigkeit K BORE (1E-6 m/s)
85	RG	5.6	23	4.11
115	RG	8.4	1.8	0.21
122	RG	4.8	2.7	0.56
146	RG	5.0	3.3	0.66
162	DR/DF	3.5	17	4.86
167.5	DR	2.8	12	4.29
178	RG	4.0	9.7	2.43
188	RG	6.2	0.25	0.04
227	RG	7.0	5.6	0.80

Source: (NAGRA NTB 92-03, 1993)

Tabelle 2: Porosität und hydraulische Durchlässigkeit der verschiedenen Architekturelemente der USM (nach (Keller, 1992))

Architekturelemente der USM	Porosität Medianwerte	Durchlässigkeit K-Wert (m/s)
RG Rinnengürtel	20 %	10^{-7} bis 10^{-4}
DFR Durchbruchsfächer und Durchbruchsrinnen	14.5 %	10^{-8} bis 10^{-5}
UW Uferwälle und Überschwemmungssande	7.5 %	10^{-10} bis 10^{-7}
UPS Überschwemmungsebene mit Paläoböden	7.5 %	10^{-11} bis 10^{-8}
LAK Lakustrische Sedimente	keine Daten	keine Daten

Source: (Keller, 1992)

Source: (NAGRA NTB 92-03, 1993)

Figure 19: Extract of information collected on a distant well.

In the article NAGRA NTB 05-02. (2005), the authors describe the structural elements of the USM. It is indicated that there is high uncertainty concerning thickness and lateral extent of the Rinnensandsteingürtel. The Swiss Geological Survey (Geomol, 2019) has produced a 3D geological model of the Swiss Plateau, which gives visualization of the geological structure beneath this densely populated part of the country in 3D. In the Bern area, a thickness of the USM of 1500 m is expected.

Among other available data, a database of geothermal properties of the Swiss molasses is available (Leu et al. 2006).

The geoportal of Bern Kanton gives contour lines for the rock surface, which is based on several borehole data and modelling work. The rock surface at Bern Forsthaus is expected at a depth of 160 m.

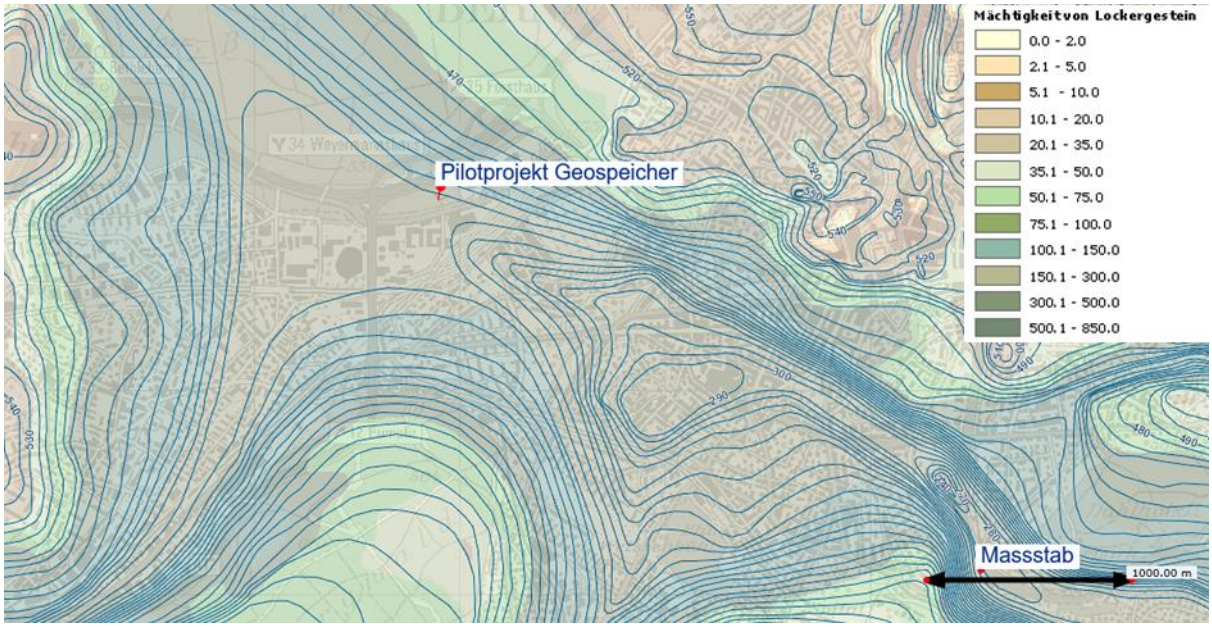

Figure 20: Overview of the contour lines for the top depth of the reservoir (source: Geoportal Kanton Bern).

3.4.2 Design parameters

As afore-mentioned, we distinguish 2 approaches:

- optimization of the exploitation scenario;
- dealing with uncertainties.

In the present exercise, we focus on uncertainties not related to the optimization of an exploitation scenario:

- The radius of the well in the reservoir is a well-controlled engineering parameter, here equal to 0.25 m.
- The planned drilling depth is 500 m. The geological horizon which is targeted continues largely deeper than the targeted drilling depth. We assume that the choice of the drilling depth has already been made in the frame of the exploitation scenario optimization. Some uncertainties may nevertheless remain: from discussion, we assume that for technical reasons, there may be 10m of uncertainties: between 490 and 510 m depth is possible, the more probable value is 500m.
- Concerning the wells configuration (see Figure 14), it is assumed that the optimal configuration (auxiliary wells forming a square, with main well at its centre), as well as the optimal distance between main depth and auxiliary wells has already been discussed. A 45 m distance is targeted, but depending on surface constraints and drilling operations, this distance may vary between 40 and 50 m.
- Concerning the orientation of the well (Figure 21), noted α, we assume that in the optimal configuration, we target α = 0°. However, considering underground uncertainties, the true main direction of permeable layers is tainted by uncertainties. In the absence of more precise information, we may assume an uncertainty range for α comprised between -10 and +10°.

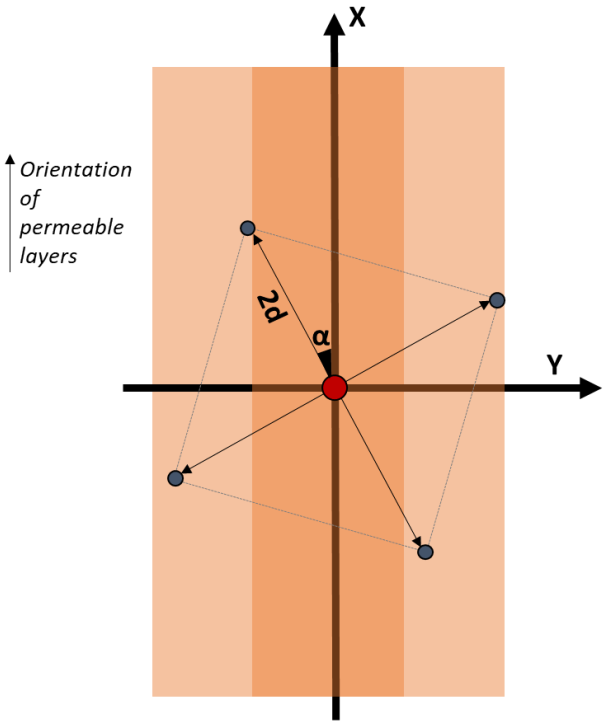

Figure 21: Illustration of the wells configuration. Orange rectangles represent permeable layers (assumed to be aligned with the X direction).

3.4.3 Storage geometry

Concerning the reservoir top depth, we use information provided in Geoportal Kanton Bern (presented in Figure 20). At the project location, the depth of the USM rock surface is 390 m (altitude relative to sea level); The topography at this location is 550 m, so the top depth best estimate is 160 m. The level lines are well fitted with a number of wells logging and geophysical data and experts are quite confident in the values (we assume more or less 5 m). Since the plume in the reservoir is inferior to 60 m and since the distance between two level lines (step 10 m elevation) is around 60 m, we can consider that a plausible range of values for the top depth is between 145 and 175 m.

Concerning the total reservoir thickness, it is computed by subtraction between the drilling depth and the top reservoir.

3.4.4 Reservoir characteristics

Different options were discussed to represent the uncertainties concerning the reservoir constitution. As aforementioned, the reservoir thickness is represented by an uncertain parameter.
We proposed as a first input parameter the number of permeable layers intersected by the well. As illustrated in Figure 12, there may be high uncertainties concerning this parameter, since permeable layers have limited extents. Even if we had drilling information very close (which is not the case), uncertainty would still exist. Based on the geological profile in Burgdorf (NAGRA, 1993), we have 10 permeable layers in the analysed section of 211 m length. This would correspond to 16 permeable layers in the reservoir (reservoir thickness around 340 m). Experts consider that 16 is thus the best estimate, but values between 11 and 21 should be considered.
Another issue was how to take into account the uncertainty on the individual thickness of permeable and separating impermeable layers, keeping in mind that the reservoir thickness is uncertain and that the number of layers is also uncertain?

- A first option would be to consider all permeable layers with equal thickness $t_{1permeable}$, and to draw only one input parameter "thickness of each permeable layer". The thickness of impermeable layers would then be computed by: $\frac{t_{reservoir}-N_{permeable}\times t1permeable}{N_{permeable}-1}$.

  Simulations leading to possible negative values (cases with low reservoir thickness, high individual thickness, high number of layers) should simply be removed. Despite its simplicity, this choice restrains the representativeness of simulations. In reality, the reservoir is a stack of irregular permeable and impermeable layers, and this may be of importance to catch the real behavior of the reservoir.

- In order to take into account the fact that the number of permeable layers and the reservoir thickness are variable, we proposed to use as input parameter the ratio $\frac{\sum thickness\ of\ permeable\ layers}{t_{reservoir}}$.

  Based on the geological profile (NAGRA, 1993), the ratio is 0.3. This can be considered as the most plausible value but in order to consider uncertainty, it may be reasonable to consider that this value may vary between 0.2 and 0.4.

- Using the afore-mentioned ratio and the total reservoir thickness, we know the parameter $\sum thickness\ of\ permeable\ layers$. We also know the number of permeable layers. It is then necessary to distribute the total thickness on the different layers. As afore-mentioned, it is of importance to reproduce the random variability between layers. We propose to introduce a new parameter, the standard deviation of permeable layers thickness. As illustrated in Figure 22, normal laws may be used to represent the random variability of permeable layers thicknesses. In order to constitute the stack of permeable layers, we propose the following: first a set of $N_{permeable}$ values (t_1, t_2, … $t_{Npermeable}$) is drawn from the following normal law: average equal to $\frac{\sum thickness\ of\ permeable\ layers}{\mathrm{Npermeable}}$, standard deviation $\sigma_{thick\_permeable}$ (input parameter). The order of values is kept random and will correspond to thickness, from top to bottom. Due to the finite random draw, the sum of random values will not be exactly equal to $\sum thickness\ of\ permeable\ layers$. A correction will thus be made on the set of values with $\lambda = \frac{\sum thickness\ of\ permeable\ layers}{\sum t_i}$: t_i values are replaced by $t_i^* = \lambda \times t_i$, so that the sum of thickness becomes perfectly equal to the sum afore-deduced. For the parameter $\sigma_{thick\_permeable}$, we have information stemming from Burgdorf measurements (NAGRA, 1993). Taking into account the complete analysed section (211 m) and the graphically represented lithology, we get 10 values for thickness of permeable layers. The standard deviation is around 1.8. Based on experts opinion, it was considered that this parameter may vary between 1 and 3, in the absence of more precise information.

- As a last parameter, in order to constitute the reservoir model, exactly the same approach is proposed for the impermeable layers, with introduction of the parameter $\sigma_{thick\_impermeable}$ (standard deviation of impermeable layers thickness), and with $N_{impermeable}$= $N_{permeable}$-1. The best estimate is 1.4, and once again in the absence of more precise data, it is proposed to consider a range of variation between 1 and 3.

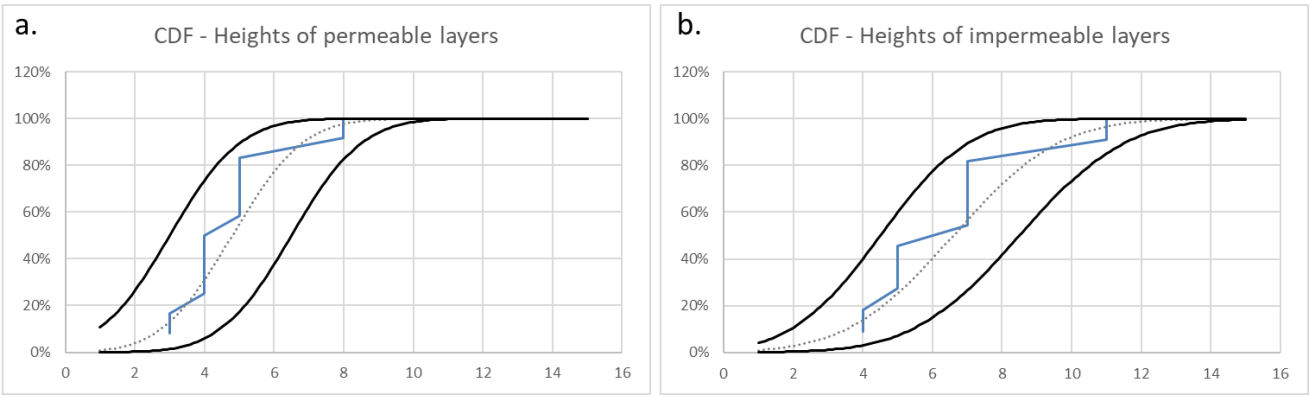

Figure 22: Construction of CDF with the limited set of data (Burgdorf, NAGRA, 1993) concerning thickness of permeable layers (on left) and of impermeable layers (on right). Approximation by normal laws (dotted line as a best estimate and plain lines as possible conservative enveloppe) appears satisfactory.

With parameters afore-mentioned, we can constitute the stack of permeable and impermeable layers. In a first approach, it was considered that permeable layers were continuous in lateral directions. Assuming that the main direction of the former riverbed is the X direction (Figure 21), we agreed with experts that assuming continuity within this direction is a satisfactory assumption. In the Y direction, by contrast, the assumption is debatable (see Figure 12). This can be integrated in modelling in different ways, with different levels of complexity. Additional discussions with experts would be necessary to enlighten the different points:

- Concerning the river width evolution with time, considering the different geological ages of the different permeable layers, is there a time-correlation between subsequent permeable layers (like geostatistical correlation length in space)? Or should we consider the width of each layer independently from the others? (Figure 23, top)
- We can decline the same question concerning the lateral position of the layers. (Figure 23, bottom)
- What is the main source of uncertainty? Random variability due to strong difference between different geological ages, or epistemic uncertainty due to knowledge limitation? (Figure 25)

Figure 23: Illustration of the different possibilities for the conceptualization of layers width (top) and lateral location (bottom).

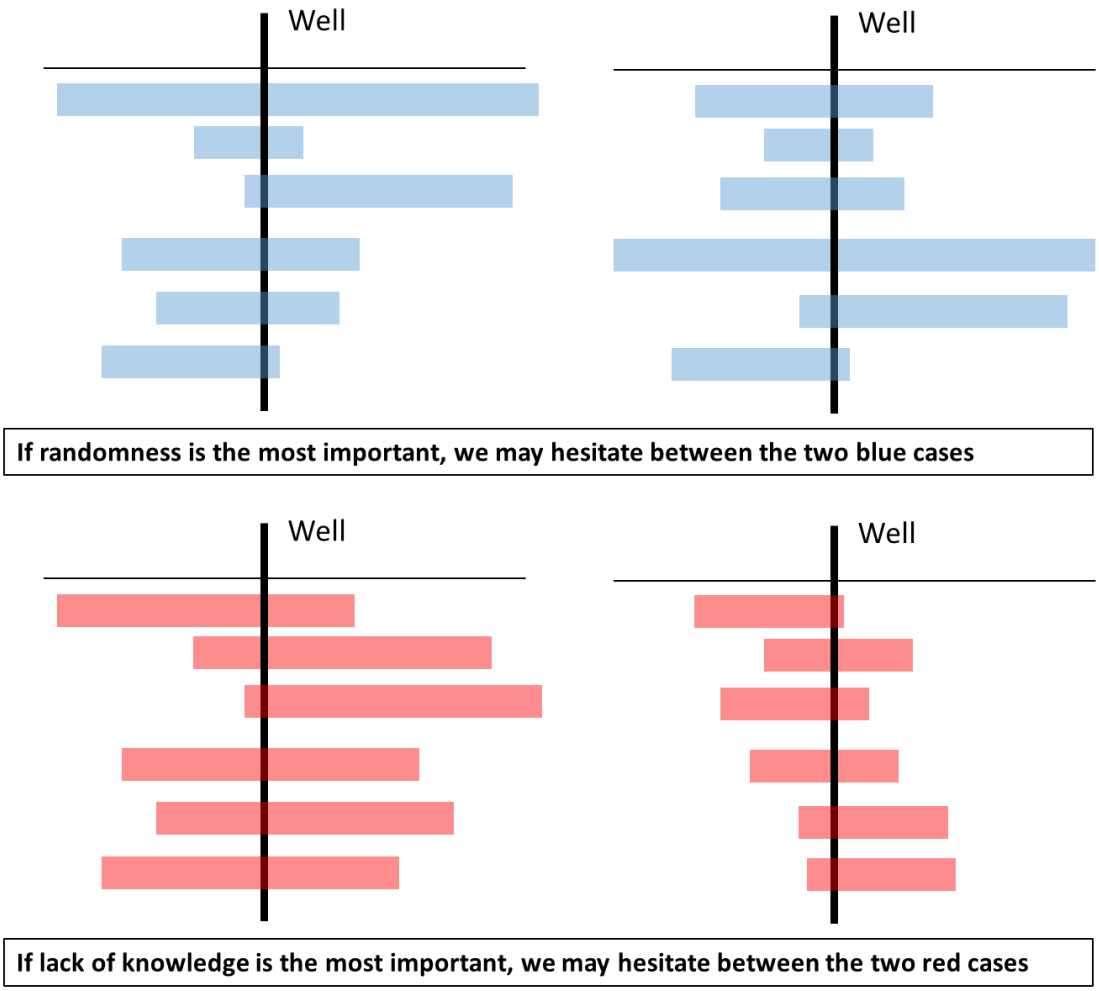

Figure 24: Illustration of the different possibility for conceptualization of layers width in case of random uncertainty (top) vs. aleatory uncertainty (bottom).

Depending on the answers to these questions, the choice of input parameters would not be the same.
In a first simple approach, we propose to consider that all layers have equal width, and to consider that the well intersects each layer at a lateral independent position. With this simple base case, we need only one parameter: the width of permeable layers. For illustration, we can for example consider that the average width is estimated between 25 and 100 m (with 60 m as a more probable value); relevant values for these parameters need further investigations and other experts opinions.
With more clues on the afore-mentioned questions, it would be possible to enrich the representation of this uncertain parameter.
Concerning width on one hand and location of intersection location with the well on the other hand:

- If there is no time-correlation between subsequent layers, it may be more appropriate to perform independent draws for the different layers. If on the contrary there is a correlation, it would be more appropriate to introduce an incremental uncertain parameter by reference to the previous layer;
- If the uncertainties are mainly epistemic but with low variability, similar characteristics for all layers, represented by a unique parameter may be relevant; if on the contrary the randomness dominates, representation by a PDF would be more physical. If randomness and epistemic uncertainties co-exist, then imprecise probabilities may be of interest.

In terms of uncertainty frameworks, depending on the afore-mentioned choice, some technical difficulties may arise, notably when dealing with dependency between different parameters represented in the possibilistic framework (not fully integrated in HyRisk).

3.4.5 Rock properties

Concerning the rock density, considering the database of geothermal properties of the Swiss molasses, the best estimate is 2535 kg/m³, an uncertain range between 2400 and 2650 may be considered.
Concerning the specific heat capacity of rock per volume, according to experts, it may vary between 1.868x10^6 and 2.653 x10^6, with 2.188x10^6 J/m^3/K as a more plausible value for impermeable layers, and between 1.736x10^6 and 2.610 x10^6, with 2.253x10^6 J/m^3/K as a more plausible value for permeable layers.
Concerning the thermal conductivity of rock, according to experts, it may vary between 2.1 and 2.8, with 2.4 W/m/K as a more plausible value for impermeable layers, and between 2 and 2.8, with 2.4 W/m/K as a more plausible value for permeable layers.

3.4.6 Fluid properties

Concerning the specific heat capacity of fluid, according to database, the base case value considered is 4180 J/kg/K. During expert elicitation exercise, the range of uncertainties could not be provided. Through a rapid literature review (Rogers, 1981), we can see that the specific heat capacity varies significantly with molality, but in the present case the molality can be considered as quite well characterized. The variation depending on temperature and pressure is less important. Considering this information, we may consider [4050 ; 4250] as a conservative range of values. It may be refined if necessary.
Concerning the thermal conductivity of fluid, once again we have at our disposal an estimate for the Swiss context of 0.60 W/m/K. In order to circumvent the range of uncertainties, we had a look at Figure 3 in Walsch et al. (2017) to assess the order of magnitude of plausible variation. Considering the range of temperature, a range of value between 0.63 and 0.66 may be proposed. Since this information is not perfectly in line with previous base case value, we decided to keep 0.60 as a more plausible value, and to consider a conservative range between 0.60 and 0.66 W/m/K. If influential, we will further investigate the parameter to characterize it more precisely.

3.4.7 Permeable layers

Concerning intrinsic properties of permeable layers, we had a number of preliminary discussions concerning the involved parameters: porosity and permeability.

Should we use homogeneous equivalent values in all cells or integrate random variations? As afore-mentioned, it is difficult here to have a refined mesh in order to keep computation time reasonable. In order to use appropriately random values for porosity and permeability, it would be necessary to characterize correlation length (over which dimensions the parameters evolve) and to build a corresponding mesh. The available data correspond to equivalent values (transmissivity obtained from aquifer tests), and thus using equivalent values for parameters appeared as more appropriate.

For permeability, should we consider isotropic values or anisotropic values? For the present case, it appeared necessary to take into account the anisotropy. The X direction (former river direction) may be considered as a principal direction, with permeability k_x. When dealing with uncertainty, obviously the parameters k_y and k_z cannot be handled independently. Thus we propose to use the ratios k_y/k_x and k_z/k_x.

For each layer, we decided to use a set of equivalent values. The question is then: how to manage possible interdependency between layers? It comes back to the question illustrated in Figure 24. For porosity and permeability, since the sedimentary deposits came from different ages, assuming different equivalent values may be more relevant. In addition to this randomness, there is also an important level of epistemic uncertainty. In order to take this into account, we propose to use a set of two parameters. The first one is the equivalent permeability (vs. porosity) of the $N_{permeable}$ layers. The second one is the standard deviation σ_k (vs. σ_Φ) between individual layers equivalent permeabilities (vs. porosities) (assuming a normal law). We propose to proceed in the following way (illustration is made for permeability, but the same is also proposed for porosity). First an equivalent permeability is drawn: k_x. Then $N_{permeable}$ values of individual permeabilities (k_{x1}, k_{x2},…, $k_{xNpermeable}$) are drawn on a normal law with average value k_x and standard deviation σ_k. In order to reproduce faithfully the equivalent permeability k_x, a correction is applied: $\gamma \sum k_{xi} \times t_i^* = k_x \times t_{reservoir}$. k_{xi} values are then replaced by $k_{xi}^* = \gamma \times k_{xi}$.

Regarding information gathering:

- Concerning equivalent porosity: Based on Keller (1992) and other measurements, a porosity value between 15 and 20 % is the more probable, but values between 10 and 20 % are plausible. In the absence of more precise information, the standard deviation to take into account individual layers different contributions to this equivalent porosity may be comprised between 0 and 5 %.
- The equivalent permeability was calculated by first determining the overall transmissivity for the 9 layers and then calculating the average hydraulic conductivity based on the total thickness of the layers at Burgdorf. The best estimate for the permeability in the X-direction is 3.45×10^{-13} m². There may be uncertainties, but it is an equivalent permeability for the $N_{permeable}$ layers and not local values, the range of expected variation is thus more limited, let's say between 1×10^{-13} m² and 10×10^{-13} m². For the standard deviation between the different layers, in the absence of more precise information, we considered that it may vary between 0 and 2×10^{-13} m².

We considered independently the parameters porosity and permeability. There may be a layer with high porosity and low permeability, and vice-versa. The choice of independent parameters is conservative in terms of risks assessment. If necessary (if parameters are found influential), it may be possible to include this correlation between both parameters to limit the resulting uncertainties on outputs.

Concerning the ratio k_y/k_x, according to experts, it is likely that there is a prefered flow direction. We consider it may vary between 0.1 and 1.

Concerning the ratio k_z/k_x, experts have no specific data for this anisotropy but as a general observation they know that the vertical permeability is much smaller than the horizontal permeability. Thus a ratio between 0.1 and 0.5 is proposed.

In a first approach, the ratios are considered identical for all layers.

3.4.8 Impermeable layers

Concerning intrinsic impermeable layers, we may proceed like for permeable layers. However, from the flow measurements, the impermeable layers are really impermeable. The porosity and permeability values were chosen so that there is almost no flux in the impermeable layers, whatever the direction. According to experts, it is thus not necessary to refine the associated parameters by integration of anisotropy ratios.
We considered a low porosity value (0.5 %) and a low isotropic permeability (2.60×10^{-17} m²). For the reason mentioned, we considered no uncertainty on these parameters, since it is a conceptualization choice.

3.4.9 Initial properties

As input parameters, we need the initial rock temperature, estimated around 13 °C. This parameter is considered as well characterized, with limited uncertainty (plus or minus 2 °C).

Concerning the initial hydraulic gradient, in the absence of data and based on experts opinion, it is assumed that there is no hydraulic gradient. However, we propose to check if it may have influence by considering a conservative range of values between 0 and 5 % in the X direction. If it appears to be influential, we will try to refine knowledge on direction and intensity.

3.4.10 Exploitation scenario

As afore-mentioned, we assume that optimization of exploitation scenario is a prior approach that was made before the present study on uncertainties. Parameters in this category are related to optimization of exploitation scenario and are thus considered as well characterized. It may be possible to introduce a limited range of uncertainty on these parameters, for instance by considering that even if the average injection temperature is fixed at 90 °C, due to technical engineering reasons, this average temperature may vary between 89 and 91 °C for instance. After discussion with experts, it was decided not to burden the case study and to consider all parameters fixed:

- Injection pressure (identical load/unload): 3 MPa
- Maximal drop pressure in production well: 1.2 MPa
- Injection temperature at main well (load phase): 90°C
- Injection temperature in auxiliary wells (production): 50 °C

- Threshold temperature for unload cycle: 55°C
- Duration of load cycle: 217 days
- Break days: 0 day
- Duration of unload cycle: 148 days

3.4.11 Modelling choices

The last category of parameters concerns modelling choices. These parameters were discussed in section 3.2, and we verified that the choices guarantee robustness of results, so no uncertainty was introduced at this stage.

3.5 Towards the choice of uncertainty framework(s): Elaboration of a possible work programme

As illustrated here, the first brick of uncertainty dealing presented in Figure 1 may represent by itself an important quantity of work:

- Choice of a model;
- Clarification of the decision frame;
- Preliminary estimation of computation time;
- Construction of a set of parameters: as illustrated here, the set of parameters finally identified in Table 4 is more sophisticated than the initial set of parameters. The identification of uncertain parameters itself raises an important number of questions and it required a number of discussions with experts and modellers in order to make conceptualization choices;
- Information gathering in order to estimate range of variations also represents a consistent work. In order to avoid useless time-consuming tasks, for some parameters, we limited investigations and preferred using conservative ranges of values, keeping in mind that the characterization may be refined if the sensitivity analysis concludes that these parameters are influential.

For the present case study, we are confronted with a relatively complex model, with a high number of uncertain parameters. Even after decorrelation of parameters that correspond to optimization of the exploitation scenario, after removing parameters corresponding to modelling choices, the number of remaining uncertain parameters is 26. The computation time is relatively high (order of magnitude: 1 or 2 hours). Even if simulations may be launched in parallel on several computation servers, it will not be possible to launch infinite numbers of simulations. Assuming for instance 10 simulations in parallel, 2 hours of computation time, it means that 840 simulations can be launched during a complete week. A thousand of simulations may appear significant, but uncertainty frameworks (and notably possibilistic framework) require huge amounts of simulations. Immediate application of the frameworks presented in section 0 would not be possible here.

Within the budget of the HEATSTORE project, it was unfortunately not possible to follow through, but we indicate below a possible work programme. It should be noted that dealing with this level of complexity remains a non-routine task and needs permanent adaptation of work programme, depending on the first results obtained. The work programme is thus an indicative basis.

In a first time, even if the possible interpretation is limited, a first OAT sensitivity analysis may be carried out. This requires 1 base case simulation and 26x2 = 52 supplementary simulations. It would enable drawing a first graphic illustration (such as Figure 5) and to have a first idea of influential parameters. Besides, it may enable highlighting and solving modelling issues related to more extreme values before undertaking a higher number of runs.

At this stage it is unrealistic to work in the possibilistic framework. We would recommend the elaboration of an experience plan in order to do a first estimation of the uncertainties on outputs and a first screening of the most influential parameters using Sobol' indices (see section 4 which presents this tool). There are different possible conclusions at this stage: either a high number of parameters has medium influence, or the uncertainties on the output are mainly related to a limited number of very influential parameters. It should be noted that the results concerning influential parameters may be different for the two outputs considered. From the first results, outputs should be analysed in order to quantify the ranges of possible variations, and to compare these ranges with the decision thresholds provided by decision makers. It may already provide some first information from a decision-making view point.

At this stage, for the most influential parameters, it is worth checking the prior information gathering exercise in order to consolidate the choices made (is it sure that the values retained are conservative? Is it possible to refine the information by collecting a few more information?). Collecting information is expensive (additional measurements/acquisition, and/or time required). This is the reason why we recommend a customized approach for the different parameters, depending on their importance for decision-making. In a first time, we collect the easily accessible information (see section 3.4), and then the collect of information is refined depending on first results. It may be possible to go further on this kind of approach considering the concepts of “value of information (VOI)”, which enables quantifying the cost that is worth spending to collect a given data, depending on the expected value from a decision viewpoint. In the present case, the idea is less sophisticated. We try to avoid spending too much time and money by proceeding iteratively, guided by common sense.

Based on the first set of results, the afore-mentioned exercise of outputs scoring and averaging could be launched. For each output, the minimal and maximal outputs values are recorded and scoring scales are established, taking into account the decision thresholds. For instance, if output varies between 1 and 100, with most values around 90 and a decision threshold at 90, if we use a linear notation scale between 0 and 100, most simulations will have a score around 9/10 and will not be discriminated, even if for the decision maker 85 is a bad score and 95 an ideal performance. In such a case, a non-linear notation scale would be more appropriate. For the present case, with two indicators, it is possible to analyse two outputs. But if we restrain to the independent analysis of the two outputs, it will not be possible to take into account the possible correlated or uncorrelated behavior between outputs (if all simulations having a bad score on one output have also a bad score on the other output, the worst scenarios will be more feared than in the opposite case).

Then, an option would be to keep the 3D complex numerical model and to perform Monte Carlo simulations in the probabilistic framework, using the whole set of uncertain parameters. This will lead to results in the form of a unique CDF for each output, and for the agglomerate score output. This kind of results may be helpful for decision making (section 2.6), but it offers only a partial view on uncertainties.

Thus we suggest as another prospective task the construction of a meta-model (or surface response model). Techniques to elaborate a meta-model are presented in section 4 for another case study. We would consider one meta-model for each output, considering the associated most influential parameter. These two meta-models will enable rapid estimation through analytical computations. Passing through a meta-model will introduce an additional uncertainty, which can be quantified and will be integrated in the results. If this step is successful, it will then be possible to use the different uncertainty frameworks, and notably the extra-possibilistic framework. It is very interesting in the present case, since from the data information collection, we can see that data are very scarce and that possibilistic representation is more faithful than probabilistic representation for almost all parameters. The level of complexity of the extra-probabilistic approach, even with a meta-model, will depend on the monotony of outputs with regard to the different inputs and on the possible consideration of dependence between the different retained inputs.

It could then be very interesting to follow the uncertainty analysis exercise with progressive enrichment of available data (notably with the first drilling). Maybe it would question the model conceptualization, maybe only the choice of parameters, and for sure the available data to characterize and represent input parameters. Subsequent adjustment of the approach and redefinition of the decision making frame would be worth of interest from a scientific viewpoint.

4 Uncertainty analysis using long-running numerical simulations

4.1 Introduction

The Bern case study presented in section 0 focuses on a specific real site study. We highlighted the important work needed to elaborate the decision-making framework, to conceptualize the situation, to establish a model, to elaborate a convenient set of input parameters and to collect information.

By contrast, the case study presented here is not a specific site-study. The approach is more generic: the work scale corresponds to similar kinds of storage operations that may be deployed in the Dogger, in the Paris basin (France). From the numerous geothermal activities already in place in the Dogger, we have an important database concerning Dogger properties. We use this set of available data in order to establish a plausible case study (non specific to a given location) and to investigate the parameters that may be influential for storage performance, with range of uncertainties that correspond to ranges of variations observed in the Dogger. Since the case study is more generic, the modelling choices, the identification of parameters and the collect of information was more simple. The work is thus more focused on subsequent steps: how to deal with a time-consuming model to identify most influential parameters, and how to elaborate a meta-model that can further be used for decision making? As mentioned in section 3.5, the approach presented here is a next step identified in the Bern work programme.

4.2 Objectives

Computer models are very useful to simulate geological heat storage and to provide an estimate of the amount of energy stored and produced over time depending on the cycles (flow rate and temperature) imposed at the wells. Yet, a large variety of different sources of uncertainty can affect these temporal estimates, for instance the reservoir properties or the choice in the design parameters of the cycles. Using the site described in section 4.3 as an application case, Figure 25 provides an illustration of four different temporal estimates during storage and re-production phases considering four different reservoir settings and designs. This raises the following questions: 1) what uncertainties drive the most this variability? 2) what uncertainties do not? 3) does this influence change over time?

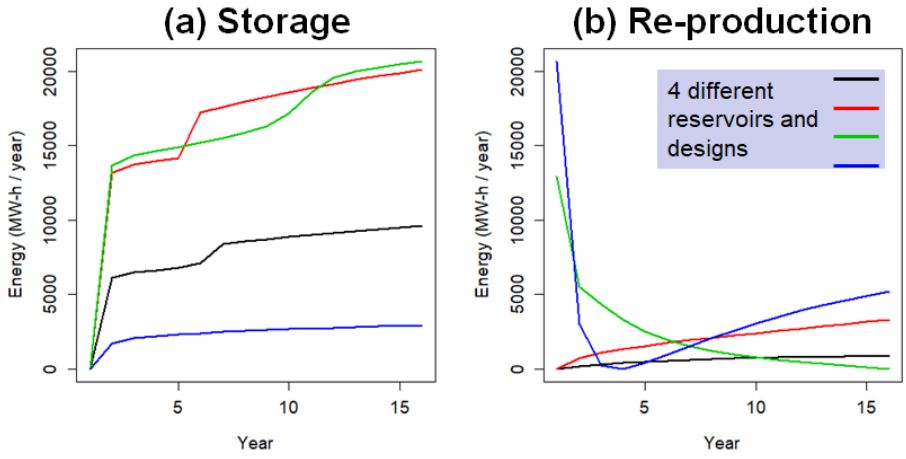

Figure 25: Temporal evolutions of the energy (MWh/year) given four simulation scenarios (reservoir characteristics and design parameters) for the storage (a) and the reproduction (b) phase considering the storage case described in section 4.3.

To analyse the influence of the uncertainties, a powerful approach relies on the tools of variance-based global sensitivity analysis, denoted VBSA (Saltelli et al., 2008); see some real case applications in the domain of reservoir engineering (Manceau and Rohmer, 2016). A major limitation in our case is that the numerical model used to compute the energy time evolution has a moderate-to-large computation time cost, i.e. large enough to limit the number of possible simulations scenarios (i.e. corresponding to the assumptions of the reservoir properties, the design parameters, etc.) to a few hundreds. VBSA imposes however a large number of

numerical simulations (typically more than 10,000). Therefore, we propose in this section a procedure combining VBSA with surrogate models (also named metamodels).

In the next sections, we first describe the application case and the physical model that was set up to simulate the energy temporal evolution given different scenarios. Then, we describe the different statistical methods (VBSA and metamodels). We then apply them and discuss the results. Finally, we explore an advanced metamodelling approach to improve the procedure.

4.3 Storage application case

4.3.1 Description of the physical model

The physical model is based on the principle and the technical feasibility of inter-seasonal heat storage system within the Dogger aquifer. The Dogger aquifer has been exploited intensively for 40 years with 50 energy geothermal plants currently operating. Aquifer Thermal Energy Storage (ATES) is a promising solution for reducing the time mismatch between energy production and demand in urban environments. The Paris area seems to be a favourable region since there is:

- locally a surplus of heat production during the summer
- an appropriate geological reservoir with good hydrodynamic and thermal properties
- and both existing and projected district heating networks that is suitable for winter unloading of the heat.

These conditions are satisfied in the Paris basin, which can be considered as a favourable area for future ATES operations:

- Incineration plants currently operated are feeding the heating networks (equivalent to the consumption of 300,000 housing-equivalents of 70 m², see https://www.syctom-paris.fr/pour-un-traitement-des-dechets-responsable/energie.html). The waste incineration is providing baseload energy to feed a large, steam heating network region and power is available during the summer low-demand period.
- A considerable database on the underlying Dogger aquifer resulting from successful experiences with low-enthalpy geothermal energy.
- The region around Paris is the most developed district heating networks and is still developing.

But in spite of this favourable context, these three criteria alone are not sufficient to assess the profitability of an ATES in the Paris region. Unlike conventional geothermal solutions, the power available to feed a heating network temperature of the resource varies over weeks and with the seasons, as does the aquifers. These reasons make necessary the use of models that enable tracking of the temperature of the geothermal resource and of the characteristics of the load (inlet and outlet temperatures, network flow rate) in order to estimate the geothermal feed power at a given time. The system is called “Aquifer Thermal Energy Storage (ATES)”, but it recovers some heat already in place, as a conventional deep geothermal installation does. It may be called “a mixed deep-conventional-doublet-ATES”. Consequently, for many simulations, energy extracted from the underground is higher than the stored energy.

In this study, the inter-seasonal heat storage system within a deep aquifer considered is based on the use of two wells, which operate alternately as producer and injector in order to store an excess energy (provided by a domestic waste incineration plants) in the form of hot water during the summer season, and then recovering the heat during the winter/heating season. Note that, in that case, the deep aquifer (the Dogger aquifer) already constitutes a geothermal resource, which is powered by a heat storage system. The loading/unloading cycle of thermal storage is a periodic sequence of 12 months. During this period the wells are reversible and operate as producer or injector. A scheme of the heat storage system functioning is provided in the Figure 25.

The deep aquifer periodic exploitation tends to result in a thermodynamic system with two sources: a cold source and a hot source, close to the cold and the hot well, respectively.

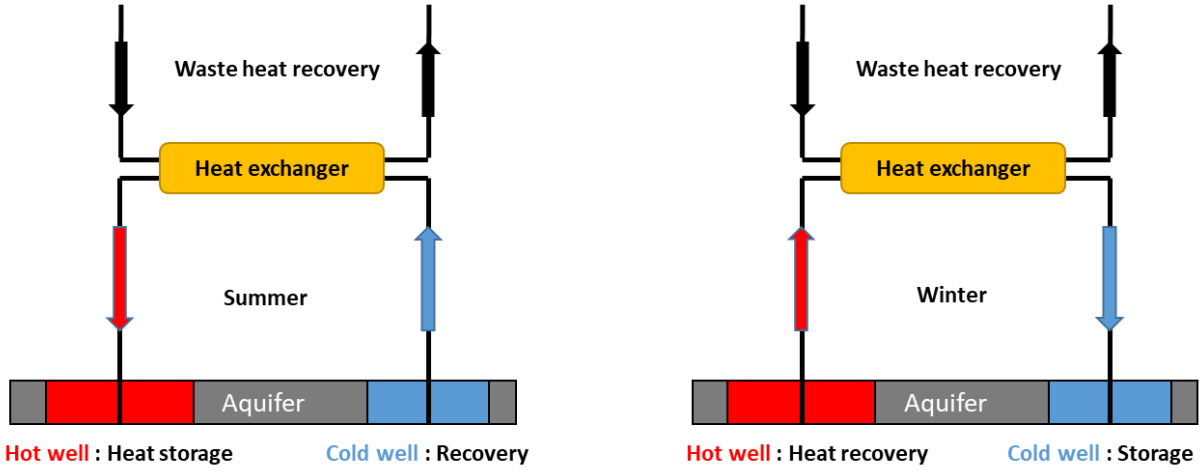

Figure 26: Diagram of a doublet for deep geothermal aquifer powered by heat storage exploitation.

The physical model is developed using the “Dogger database”. This database was set up to follow detailed information on geothermal operations targeting the hydrogeological formation of the Dogger limestone in the Paris basin. This database constitutes the "memory" of the Dogger geothermal exploitation since the 70’s. The aquifer’s characteristics are therefore well known thanks to production tests, flow meter logs and NPHI (Neutron porosity logs) logs which give valuable information on aquifer porosity, intrinsic transmissivity, number and thickness of productive layers and interstrata.

Then the numerical model used in this study is built using the constraints provided by the “Dogger database” as well as the scheme of the heat storage exploitation. The conceptual model used for hydrothermal modeling is based on one or multiple-layers structure that represents the reservoir (deep geothermal resource/aquifer). Note that the thickness of the aquifer is still 10 m using one or multiple layers structure. The model uses a vertical plan of symmetry in the middle of the aquifer (especially to reduce computational time). The two wells are located at the middle of the model and separated by a distance “D”. The domain is a three-dimensional model measuring 10 km x 5 km x 90 m in x, y and z directions, respectively. The model is based on a three-dimensional prismatic meshing with 45 layers and a refined mesh close to the wells and comprised approximately 30,000 cells. The mesh has been generated using the CGAL library (*Computational Geometry Algorithms Library).*

The simulations presented in this study were performed using the ComPASS Platform, which is currently in development (https://charms.gitlabpages.inria.fr/ComPASS/ and http://www.anr-charms.org/page/compass-code). ComPASS aims at being an open, evolutive platform for hydrothermal modeling. It implements state of the art numerical scheme to discretize multiphase Darcean flows on generic unstructured meshes. The reader interested in further details is referred to the works of Xing et al., (2017) for the description of the theoretical and numerical aspects of the modeling of compositional multiphase flows in fractured media, Beaude et al.,(2017) for the integration of complex well architectures (Beaude et al., 2017b) and the specification of complex boundary conditions (Beaude et al., 2018).

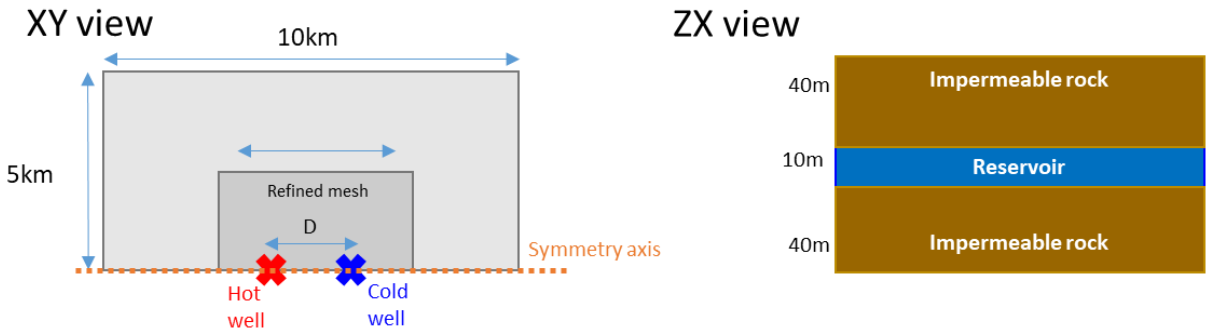

Figure 27: Geometry of the numerical model.

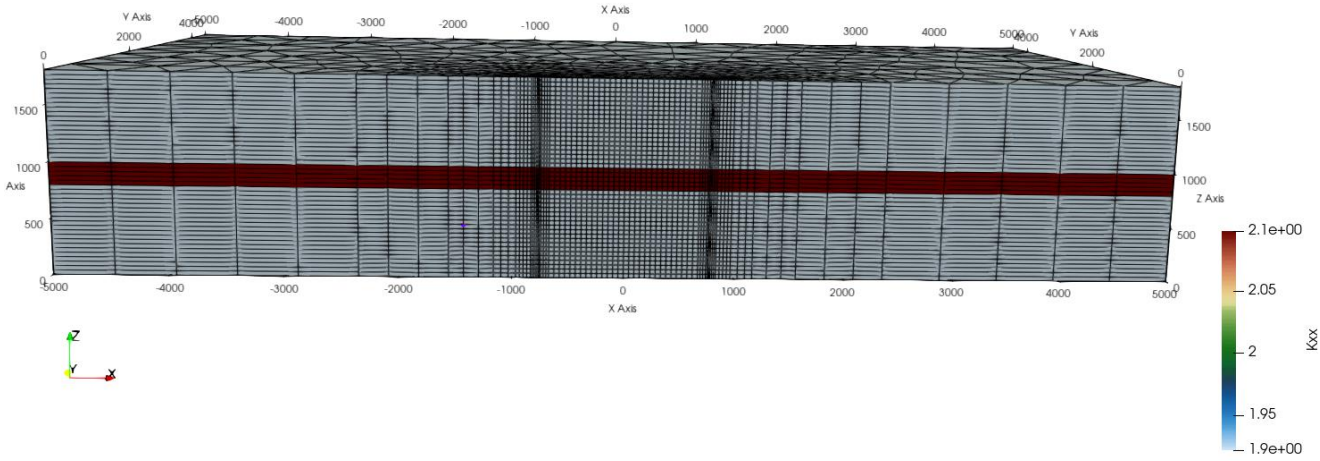

Figure 28: Geometry with the prismatic meshing of the numerical model (vertical exaggeration: 20) Example with the one layer (10m) structure for the reservoir.

The ATES system considered in this study produces a hot plume in the reservoir around the hot storage well during the summer period (the hot well operates as an injector while the cold well is a producer) and a cold plume around the cold storage well during the winter period (the cold well operates as an injector while the hot well is a producer). The ATES system was simulated for approximately 15 one-year cycles (depending on the parameters issued from the statistical methods, see 55), where each cycle consists of (see on example in Figure 33):

- 10 to 15 weeks of hot fluid storage at a constant flow rate ranging from 175 to 375 m^3/h and at a temperature ranging from 75 to 115°C, while water is unloading from the cold well;
- 30 to 35 weeks of hot fluid unloading at a constant flow rate;
- 3 weeks delay time at the end of each period.

Note that, this baseline operating conditions is a hypothesis based on the fact that it maximized the use of geothermal energy on the heating network.

To perform numerical simulations initial and boundary conditions are specified for the model boundaries. For the lateral : North, East and West model boundaries Dirichlet boundary condition are applied (temperature and pressure) and for the South model boundary a no-flow boundary condition is considered (in accordance with the symmetry axis). For the initial state, a hydrostatic state is assumed for the reservoir, the pressure is prescribed in accordance with the depth of the top of the reservoir as well as the initial temperature of the reservoir, which is considered constant on the whole height. Note that the East and West model boundaries are used to prescribed a hydraulic gradient for the reservoir (Figure 29).
The hydraulic and thermal properties are prescribed for the reservoir and the impermeable layers related to a randomly selected simulation scenario (see Table 5).

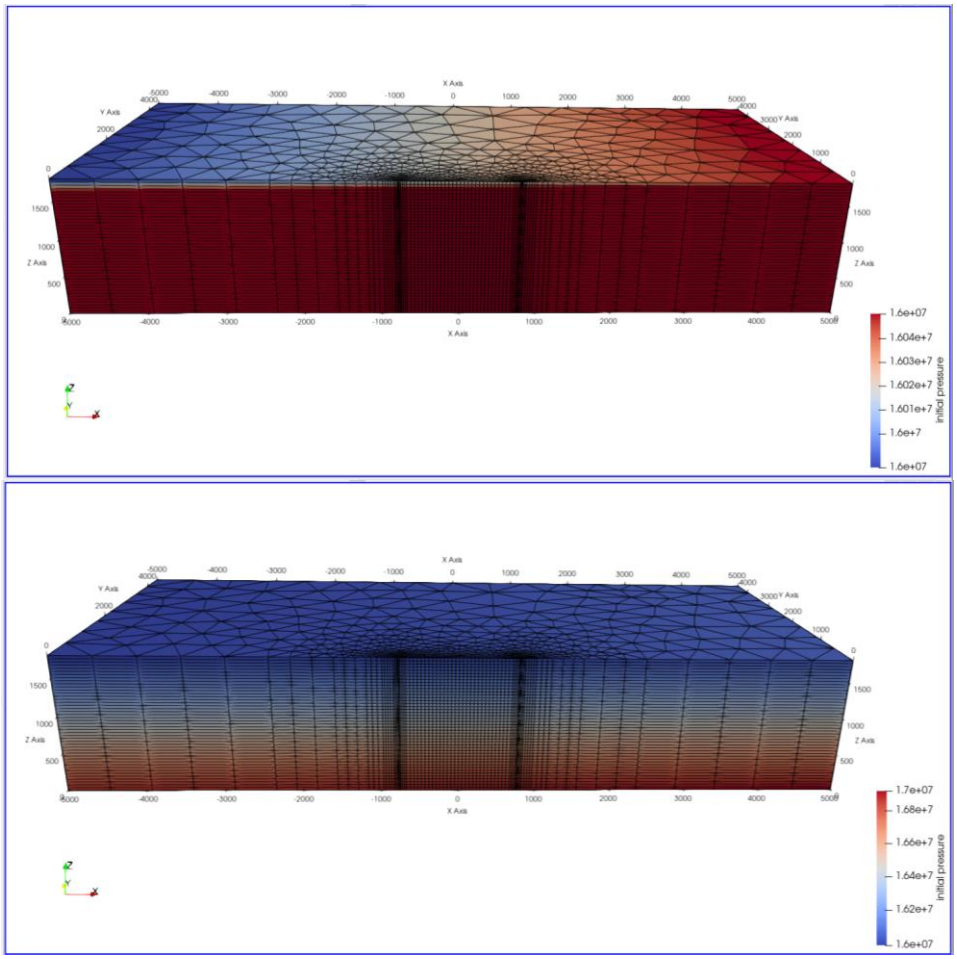

Figure 29: Initial pressure distribution. Top: Hydraulic gradient from the East to the West boundary. Bottom: Initial pressure distribution for the whole domain (hydrostatic).

For this study, 140 numerical simulations were performed; each numerical simulation being related to a randomly selected simulation scenario (reservoir and design parameters). Hereafter, we described the results obtained for one scenario. For that case, the parameters used are summarized (the very precise values indicated here come from statistical averaging over the Dogger database):

- the reservoir structure corresponds to the one-layer scenario (as presented in the Figure 28)
- Distance (D) between the wells : 802.22 m
- Anisotropic condition (x,y,z) : $K_{xx}=K_{yy} > K_{zz}$
- Hydraulic gradient : 0.12 bar/km
- Initial reservoir temperature: 83.56 °C
- Injection temperature (hot well) : 87.78 °C
- Injection temperature (cold well) : 60.62 °C
- Flow rate : 222.22 m^3/h
- Reservoir permeability : $3.8x10^{-12}$ m^2
- Reservoir porosity: 0.1488
- Impermeable layers porosity: 0.0288
- Impermeable layers permeability : $1x10^{-20}$ m^2
- Well radius : 0.1
- Initial reservoir pressure : 160 bar
- Reservoir thermal conductivity : 2.5 $W.m^{-1}.K^{-1}$
- Fluid thermal conductivity : 0.664 $W.m^{-1}.K^{-1}$
- Impermeable layer thermal conductivity : 2.0 $W.m^{-1}.K^{-1}$
- Rock density : 2800 $kg.m^3$
- Rock volumetric heat capacity : $2.5x10^6$ [$MJ/m^3/°C$]

The results are presented in Figure 31 and Figure 32. Figure 31 shows the evolution of the temperature field around the hot and cold wells at different time steps. For the first three snapshots, the hot well is in production phase (unloading) while the cold well is loading the cold fluid (as demonstrated by the arrows that represent the total mass flux). The last snapshot correspond to the temperature field and the mass flux at the end of the simulation (15.7 years). We can observe that after approximately 6 years the cold plume around the cold well reaches the hot well, then the fluid temperature produced at the hot well is decreasing. The Figure 32 present the loading and unloading temperature at the hot and cold well, where the aquifer is initially at a uniform temperature of 83.56°C. We can observe the decrease of the average temperature for the cold well as function of time (formation of the cold plume) and we can notice that the steady state is not reached at the end of the simulation. For the hot well the maximum average temperature increases over time (for the loading phase) and the minimum average temperature (for the unloading phase) increases to approximately 6 years and then decreases due to the extent of the cold plume.

The parallel computation implemented into the ComPASS platform makes it possible to obtain reasonable computation times. This simulation was performed using 4 MPI (Message Passing Interface) processes and the total computation time in minutes obtained was 106 minutes. For all numerical simulations performed (using 4 MPI processes), the total computation time for each case ranged from less than 1 hour to 14 hours (Figure 30). Note that the computing time is less than 2 hours for more than 75% of the simulations performed.

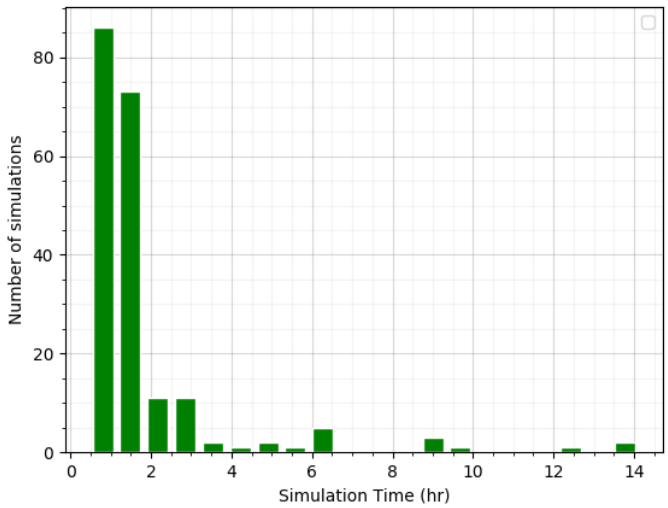

Figure 30 : Histogramm of computing time.

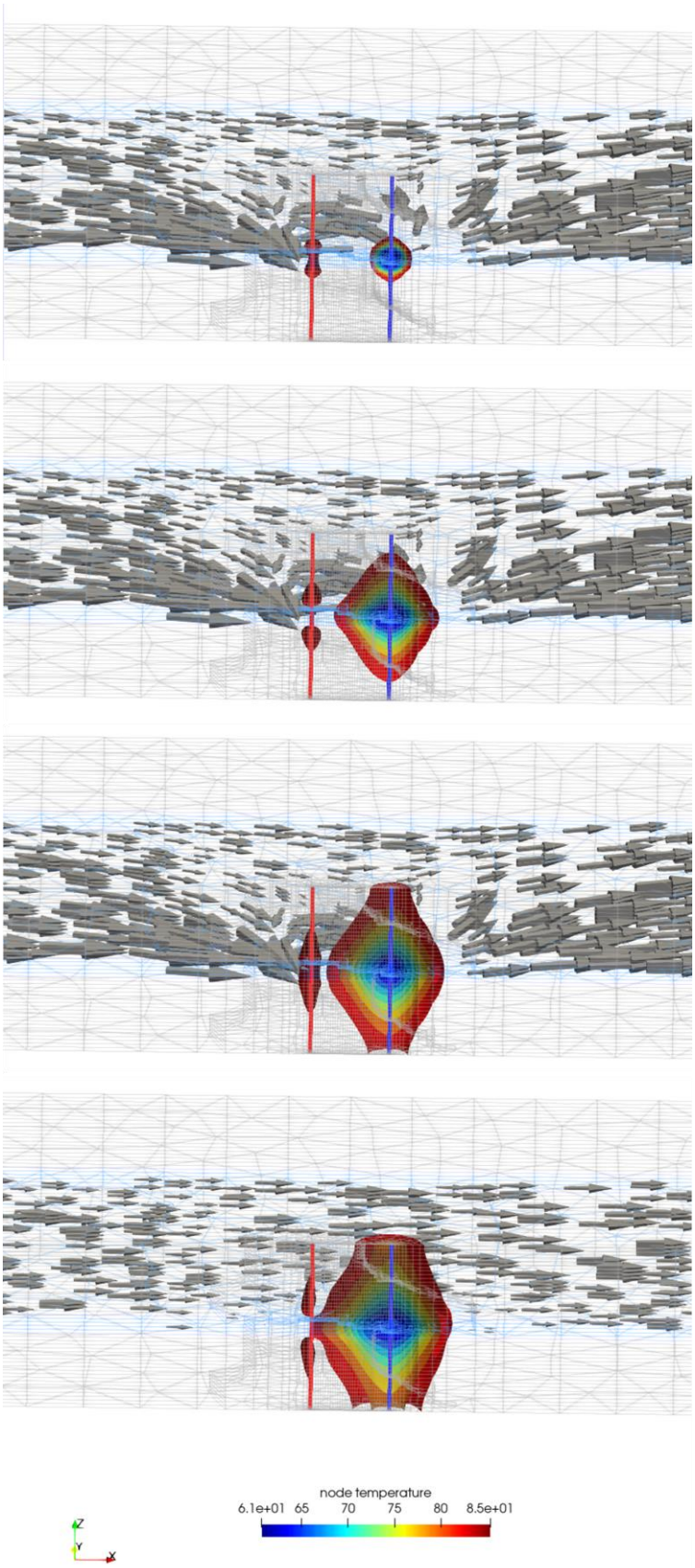

Figure 31: Contours of temperature field around the wells (hot in red, cold in blue) at different time steps (0.7, 5.7, 10.7 and 15.7 years). Arrows correspond to the total mass flux within the reservoir.

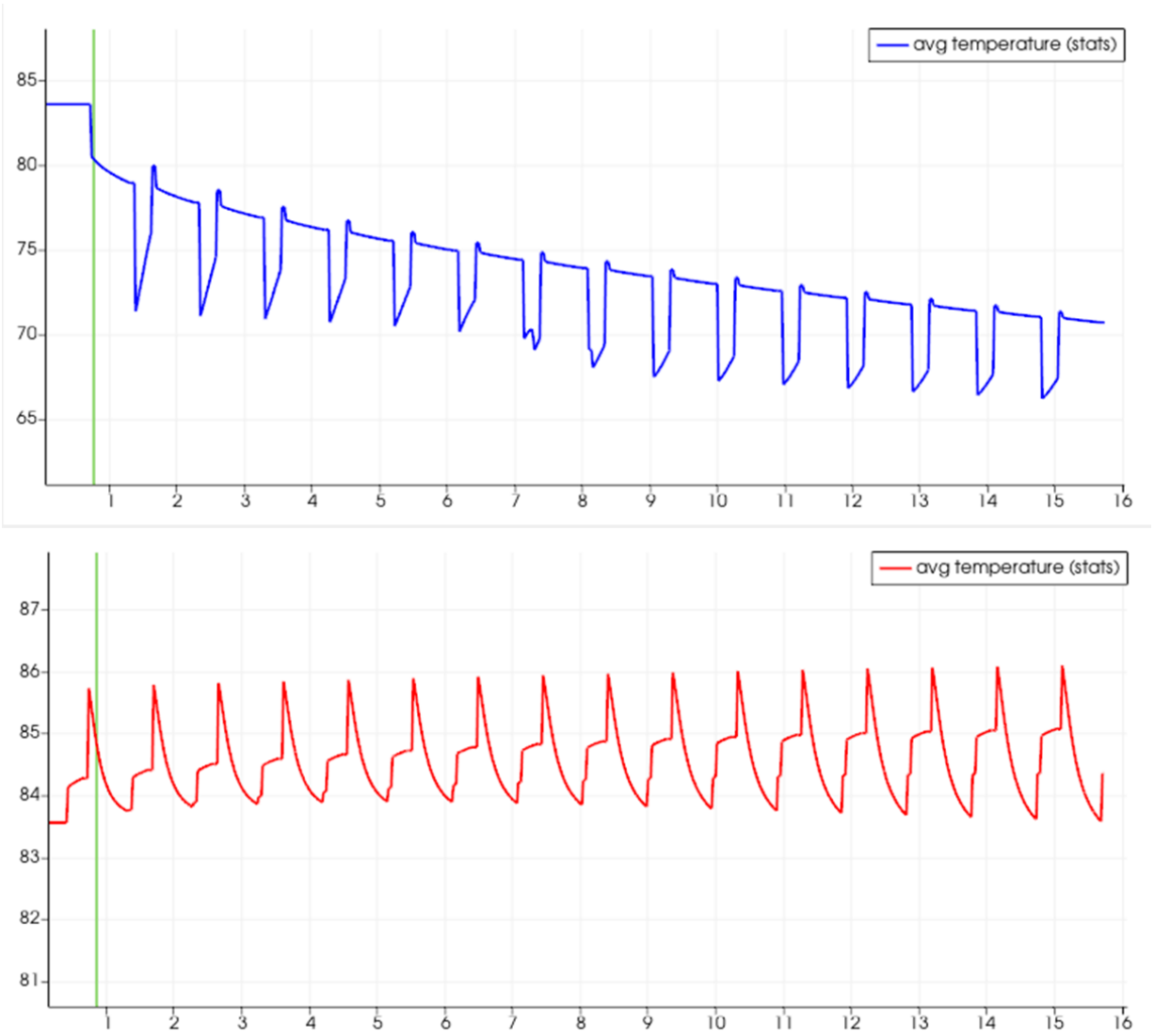

Figure 32: Average temperature curves at the cold and hot wells as function of time.

4.3.2 Input uncertainties

A total of 14 different input uncertainties are accounted for (Table 5). The first category corresponds to design parameters, namely the inter-well distance D and the parameters describing the production cycle at the hot and cold wells. Figure 33 provides an example of production cycle.

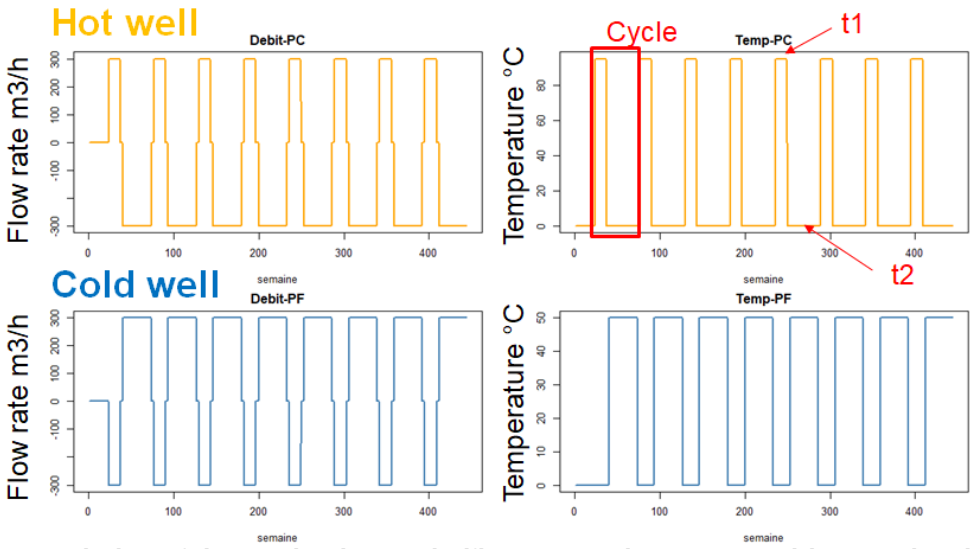

Figure 33: Description of the production cycle (flow rate and temperature) imposed at the hot and cold well.

The second category of input uncertainties relate to the hydro-geological factors and correspond either to the reservoir, caprock properties or to the hydrogeological setting. Note that most of these uncertain parameters correspond to continuous scalar variables, but some correspond to scenario-like variables, i.e. variables that can only take discrete values. These correspond to the reservoir architecture (see Figure 34), regional water flow direction (scenario W-E or E-W), and reservoir permeability anisotropy ($K_{xx}=K_{yy} > K_{zz}$; $K_{xx}>K_{yy}>K_{zz}$; $K_{yy}>K_{xx}>K_{zz}$).

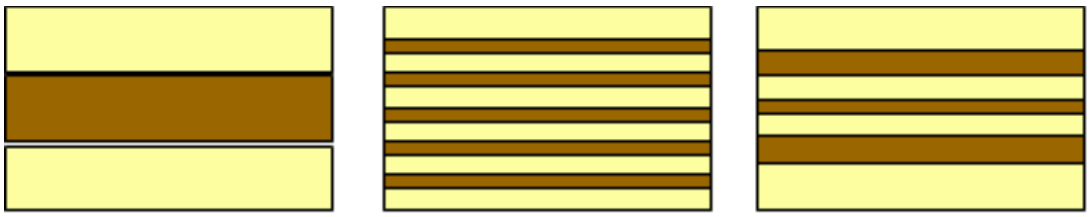

Figure 34: Three scenarios of reservoir architectures.

Table 5. Lower and upper bounds of each parameter. Scenario-like parameters are indicated.

Parameter	Symbol	Lower bound	Upper bound	Unit
Hydrogeological setting				
Gradient	Grad	0.01	0.3	bar/km
Direction	Dir	2 scenarios		
Reservoir				
Intrinsic permeability	K_res	11	12.3	-log10()
Porosity	p_res	10	25	%
Initial temperature	T_res	45	85	°C
Anisotropy	Ani	3 scenarios		
Architecture	Archi	3 scenarios		
Caprock				
Porosity	p_cap	0.1	10	%
Design parameters				
Inter-well distance	D	800	1600	m
Time duration of the 1st part of the stair-like cycle	t1	10	15	weeks
Time duration of the 2nd part of the stair-like cycle	t2	30	35	weeks
Maximum flow rate	Q	175	375	m^3/h
Temperature at the hot well (HW)	T_HW	75	115	°C
Temperature at the cold well (CW)	T_CW	30	65	°C

4.4 Statistical methods

4.4.1 Overall procedure

The proposed procedure holds as follows:

Step 1. Computer experiments

- Define a limited number *n* of random configurations for the uncertain parameters;
- Perform *n* numerical simulations;
- Compute the energy (storage / reproduction) over time (similarly as for Figure 25).

Step 2. Metamodelling

- Set up (construct) a metamodel at each time step to replace the long-running numerical code;
- Validate the predictability of the metamodel at each time instant;
- Technical details are provided in section 4.4.2.

Step 3. Uncertainty analysis

- Decompose the uncertainty into contributions of each uncertain parameters. These contributions correspond to sensitivity measures;
- The analysis is performed at the different time instants;
- Technical details are provided in section 4.4.3.

4.4.2 Metamodelling

A metamodel aims at approximating the computer code's output (here the energy) as a function of the scenario parameters ***x*** (the design and reservoir parameters) using a limited number of numerical simulation results *n*; each numerical result being related to a randomly selected configuration of the scenario parameters. Figure 35 provides a schematic overview of the approach.

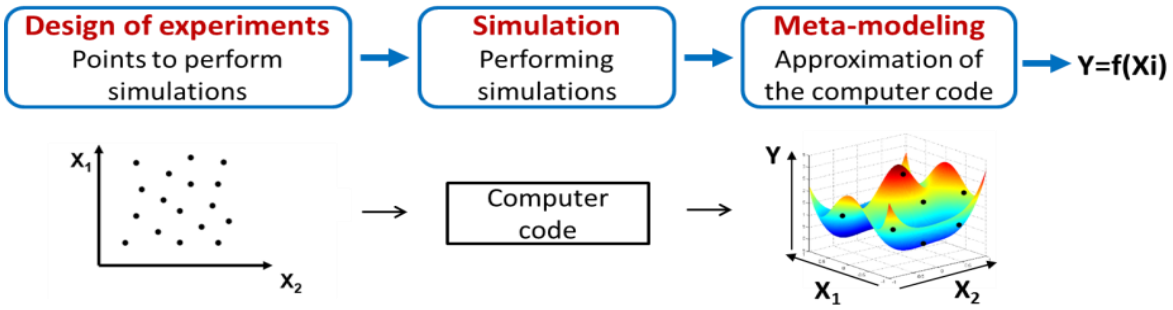

Figure 35: Schematic overview of the metamodeling approach.

The selected metamodeling technique is the kriging method (also known as Gaussian Process GP) which enables to learn in a nonparametric manner the statistical link between the scenario parameters and the energy. Basic concepts are briefly described in the following for the scalar case. For a more complete introduction to kriging metamodelling and full derivation of equations, the interested reader can refer to Roustant et al. (2012).

A practical difficulty in our case is related to the account of scenario-like inputs (reservoir architecture, regional water flow direction, and permeability anisotropy). To integrate these types of variable in the metamodel, we rely on the recent developments by Roustant et al. (2020).

Let us consider the set of d continuous input variables $\mathbf{x}=(x_1,\ldots,x_d)$, and the set of J categorical inputs $\mathbf{u}=(u_1,\ldots u_J)$ with $L_1,\ldots, L_J$ levels that represent the scenario-like inputs. The output *y* is then computed using the numerical environmental simulator f(.) as $y = \mathrm{f}(\mathbf{x},\mathbf{u}) = \mathrm{f}(\mathbf{w})$. In the context of GP metamodelling, the function f(.) is assumed to be a realization of a GP ($Y(\mathbf{w})$) with a constant mean *m* and a covariance function *k*(.,.), named kernel, that can be written as follows:

$$\forall \mathbf{w},\mathbf{w}', \mathrm{k}(\mathbf{w},\mathbf{w}') = \mathrm{cov}\big(Y(\mathbf{w}), Y(\mathbf{w}')\big) \quad (1)$$

Let denote $(\mathbf{w}^1,\ldots,\mathbf{w}^n)$ the training samples and $\boldsymbol{y} = (\mathrm{y}^1 = \mathrm{f}(\boldsymbol{w}^1),\ldots, y^n = \mathrm{f}(\boldsymbol{w}^n))$ the corresponding results. The prediction at a new observation $\mathbf{w}^*$ is given by the kriging mean $\hat{Y}(\mathbf{w}^*)$ as follows:

$$\hat{Y}(\mathbf{w}^*) = \mathrm{E}(Y(\mathbf{w}^*)|Y(\mathbf{w}^1) = y^1,\ldots,Y(\mathbf{w}^n) = y^n) = m + \boldsymbol{c}_{\mathbf{w}^*}^T.\mathbf{C}^{-1}.(\boldsymbol{y} - m\mathbf{I}) \quad (2)$$

where **C** is the covariance matrix between the points $Y(\mathbf{w}^1),\ldots,Y(\mathbf{w}^n)$ whose element is $C[\mathrm{i},\mathrm{j}] = k(\mathbf{w}^i,\mathbf{w}^j)$; $\boldsymbol{c}_{\mathbf{w}^*}$ is the vector composed of the covariance between $\mathrm{Y}(\mathbf{w}^*)$ and the points $Y(\mathbf{w}^1),\ldots, Y(\mathbf{w}^n)$, and **I** is the vector of ones of length n.

The prediction at $\mathbf{w}^*$ can be associated to an error estimate provided by the kriging variance $\hat{\sigma}^2$ given by:

$$\hat{\sigma}^2(\mathbf{w}^*) = \mathrm{Var}(Y(\mathbf{w}^*)|Y(\mathbf{w}^1) = y^1,\ldots,Y(\mathbf{w}^n) = y^n) = \mathrm{C}(\mathbf{w}^*,\mathbf{w}^*) - c_{\mathbf{w}^*}^T.\mathbf{C}^{-1}.c_{\mathbf{w}^*} \quad (3)$$

Accounting for a mixture of input variables' types - continuous or categorical (ordinal or nominal) - is made via the covariance function $k(\mathbf{w},\mathbf{w}')$. Here, it is assumed to be the tensor product of the covariance function for the continuous inputs $k_{\mathrm{cont}}(\mathbf{x},\mathbf{x}')$ and the one for the categorical inputs $k_{\mathrm{cat}}(\mathbf{u},\mathbf{u}')$ as $k(\mathbf{w},\mathbf{w}') = k_{\mathrm{cont}}(\mathbf{x},\mathbf{x}')\prod_{i=1}^{J} k_{\mathrm{cat}}^i(u_i,u'_i)$. Hence, the covariance function k_{cont} can be described by kernel models that are commonly-used in the computer experiment community. In the present study, we restrict the analysis to the stationary two differentiable Matérn 5/2 model (Santner et al., 2003).

The categorical covariance functions $k_{\mathrm{cat}}^i\ (i = 1,\ldots,\mathrm{J})$ can be described in different manners (Roustant et al., 2020). In our case, we assume that the variable of interest (here the energy) will act differently depending on the considered scenario, but without excluding some dependencies between these different responses, k_{cat} can then be described by the most general (and complex) dependence structure where each pairwise

coefficient can take a different value depending on the considered levels u, u'. The covariance function reads as follows:

$$k_{\text{cat}}^{\text{Gen}}(u,u') = \begin{cases} c_{u,u'} & \text{if } u \neq u' \\ v_u & \text{if } u = u' \end{cases} \quad (4)$$

When constructing a GP metamodel, a key issue is related to its *predictability*, i.e. whether the GP model is capable of predicting "yet-unseen" input configurations, i.e. samples that have not been used for training. This can be examined by using cross-validation approaches (e.g. Hastie et al., 2009). To measure predictability, the performance indicator, denoted Q^2, is defined to measure the deviation from the true output value. Given a test set $\boldsymbol{T}$, Q^2 is defined as follows:

$$Q^2 = 1 - \frac{\sum_{i \in \boldsymbol{T}} (y_i - \hat{y}_i)^2}{\sum_{i \in \boldsymbol{T}} (y_i - \bar{y})^2} \quad (5)$$

where $\hat{y}_i$ is the ith GP-based prediction of the model output y_i, and $\bar{y} = \frac{1}{|\boldsymbol{T}|} \sum_{i \in \boldsymbol{T}} (y_i)$ is the average value for the test set. A coefficient Q^2 close to 1.0 indicates that the GP model is successful in matching the new observations that have not been used for the training. A typical threshold of 80% is often used to evaluate the validation quality.

4.4.3 Variance-based Sensitivity Analysis

In order to quantify the contribution of each uncertainty source (Table 5) to the overall uncertainty (measured by the variance) of the energy, we rely on a global sensitivity analysis which presents the advantages of exploring the sensitivity in a global manner by covering all plausible scenarios for the uncertainties and by fully accounting for possible interactions between them. In the present study, we opt for a variance-based global sensitivity analysis, denoted VBSA (Saltelli et al., 2008), which aims at decomposing the total variance of the energy into the respective contributions of each uncertainty; this percentage being a measure of sensitivity and can be modelled by the Sobol' indices.

Formally, let us consider the *n*-dimensional vector $\boldsymbol{X}$ as a random vector of random input variables X_i (i=1,2,…,*d*) that are assigned to the uncertainties described in Table 1. VBSA determines the part of the total unconditional variance Var(*Y*) of the energy resulting from each input random variable X_i. Formally, VBSA relies on the first-order Sobol' indices – also named as "main effects" (ranging between 0 and 1), which can be defined as:

$$S_i = \frac{\text{Var}(\text{E}(Y|X_i))}{\text{Var}(Y)} \quad (6)$$

where E(.) is the expectation operator.

The index S_i corresponds to the main effect of X_i, i.e. the proportion of the variance reduction of *Y* (i.e. representing the uncertainty in the energy) that is solely induced by varying X_i. The higher the influence of X_i, the lower the variance when fixing X_i (corresponding to the term $Var(Y|X_i)$ in Eq. 6), hence the closer S_i to one. Thus, this index provides a measure of importance useful to rank in terms of importance the different input parameters within a "factors' prioritizing setting" (Saltelli et al., 2008). Higher order Sobol' indices can also be defined by evaluating $Var\big(E(Y|X_i, X_j)\big)$, and represent the combined effects of the parameters X_i, X_j. A measure of these higher order interaction terms is $1 - \sum S_i$, which is generally ≤1; the closer to one, the higher the interactions (see Saltelli et al., 2008).

In practice, Monte-Carlo sampling procedures are used to estimate S_i, hence the need for a combination with metamodeling to alleviate the computational burden when the computer code is expensive to evaluate (e.g. Manceau and Rohmer, 2016).

In our case, an additional difficulty is related to the presence of dependence among the input variables, namely the reservoir initial temperature (T_res), the HW and CW temperatures (T_HW and T_CW), which makes the interpretation of Eq. 6 as a variance contribution more difficult. To overcome this problem, we rely on the approach proposed by Jacques et al. (2006), which consists in estimating the main effect for the group of variables (T_res, T_HW, T_CW).

4.5 Results

We use a series of 140 numerical simulations; each numerical simulation being related to a randomly selected simulation scenario (reservoir and design parameters). The random selection was performed by combining the Sliced Latin Hypercube Design approach by Ba et al. (2015) and a filtering approach to ensure physical constraints on the temperature (i.e. T_res>T_CW and T_res<T_HW). Figure 25 provides some examples of simulation results for the storage and re-production phase.

On this basis, a GP metamodel is constructed at each time instant to predict the amount of energy during the storage and re-production stage. Figure 36 (top) provides the time evolution of the Q^2 performance indicator (calculated based on 10-fold cross validation procedure) for the storage phase. This shows that over time, the predictability remains of satisfactory level. This is also confirmed by checking the predicted values versus the "true" simulated ones (Figure 36, bottom). Similarly Figure 37 provides the analysis for the reproduction phase, which shows similar satisfactory predictability level.

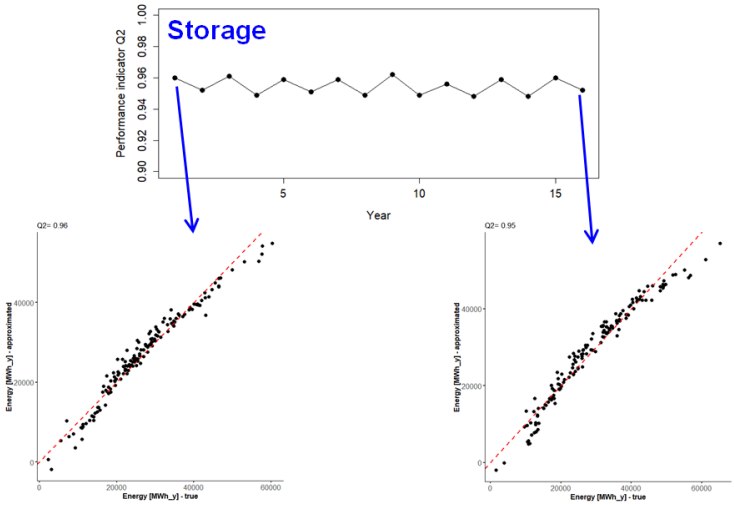

Figure 36: (top) Time evolution of the Q^2 performance indicator (calculated based on 10-fold cross validation procedure) for the storage phase. (bottom) Predicted values versus the "true" simulated ones.

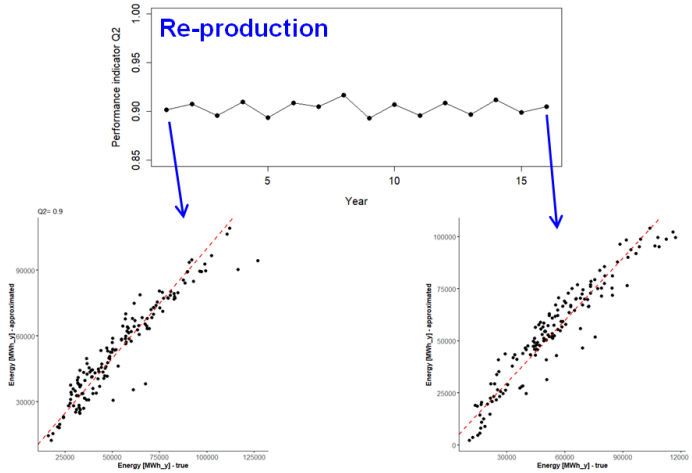

Figure 37: (top) Time evolution of the Q^2 performance indicator (calculated based on 10-fold cross validation procedure) for the re-production phase. (bottom) Predicted values versus the "true" simulated ones.

Once the metamodels are validated, we can use them to compute the main effects using the Monte-Carlo-based approach of Jacques et al. (2006) with >100,000 random simulations. Clearly the computation would have not been feasible with the computer model described in section 4.3.

The results for both phases are provided in Figure 38. Several conclusions can be made:

1) This shows the huge importance of the temperature parameters (T_res,T_HW, T_CW) with a variance contribution (main effect) of ~50% (stored energy - Figure 38(a)), and of ~75% (re-produced energy - Figure 38(b)).
2) Based on the values of the main effects, we can also identify, the flow rate Q (with a contribution of ~20-25%) as well as the time duration t1 (stored energy only, with a contribution of ~10%) as the second most important parameters.
3) The influence of the afore-mentioned parameters appears to be quasi- constant over time; at the exception of the stored energy, where the temperature parameters' influence decreases from 75 to 50% over the first two years.
4) The hydro- geological factors do not seem to influence much (in comparison to the design parameters).

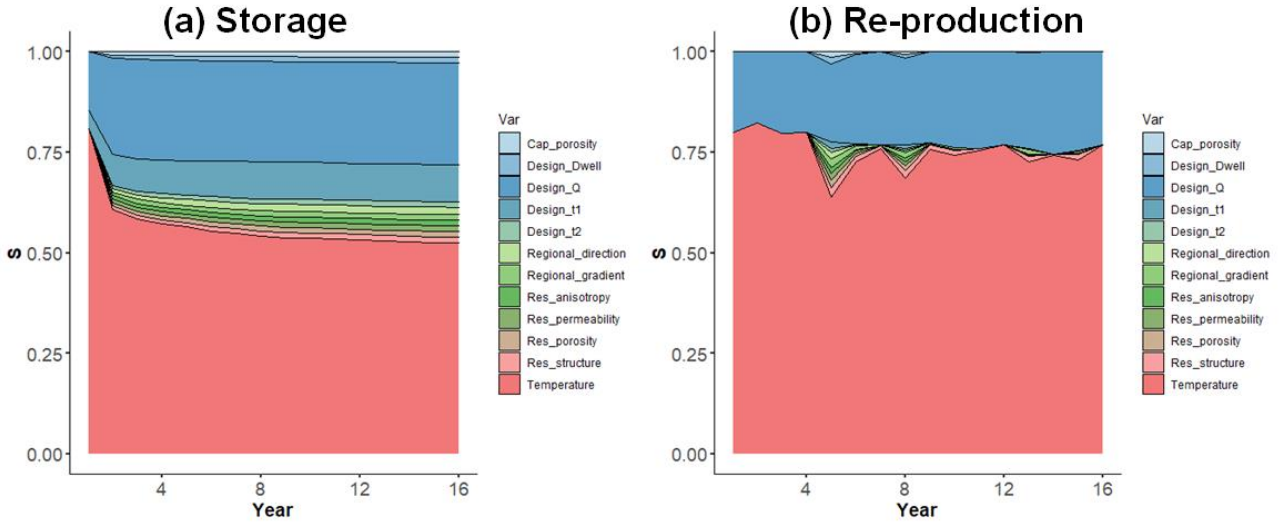

Figure 38: Main effects computed for the different input uncertainties for the storage (a) and the re-production phase (b).

4.6 Towards metamodel-based time series prediction

A major assumption of our analysis is that we construct a metamodel at each time instant. This imposes to process 16 different metamodels (one for each time step), which can be difficult in practice.

A possible improvement could consist in reducing the dimension of the time series through Singular Value Decomposition SVD, as proposed for instance by Rohmer et al. (2016) in the context of ocean modelling. This consists in projecting the set of time series (normalized, Figure 39, top-right) onto a limited number of new mathematical basis (called SVD1,2, and 3).

Figure 39 shows the respective projection of the original data onto SVD1, 2, and 3 as well the reconstruction and the corresponding residuals (Figure 39, bottom, left). Interestingly the reconstruction error using only three basis is very satisfactory: this shows that the dimension of the time series can be reduced from 16 to 3, i.e. only three metamodels could be constructed (instead of 16).

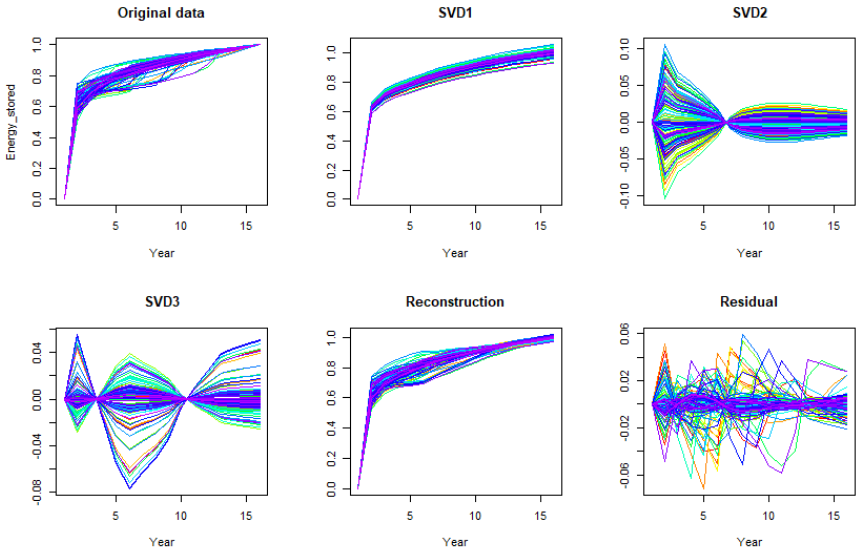

Figure 39: Application of Singular Value Decomposition to the set of energy time series during the storage phase.

The comparison of the predictions using the SVD-based metamodels with the original ones shows satisfactory predictability results (Figure 40). This confirms that this approach constitutes a promising direction for further research.

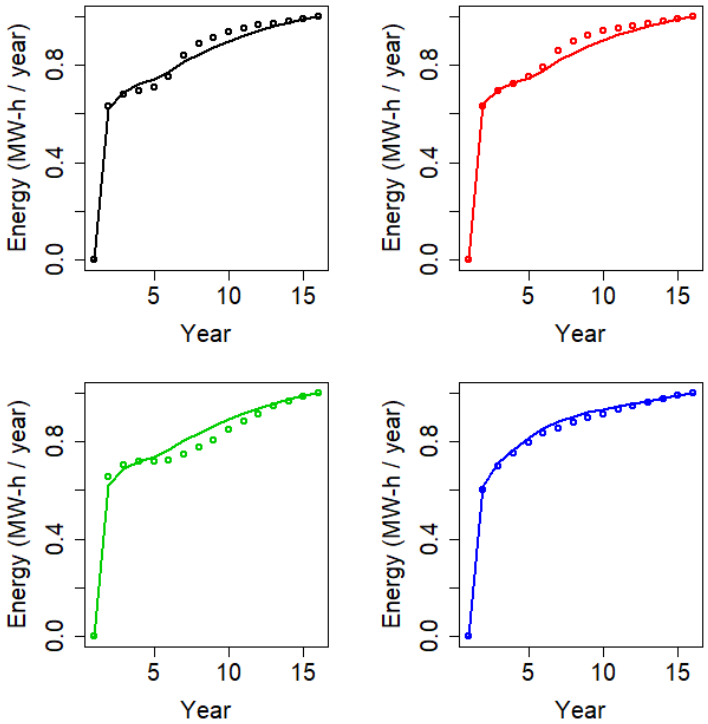

Figure 40: Comparison between four time series (dots) of normalized energy during storage phase with the predictions using metamodels (straight lines) constructed using the time series projected onto 3 SVD basis (see Figure 39).

5 Uncertainty in geological modelling

In the two previous case studies, numerical models used simplified representation of geological characteristics: we assumed parallel layers, with constant thickness and with homogeneous properties. These conceptualization choices were made by geologists and hydrogeologists in order to represent as faithfully as possible and with limited complexity the main processes, in the absence of sufficient data to elaborate a geological model. Depending on the modelling purposes, on the considered scale and on the density of data, a more refined geological modelling may be proposed. Such a geological model can be more or less detailed and more or less certain, and the uncertainty of the subsurface geological model will be part of the overall uncertainty of the entire storage system. In this section, we introduce the main issues related to geological modelling as well as the two different kinds of assessments that may be deployed: qualitative assessment vs. quantitative assessment.

5.1 Challenges

When dealing with modelling of Underground Thermal Energy Storage (UTES) systems, a geological model of the subsurface is inevitably part of the model-representation of the system. The requirements for detailing the geological model will typically increase from PTES (Pit Thermal Energy Storage) to BTES (Borehole Thermal Energy Storage) to ATES (Aquifer Thermal Energy Storage) and with models for MTES (Mine Thermal Energy Storage) being partly geological, partly “technical”.

When establishing geological models representing the subsurface geological conditions in more or less detail, they are always subject to a certain degree of uncertainty. All the different types of data involved in the geological interpretation of a given area and the correlation between different points - or spatial information are subject to different specific uncertainty and the data density and its variations throughout the model area introduces uncertainty. There can be specific uncertainties on measured data and/or processing of data, e.g. geophysical data like DC (Direct Current) or EM (Electro-Magnetic) data, well log measurements and seismic data/GPR (Ground Penetrating Radar) data, but there can also be more subjective uncertainties related to the interpretation of such data as well as on the more direct geological information like descriptions of borehole samples or cores (Sandersen, 2008).

Borehole data are often/sometimes regarded as “hard data/hard evidence”, and this may count for cores from boreholes, which are unfortunately very costly and therefore often rare for shallow applications. But for other types of borehole samples, it can be questioned if the sample represents the depth interval assumed and if all the material from a given depth is represented in the sample, and thereby what the sample actually represents, depending on the actual drilling method. For example, with rotary drilling and air lift drillings, the finer sediments can be flushed out and the driller could potentially misinterpret a clay layer as more sandy (Høyer et al. 2017). Also, the sample interval can vary over time and with purpose of drilling, with more samples obviously resulting in a higher certainty than few samples. During the geological modelling phase, a skilled geologist should go through all the borehole records, check for inconsistencies and assign a quality rating to each borehole, based on these different pieces of information.

Hence, the uncertainty of a given subsurface geological model cannot easily be quantified, but depends to a large extent on the amount and nature of available data, the geological complexity of the model area, the type, detail and focus of the model itself, and the uncertainty may also vary within the modelled area.

A geological model will always be (much) simpler than the actual geological conditions, and the key of successful geological modelling relies on making the right choices and interpretations in the process of simplifying more or less complex geological conditions to something which is relevant and feasible within the frame of a given project in terms of resources, deadlines and needs.

And when first the geological model is established, this model may even be further simplified for calculation purposes, e.g. for groundwater modelling/thermal modelling and/or modelling of combined energy systems involving the dynamics of the subsurface in one way or the other.

There are different ways to assess the uncertainty of geological models and hence their contribution to further purpose-specific modelling (again e.g. hydrological/thermal/energy system modelling).

5.2 Qualitative assessment

Sandersen (2008) proposes a simple method for qualitative assessment of the uncertainty of cognitive layer-based geological models, taking the uncertainties related to the data sets, the density of data points, as well as the uncertainties related to the geological interpretations into consideration.

As described above, the construction of geological models typically includes the use of several different data sets, each with their own uncertainties. When combining these data sets, uncertainties related to the geological interpretations are introduced, in addition to the uncertainties of the individual data sets as well as uncertainties related to differences in data types and data density within the model area.

A quantification of the uncertainties may be carried out objectively for the individual data sets based on equipment, sampling, processing, data interpretation etc., but this can be complicated and time-consuming. Besides, the uncertainties of the individual data sets are not necessarily additive. On the contrary, the data sets typically support each other, resulting in a lower degree of uncertainty of the model as a whole.

Highly subjective decisions in the geological interpretation are made based on a combination of the data, knowledge about the methods providing the data and knowledge of the geology of the area. Assessment of the uncertainties of the geological model can be made using a qualitative approach. Sandersen (2008) suggest assessing and communicating the uncertainty of a geological model to the users of the model by e.g. visualization along selected and regularly spaced profiles.

The assessment of uncertainties of the geological model is performed after the geological modelling is completed along geological profiles also displaying the available geological and geophysical data. It comprises a subjective assessment of the data uncertainties as well as the uncertainty introduced by geological interpretations and by modelling. Accordingly, the assessment reflects the geologist's own evaluation of the reliability of the model interpretation along the profile. The degree of uncertainty can be divided into a number of intervals and drawn onto the profiles with coloured or shaded bars above the profile. It can further be visualized on a map, thus giving an overview of the entire model area. The following uncertainty intervals are suggested as an example:

- Low uncertainty of the geological model interpretation: an adequate amount of reliable data ensures that a credible geological interpretation can be made. The data can stand alone and the interpretation is not dependent on data from adjacent areas.
- Intermediate uncertainty of the geological model interpretation: A limited amount of data and/or lower data quality. The geological interpretation is to a certain degree made on the basis of information from adjacent areas and from indirect information such as topography or hydraulic head measurements.
- High uncertainty of the geological model interpretation: No, or only a limited amount of data and/or poor data quality. The geological interpretation is primarily based on extrapolations from adjacent areas.

The uncertainty assessments are relative and the intervals used should be adjusted to the area in question in order to obtain a suitable description of the variations. Apart from varying geology, individual geological models will also vary in purpose, degree of detail, data types, etc. Therefore, it is not necessarily possible to compare uncertainty assessments of different geological models and if an existing geological model is to be used for new purposes it can be worth/necessary to examine initial assessments of the quality and uncertainty of the model from when it was established.

Another way to carry out qualitative assessment is to apply a qualitative uncertainty estimate to each interpretation point in the model. In a layer-based model, the layers are typically constructed by placing interpretation points throughout the area and by performing interpolation between these to generate the corresponding stratigraphic surfaces. The initial interpretation points are typically placed at locations with reliable data and when necessary, free interpretation points are added between these to control the surfaces. Each interpretation point can then be assigned a qualitative uncertainty estimate ranging from e.g. 1) low uncertainty to 4) free interpretation point, representing the highest uncertainty (Høyer et al. 2019).

5.3 Quantitative assessment

An approach to obtain more quantitative measures for the uncertainty of geological models, is the use of multiple realisations to illustrate the structural variation based on the given data basis (e.g. Barfod et al., 2018;

Feyen and Caers, 2006; He et al., 2013; Huysmans and Dassargues, 2009; Pirot et al., 2015; Refsgaard et al., 2012; Troldborg et al., 2010). This is done by stochastic modelling using geostatistical methods to establish an interpretation/correlation of the existing data and information. This method can result in establishing a suite of different equally likely models, all representing/reflecting the available data in an acceptable way and the variation of these models is then to some extent reflecting the uncertainty of the geology of the model area and can to some extent be quantified.

Stochastic models have primarily been used to simulate smaller-scale phenomena that cannot be accurately observed or modelled. This can be e.g. hydraulic conductivities varying significantly within the same type of deposit, depending on factors like; (1) sorting, (2) heterogeneity, (3) compaction, and (4) fractures (e.g. Berkowitz, 2002; Keller et al., 1986) and stochastic modelling can be a way of estimating facies-level structural uncertainty and representing the average effect of unresolved phenomena on larger-scale phenomena. There are, however, also recent attempts to setup practical workflows to perform more large-scale geostatistical modelling of e.g. a Miocene succession characterized by large and relatively uniform sand and clay structures in Denmark (Høyer et al 2017).

Recently, machine learning techniques also enabled advances in order to quantify geological uncertainty. This is illustrated on a case study in next section.

6 Underground uncertainty quantification analysis for Geneva demosite using geostatistics and machine learning

In the previous section, we highlighted numerous questions related to the integration of uncertainty concerning rock properties. In the afore-mentioned case studies, we made the choice to represent the rock properties parameters by equivalent values for several reasons: i. difficulty to collect geostatistical information; ii. difficulty to elaborate a 3D numerical model with refined mesh and with reasonable computation time. However, as mentioned in previous sections, it constitutes a limitation of models, and some physical reservoir behaviors cannot be faithfully modelled without considering a complete spatial representation of the reservoir properties such as porosity and permeability. In the present section, the question of correct prediction and representation of rock properties is thus tackled.

Predicting rock properties at unsampled locations and forecasting the future flow behavior of complex geological and engineering systems is difficult and uncertain. This is achieved through reservoir modelling which goals consist of a complete representation of the reservoir properties such as porosity and permeability. Since this is not achievable with accuracy and certainty, we use instead geostatistical techniques to generate multiple realizations. Realizations are typically simulated with a conditional simulation algorithm that respects all available hard data and spatial continuity models. These realizations capture the stochastic uncertainty related to inference of reservoir properties away from *primary* data (e.g., wells) and with correlated *secondary* data (e.g., seismic). Geostatistical simulation techniques allow for full property variability, conversely to the conventional mapping algorithms such as kriging, splines and inverse distance, that remove high frequency property variations. The latter have the goal to reveal the large-scale geological trends, however, for fluid flow problems, the spatial patterns of extreme high and low value of porosity and permeability often have a large effect on the flow response and geostatistical simulation is more appropriate for predicting flow performance and modelling uncertainty.
Machine learning techniques are increasingly applied to geoscience and reservoir modeling (Brusova et al., 2020). Machine learning can be divided into unsupervised and supervised learning. While the former is more adapted for exploratory data analysis in the early stage of reservoir modeling, the latter use labelled datasets to train algorithms that can classify or predict outcomes accurately.
By integrating primary and secondary data, geostatistics and machine learning techniques are powerful tools to accurately predict and quantify uncertainty of reservoir properties.

6.1 Available dataset for the Geneva demosite

Since 1960s, several 2D seismic lines have been acquired in the Geneva area with the scope to explore for hydrocarbons and geothermal potential. As the Figure 41 shows, the seismic lines cover the entire Geneva canton, with a focus on the center and south part of it. Few wells are also available with a depth spanning from few hundreds of meters to 3 km.

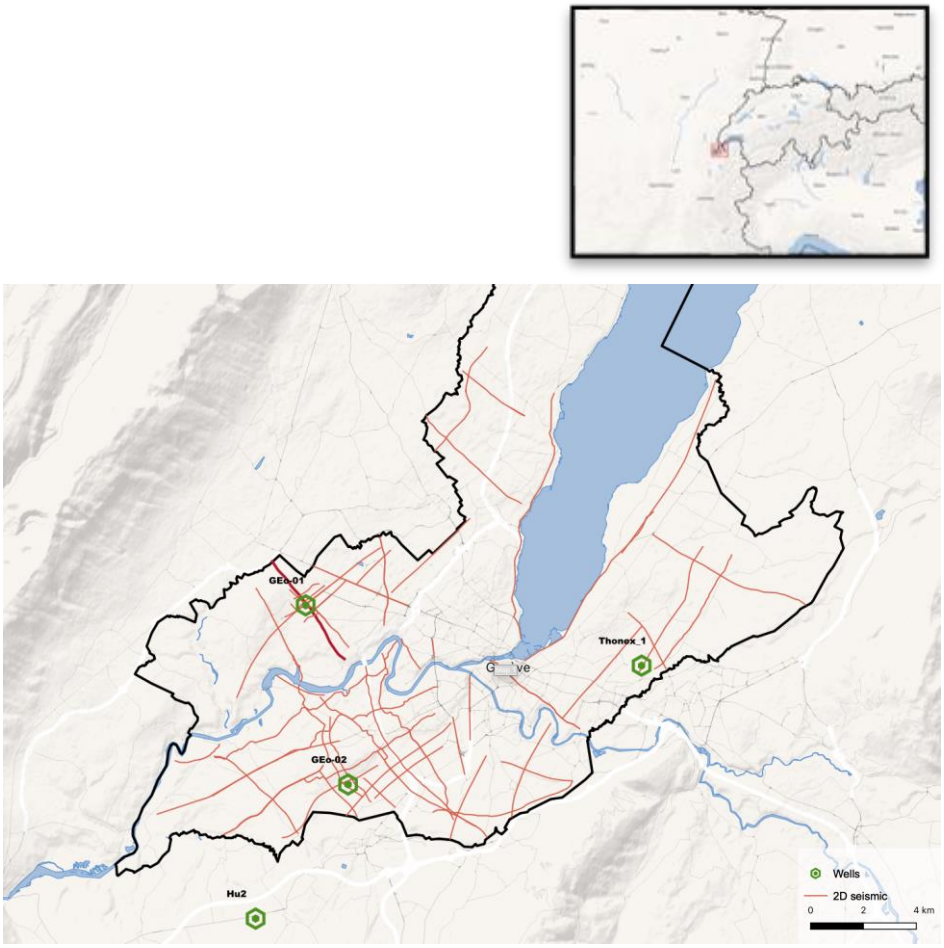

Figure 41: Geneva area available dataset.

6.2 Methodology

Classical methods to obtain reservoir properties from seismic data require a well to seismic calibration, wavelet extraction and estimation of low frequency model. Then a seismic inversion approach is carried out to derive acoustic impedance (AI) and the petrophysical properties of the reservoir such as porosity or geomechanical properties. The inversion of seismic data for elastic properties can be posed as a deterministic problem or as a stochastic problem, i.e., model random parameters characterized by probability densities (Bosch et al., 2010). These techniques work well when the wells could be calibrated to the seismic. However, they are difficult to apply in absence of well or where the wells coverage is sparse, as in the case of the Geneva area.
For this work we propose to apply a machine learning pattern-recognition techniques to the wells to obtain a predictive model that can be then applied to the seismic inverted data to get a porosity field distribution. This distribution is then used as a secondary data in a collocated sequential Gaussian simulation approach to generate realizations of the porosity distribution.

6.2.1 Machine learning applied to the wells

Even if only few wells are available in the Geneva area, some of them go through the whole geological sedimentary sequence of the region. By integrating all the wells in a machine learning approach, we can obtain a predictive model that can be then applied to the seismic dataset.
Machine learning is a subcategory of artificial intelligence which algorithms are exposed to large amount of data to build a predictive model. They can be divided into deep learning algorithms and traditional machine learning algorithms. Generally, traditional machine learning algorithms are best suited for problems that involve "small" amounts of data (< 500k) and deep learning performs better when the amount of data is huge as shown in the Figure 42.
We applied an Extreme Gradient Boosting or XGBoost algorithm (Chen et al., 2016), that uses decision tree ensemble models, which consist of a set of classification and regression trees (Breiman et al., 1984). Those

trees are poor models individually, but when they are grouped, they can be really performant. XGBoost builds really short and simple decision trees iteratively. Each tree is called a "weak learner" for their high bias. XGBoost starts by creating a first simple tree which has poor performance by itself. It then builds another tree which is trained to predict what the first tree was not able to and is itself a weak learner too. The algorithm goes on by sequentially building weaker learners, each one correcting the previous tree until a stopping condition is reached, such as the number of trees (estimators) to build.

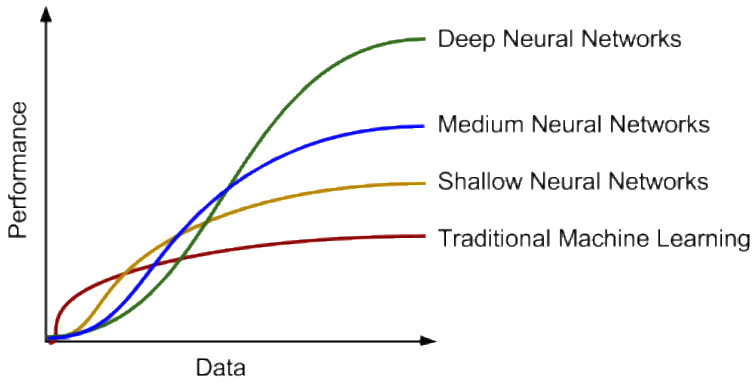

Figure 42: Performance of machine learning algorithms vs. amount of (labelled) data. Image source: deeplearning.ai

Gradient boosting is currently one of the most popular techniques for efficient modelling of tabular datasets of all sizes. It is a very fast, scalable implementation of gradient boosting that has taken data science by storm, with models using XGBoost regularly winning many online data science competitions and used at scale across different industries.

Some pre-processing is needed to prepare the well data for the training phase. While some wells have a complete set of well logs measurements, such as compressional sonic (DT), neutron porosity (NPHI) and bulk density (RHOB), others need some rock physics modelling to retrieve these data. The objective of the pre-processing phase is to build a well database in which we have AI values (i.e., the product of the bulk density and the compressional waves velocity) and porosity values, for the entire sedimentary sequence of the Geneva area. This dataset is then used by the XGBoost algorithms to learn (and train) the AI response on the neutron porosity and build a predictive model. The trained model is then applied to the seismic inverted data to obtain a ML porosity distribution for each seismic section. The inverted seismic data are obtained through a colored inversion (Lancaster and Whitcombe, 2000).

6.2.2 Geostatistical realization of porosity

The ML porosity distribution obtained in the previous section is deterministic and do not account for uncertainty quantification. To assess porosity distribution uncertainty, we propose to use the ML result obtained in the previous section as a secondary data, in a sequential Gaussian simulation workflow that employs collocated cokriging under a Markov model (Xu et al., 1992, Almeida and Journel, 1994, Goovaerts, 1997). This approach is commonly applied to integrate seismic data and to cosimulate multiple variables.
While the well data provide the most accurate measurements of depths there are rarely enough wells to permit an accurate appraisal from well data alone. On the other hand, the seismic data are generally less precise but more abundant.
The proposed sequential Gaussian cosimulation approach use a Markov model II (Journel, 1999) of coregionalization to model the cross variogram between the few available primary data, which is the porosity form well logs, and the secondary data which comes from the ML porosity distribution result of the previous section. This model assumes that secondary data Y prevail over primary data Z and the cross-variogram is given by

$$C_{ZY}(h) = B \cdot C_Y(h)$$

where B = $\sqrt{\sigma_Z^2/\sigma_Y^2}\cdot\rho_{ZY}(0)$, σ_Z^2, σ_Y^2 are the variances of primary and secondary data respectively, and $\rho_{ZY}(0)$, is the correlation coefficient of collocated data. The application of this model of coregionalization requires the covariance of the secondary data variable ($\sigma_Y^2 - \gamma_Z(h)$) and the correlation coefficient of collocated data. The covariance of the secondary data is defined by the experimental variogram that is a chart of geological variability vs direction which is calculated from the results obtained in the previous section.
We then compute 50 stochastic realizations of porosity distribution that are then postprocessed to quantify local uncertainty.

6.3 Results

The XGBoost porosity field distribution for the seismic line GG8702, located in the NW of the Geneva canton and represented in bold on Figure 41, is presented at Figure 43a. This porosity distribution corresponds to the secondary data for the collocated sequential Gaussian simulation algorithm. Since the variogram cannot be fit reliably form the primary data (well logs measurements), we apply a Markov model II of coregionalization model and fit the variogram on the secondary data, and we fix the correlation coefficient of collocated data to 0.7. Figure 43b and c show the variogram for the major and minor direction of spatial continuity, with the modeled parameters that are then used in the collocated sequential Gaussian simulation workflow.
Figure 44 shows the results of the geostatistical workflow. The postprocessing analysis of the 50 realizations focus on a few local statistical summaries such as the local expectation (e-type) and the conditional standard deviation which correspond to the local standard deviation over the entire set of realizations. The local expectation (Figure 44d) can be considered as a smoothed mean of the fifty realizations. Figure 44c shows the local standard deviation of the fifty realizations. As expected, the uncertainty is higher away from the well data, which are primary data used in this collocated simulation approach.

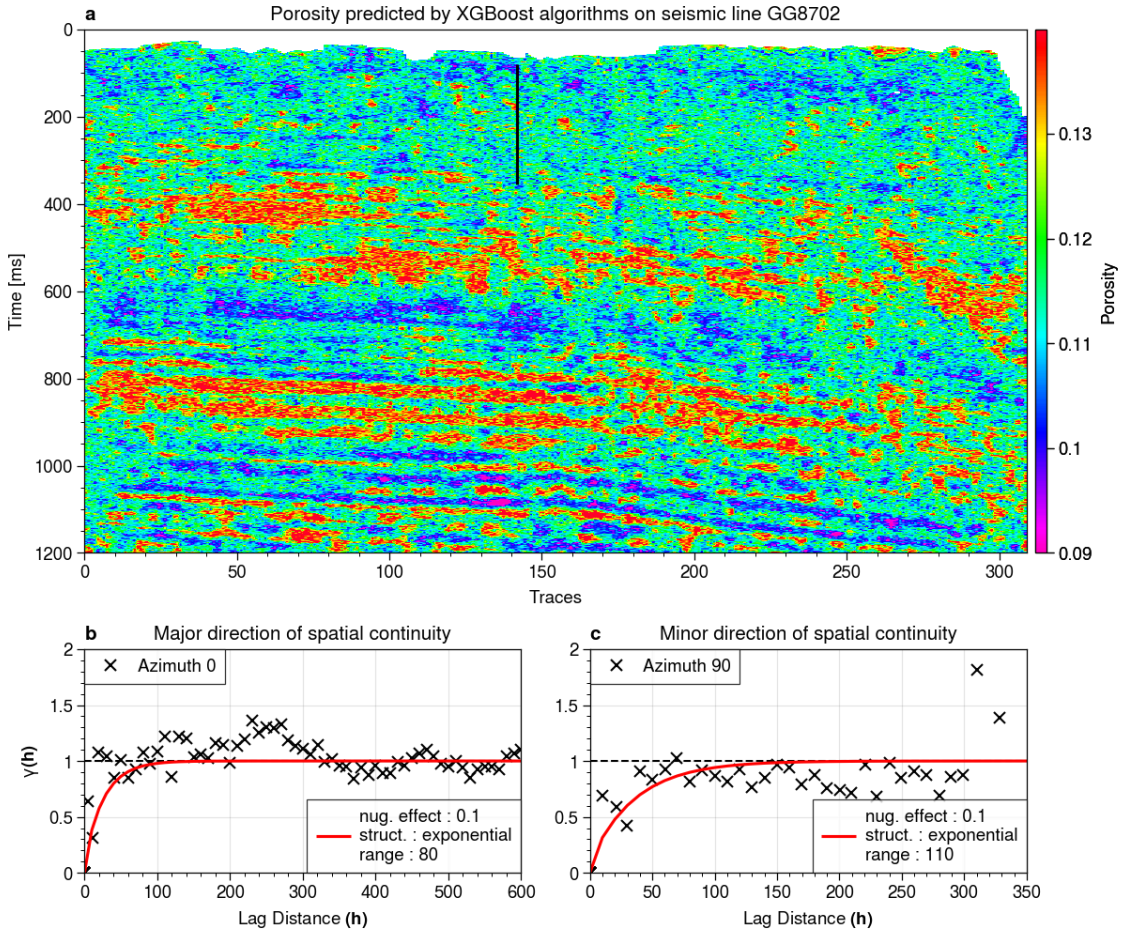

Figure 43: a) XGBoost distribution of porosity on seismic line GG8702; b) and c) Variogram for major and minor direction of continuity.

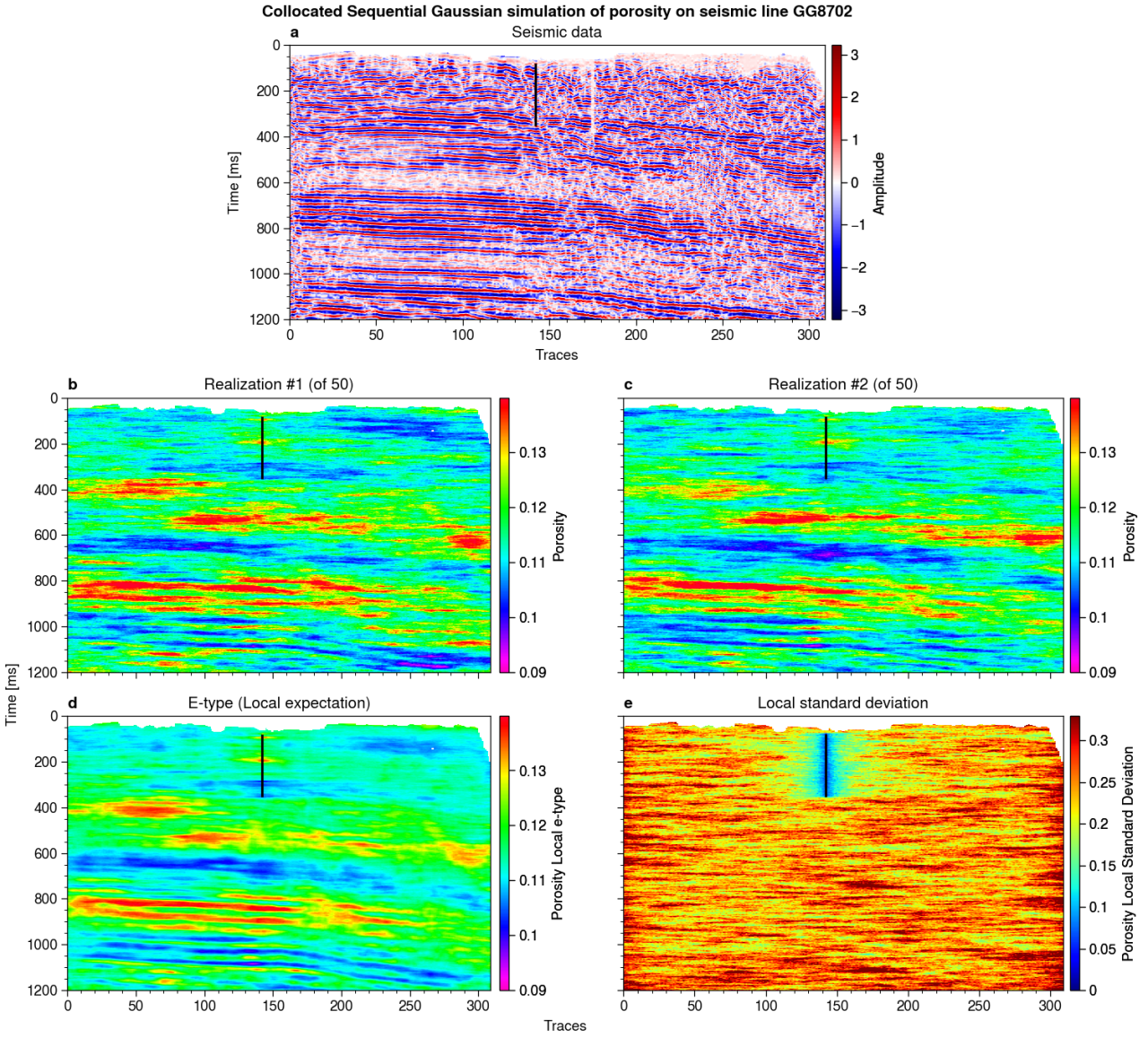

Figure 44: Postprocessed collocated Sequential Gaussian simulation of porosity for seismic line GG8702. a) original seismic amplitude; b) and c) two random porosity realizations; d) local expectation; e) local standard deviation.

7 Conclusion

The design of complex systems such as Underground Thermal Energy Storage (UTES) requires not only the modelling of the whole installation and optimisation of the overall design but also to consider the large variety of different uncertainty sources that affect each stage of the modelling chain.

This report provides an overview on the different methods that are available to deal with uncertainties, to discuss how they may be helpful for decision-making, and to highlight their advantages and limitations, focusing on an illustrative case study that consists in prior assessment of a go/no-go for a heat storage, depending on the storage efficiency. The different steps of uncertainty treatment are presented:

- Identification of uncertainty and information gathering;
- Representation of uncertain parameters;
- Propagation of uncertainties;
- Sensitivity analysis to identify the most influential parameters;
- Decision making;
- Reduction of epistemic uncertainty by new data acquisition and by re-starting the information-gathering step.

The exercise of representation, propagation, and use for decision-making are deployed with different approaches:

- OAT approach is a very simple and rapid sensitivity analysis tool, which is not appropriate for decision-making. It investigates very limited and non-conservative sets of values.
- Probabilistic framework: the level of complexity is moderate, it investigates the entire range of values but additional assumptions are made at the representation step, and thus the results should be used cautiously, since they underestimate the uncertainty. It is possible to perform sensitivity analysis.
- Extra-probabilistic framework: this sophisticated framework enables a very limited number of additional assumptions. The results can be used for decision-making and give a good idea of the true level of uncertainty. The decision-maker may feel confused by the form of the result and should be guided to interpret and use results. It is possible to perform sensitivity analysis.

We then tried to deploy the afore-mentioned approach on a real case study: the Bern demo site. We assumed that the choice of drilling the first well had not been made, and that we had to support this decision through a comprehensive analysis of uncertainties. Due to time and budget constraints, the work focused on preliminary steps and on definition of a work programme. The model was quite complex (3D numerical model); the decision framework was clarified and two decisional outputs were selected; a number of questions were raised when identifying a relevant set of parameters to deal with uncertainties and different choices were made; once input parameters were identified, we tried to gather information to characterize the different parameters and to propose appropriate representation in the probabilistic/extra-probabilistic framework. When confronted with such a complex and time-consuming model (~2 hours), with high-number of uncertain parameters (26), afore-mentioned approaches cannot routinely be deployed.

A second case study, working at a more regional scale and with a generic storage case study in the Dogger Paris basin was considered and gives a good illustration of the next possible steps for the Bern case study. Once again, the modelling needs long-running numerical simulations (typical computation time cost of the order of several hours). In order to conduct the analysis of the parametric uncertainties affecting the system: i. a metamodel was set up at each time step from a limited number of simulations run with the long-running numerical code and its predictability was validated (as specific difficulty, we dealt with scenario-like inputs); ii. uncertainty analysis was carried out using VBSA techniques (as specific difficulty, the presence of dependence among the input variables was accounted). Using the available database for the Dogger, the most influential parameters identified are the temperature parameters, the flow rate and the time duration.

For the Bern and Dogger case studies, we made the choice to represent the rock properties parameters by equivalent values but it constitutes a limitation of models, and some physical reservoir behaviors cannot be faithfully modelled without considering a complete representation of the reservoir properties such as porosity and permeability. Depending on the modelling objectives and on the availability of data, a more refined geological model may be key to move closer to reality. Uncertainties related to geological modelling may be assessed either by qualitative assessment or by quantitative assessment. A last case study was proposed to

demonstrate how rock properties (porosity and permeability) could be predicted at unsampled locations for a demonstration site around Geneva, using geostatistics and machine learning. These techniques were successfully applied to elaborate rock properties maps.

As a conclusion, through a rapid overview on a fictive basic case study, and through 3 consistent case studies focusing on different specific bricks of uncertainty treatment, the present report proposes a number of advanced tools to deal with uncertainties in highly uncertain contexts that are expected in heat storage activities. Discussions concerning these different contributions between partners involved in WP5 were also the occasion to discuss limitations, strengths, possible improvements and perspectives of future work.

8 Bibliography

Almeida, A. S., & Journel, A. G. (1994). Joint simulation of multiple variables with a Markov-type coregionalization model. Mathematical geology, 26(5), 565-588.

Barfod, A.A.S., Vilhelmsen, T.N., Jørgensen, F., Christiansen, A.V., Høyer, A.-S., Straubhaar, J., Møller, I., 2018. Contributions to uncertainty related to hydrostratigraphic modeling using multiple-point statistics. Hydrol. Earth Syst. Sci. 22, 5485–5508.

Ba, S., Brenneman, W. A. and Myers, W. R. (2015), "Optimal Sliced Latin Hypercube Designs," Technometrics.

Baudrit, C, Couso, I, Dubois, D (2007). "Joint propagation of probability and possibility in risk analysis: Towards a formal framework." International Journal of Approximate Reasoning, 45(1), 82–105.

Baudrit, C, Dubois, D, Perrot, N (2008). "Representing parametric probabilistic models tainted with imprecision." Fuzzy sets and systems, 159(15), 1913–1928.

Beer M, Ferson S, Kreinovich V (2013). "Imprecise probabilities in engineering analyses." Mechanical Systems and Signal Processing, 37(1), 4–29.

Berkowitz, B., 2002. Characterizing flow and transport in fractured geological media: a review. Adv. Water Resour. 25 (8–12), 861–884.

Bosch, M., Mukerji, T., & Gonzalez, E. F. (2010). Seismic inversion for reservoir properties combining statistical rock physics and geostatistics: A review. Geophysics, 75(5), 75A165-75A176.

Breiman, L. Friedman J., Stone C.J., and Olshen R.A.. (1984) Classification and Regression Trees. The Wadsworth and Brooks-Cole statistics-probability series. Taylor & Francis.

Brusova, O., Corzo, M., & Pyrcz, M. J. (2020). Introduction to this special section: Machine learning and AI. The Leading Edge, 39(10), 700-700.

Dubois, D., Guyonnet, D. (2011). "Risk-informed decision-making in the presence of epistemic uncertainty." International Journal of General Systems, 40(02), 145–167.

Ferson, S., Tucker, T. (2006). "Sensitivity analysis using probability bounding." Reliability Engineering & System Safety, 91(10), 1435–1442.

Feyen, L., Caers, J., 2006. Quantifying geological uncertainty for flow and transport modeling in multi-modal heterogeneous formations. Adv. Water Resour. 29 (6), 912–929.

GeoMol. (2019). Ein geologisches 3D-Modell des Schweizer Mittellands. https://www.swisstopo.admin.ch/de/wissen-fakten/geologie/geologische-daten/3d-geologie/tief/geomol.html.

Geoportal Kanton Bern, internet online database, access June 2021. https://www.map.apps.be.ch/pub/synserver?project=a42pub_frk&userprofile=geo&client=core&language=de

Goovaerts, P. (1997). Geostatistics for natural resources evaluation. Oxford University Press on Demand.

Hastie, T., Tibshirani, R., Friedman, J. (2009). The elements of statistical learning: data mining, inference, and prediction. Springer-Verlag, New York.

He, X., Sonnenborg, T.O., Jørgensen, F., Høyer, A.-S., Møller, R.R., Jensen, K.H., 2013. Analyzing the effects of geological and parameter uncertainty on prediction of groundwater head and travel time. Hydrol. Earth Syst. Sci. 10, 2789–2833.

Høyer, A.-S., Vignoli, G., Hansen, T.M., Vu, L.T., Keefer, D.A., Jørgensen, F. 2017. Multiple-point statistical simulation for hydrogeological models: 3D training image development and conditioning strategies. Hydrol. Earth Syst. Sci., 21, 6069–6089.

Høyer, A.S., Klint, K.E.S., Fiandaca, G., Maurya, P.K., Christiansen, A.V., Balbarini, N., Bjerg, P.L., Hansen, T.B., Møller, I. 2019. Development of a high-resolution 3D geological model for landfill leachate risk assessment. Engineering Geology 249, 45–59.

Huysmans, M., Dassargues, A., 2009. Application of multiple-point geostatistics on modelling groundwater flow and transport in a cross-bedded aquifer (Belgium). Hydrogeol. J 17 (8)

Jacques, J. Lavergne, C., Devictor, N., (2006). Sensitivity Analysis in presence of Model Uncertainty and Correlated Inputs, Reliability Engineering and System Safety 91, 1126-1134.

Journel, A. G. (1999). Markov models for cross-covariances. Mathematical Geology, 31(8), 955-964.

Keller, C.K., van der Kamp, G., Cherry, J.A., 1986. Fracture permeability and groundwater flow in clayey till near Saskatoon, Saskatchewan. Can. Geotech. J. 23 (2), 229–240.

Keller, B. (1992). Hydrogeologie des schweizerischen Molasse-Beckens: Aktueller Wissensstand und weiterführende Betrachtungen. Eclogae geologicae Helvetiae(85), S. 611-651.

Lancaster, S., & Whitcombe, D. (2000). Fast-track 'coloured'inversion. In SEG Technical Program Expanded Abstracts 2000 (pp. 1572-1575). Society of Exploration Geophysicists.

Leu W., et. al.(2006) Geothermische Eigenschaften der Schweizer Molasse (Tiefenbereich 0 – 500 m)

Manceau, J. C., Rohmer, J., 2016. Post-injection trapping of mobile CO 2 in deep aquifers: Assessing the importance of model and parameter uncertainties. Computational Geosciences 20(6), 1251-1267.

NAGRA (1993). Amman, M., Birckhäuser, P., Bläsli, H. R., Lavanchy, J. M., Löw, S., Meier, B., et al. (1993). TB 92-03. Untere Süsswassermolasse im Erdsondenfeld Burgdorf. Wetttingen: NAGRA. (NAGRA NTB 92-03, 1993)

NAGRA (1993) O. Voborny, P. Adank, W. Hürlimann, B.M. Thompson, 1993. Hydrogeologische Modellierung im Opalinus-Ton und in der Unteren Süsswasser-Molasse der Nordostschweiz. NAGRA NTB 90 14 (1993)

NAGRA (2005). Geologische Tiefenlagerung der abgebrannten Brennelemente, der hochaktiven und langlebigen mittelaktiven Abfälle – Darstellung und Beurteilung der aus sicherheitstechnisch-geologischer Sicht möglichen Wirtgesteine und Gebiete. NAGRA NTB 05-02, 2005

Pirot, G., Renard, P., Huber, E., Straubhaar, J., Huggenberger, P., 2015. Influence of conceptual model uncertainty on contaminant transport forecasting in braided river aquifers. J. Hydrol. 531, 124–141.

Refsgaard, J.C., Christensen, S., Sonnenborg, T.O., Seifert, D., Højbjerg, A.L., Troldborg, L., 2012. Review of strategies for handling geological uncertainty in groundwater flow and transport modeling. Adv. Water Resour. Vol. 36, 36–50.

Rogers (1981). Thermodynamics of geothermal fluids, Geothermal Energy.

Rohmer, J., Lecacheux, S., Pedreros, R., Quetelard, H., Bonnardot, F., Idier, D. (2016). Dynamic parameter sensitivity in numerical modelling of cyclone-induced waves: a multi-look approach using advanced meta-modelling techniques. Natural Hazards 84(3), 1765-1792.

Rohmer, J., Manceau, J.C., Guyonnet, D., Boulahya, F., Dudois, D. (2018). HYRISK : An R package for hybrid uncertainty analysis using probability, imprecise probability and possibility distributions. Non-peer reviewed article published at EarthArXiv.

Roustant, O., Padonou, E., Deville, Y., Clément, A., Perrin, G., Giorla, J., Wynn, H., 2020. Group kernels for Gaussian process metamodels with categorical inputs. SIAM/ASA Journal on Uncertainty Quantification 8(2), 775-806.

Roustant, O., Ginsbourger, D., & Deville, Y. (2012). Dicekriging, Diceoptim: Two R packages for the analysis of computer experiments by kriging-based metamodelling and optimization. Journal of Statistical Software, 51(1), 54p.

Saltelli, A.; Ratto, M.; Andres, T.; Campolongo, F.; Cariboni, J.; Gatelli, D.; Saisana, M.; Tarantola (2008). S. Global sensitivity analysis: the primer. JohnWiley & Sons, 2008.

Sandersen, P.B.E., 2008. Uncertainty assessment of geological models - a qualitative approach. In: Refsgaard, J.C., Kovar, K., Haarder, E., Nygaard, E. (eds), 2008. Credibility of Modelling. IAHS Publication, Calibration and Reliability in Groundwater modelling, 337–344.

Santner, T. J., Williams, B. J., Notz, W. I., & Williams, B. J. (2003). The design and analysis of computer experiments (Vol. 1). Springer, New York.

Schout, G., Drijver, B., Gutierrez-Neri M., Schotting R. (2014). Analysis of recovery efficiency in high-temperature aquifer thermal energy storage: a Rayligh-based method. Hydrogeology Journal (2014) 22: 281-291

Tianqi Chen and Carlos Guestrin. (2016) “XGBoost: A Scalable Tree Boosting System”. In: Proceedings of the 22Nd ACM SIGKDD International Conference on Knowledge Discovery and Data Mining. KDD ’16. San Francisco, California, USA, pages 785–794

Troldborg, M., Nowak, W., Tuxen, N., Bjerg, P.L., Helmig, R., Binning, P.J., 2010. Uncertainty evaluation of mass discharge estimates from a contaminated site using a fully Bayesian framework. Water Resour. Res. 46, W12552

Van den Heuvel, D. et al (2020), Pre-study of the Forsthaus Geospeicher heat storage and utilisation project: Geological and geochemical aspects

Walsch et al. (2017). Calculating thermophysical fluid properties during geothermal energy production with NESS and Reaktoro, Geothermics, 70: 146-154

Xu, W., Tran, T. T., Srivastava, R. M., & Journel, A. G. (1992). Integrating seismic data in reservoir modeling: the collocated cokriging alternative. In SPE annual technical conference and exhibition. OnePetro.